ÇUKUROVA UNIVERSITY
INSTITUTE OF NATURAL AND APPLIED SCIENCES

MSc. THESIS

Murat KARATAŞ

OPTIMIZATION OF GMAW PROCESS PARAMETERS FOR IMPROVING MECHANICAL PROPERTIES OF DP1000 STEEL JOINT

THE DEPARTMENT OF MECHANICAL ENGINEERING

ADANA-2018

ÇUKUROVA UNIVERSITY
INSTITUTE OF NATURAL AND APPLIED SCIENCES

OPTIMIZATION OF GMAW PROCESS PARAMETERS FOR IMPROVING MECHANICAL PROPERTIES OF DP1000 STEEL JOINT

Murat KARATAŞ

MSc THESIS

THE DEPARTMENT OF MECHANICAL ENGINEERING

We certify that the thesis titled above was reviewed and approved for the award of degree of the Master of Science by the board of jury on 20/02/2018.

………………………………	….……………………	.... …………………….
Prof. Dr. Melih BAYRAMOĞLU	Prof. Dr. Necdet GEREN	Prof. Dr. Uğur EŞME
SUPERVISOR	MEMBER	MEMBER

This MSc Thesis is written at the Department of Institute of Natural and Applied Sciences of Çukurova University.
Registration Number:

Prof. Dr. Mustafa GÖK
Director
Institute of Natural and Applied Sciences

ABSTRACT

MSc THESIS

OPTIMIZATION OF GMAW PROCESS PARAMETERS FOR IMPROVING MECHANICAL PROPERTIES OF DP1000 STEEL JOINT

Murat KARATAŞ

ÇUKUROVA UNIVERSITY
INSTITUTE OF NATURAL AND APPLIED SCIENCES
THE DEPARTMENT OF MECHANICAL ENGINEERING

Supervisor : Prof. Dr. Melih BAYRAMOĞLU
Year: 2018, Pages:107
Jury : Prof. Dr. Melih BAYRAMOĞLU
: Prof. Dr. Necdet GEREN
: Prof. Dr. Uğur EŞME

Euro-6 norms for reduction of CO_2 emissions and ECE-R66-01 regulation for safer passenger transportation became legislative obligations for bus builders. These two adaptations increase the weight of a bus as nearly 600kg which also increases the fuel consumption nearly 1.5-3%. Dual phase (DP) steels can compensate these increases by decreasing the thickness of the components. Because, ferrite provides the steel with good formability and martensite increases the hardness and ultimate tensile strength (UTS) in DP steels. But, the literature reviews showed that increase in heat input of Gas Metal Arc Welding (GMAW) can decompose the martensite islands and increase the ferrite grain size. As a result, hardness and UTS of the welded joint can decrease critically. Thus, this study focused on the optimization of GMAW process parameters for improving mechanical properties of DP1000 steel joint. In this aim, visual and microstructural inspections, Vickers hardness measurements and tensile tests were applied. As a result of the tensile tests, 100% of welded DP1000 samples fractured in subcritical (SC) region. The minimum decrease in UTS was calculated as 21,85% and the maximum decrease in UTS was defined as 26,55%. Increase in heat input (HI) also increased the martensite tempering effect and decreased the hardness and UTS. Welding speed, wire feed rate and voltage had 30.41%, 26.58% and 18,30% weightiness respectively on UTS. As a result, the optimum butt welding parameter combination of 1.20mm DP1000 steel was defined as 17.5V arc voltage, 380mm/min welding speed and 2.2m/min WFR and 45A arc current to provide the highest mechanical properties.

Key Words: DP1000, GMAW, Heat Input, Martensite Tempering, Tensile Strength

ÖZ

YÜKSEK LİSANS TEZİ

DP1000 ÇELİK BİRLEŞİMİNİN MEKANİK ÖZELLİKLERİNİ GELİŞTİRMEK İÇİN GMAW PROSES PARAMETRELERİNİN OPTİMİZASYONU

Murat KARATAŞ

ÇUKUROVA ÜNİVERSİTESİ
FEN BİLİMLERİ ENSTİTÜSÜ
MAKİNE MÜHENDİSLİĞİ ANABİLİM DALI

Danışman : Prof. Dr. Melih BAYRAMOĞLU
Yıl: 2018, Sayfa:107
Jüri : Prof. Dr. Melih BAYRAMOĞLU
: Prof. Dr. Necdet GEREN
: Prof. Dr. Uğur EŞME

CO_2 emisyonunu sınırlayan Euro-6 normu ve yolcu güvenliğini artıran ECE-R66-01 regülasyonu otobüs üreticileri için yasal zorunluluk haline gelmiştir. Bu adaptasyonlar bir otobüsünün ağırlığını yaklaşık 600kg ve yakıt tüketimi de yaklaşık %1.5-3 oranında artırmaktadır. Çift fazlı çeliklerin kullanılıp parçaların kalınlıklarının azaltılmasıyla bu artışlar kompanse edilebilmektedir. Çünkü, çift fazlı çeliklerdeki ferrit fazı çeliğe iyi şekillendirilebilirlik kazandırırken ve martensit fazı da çeliğin sertliğini ve çekme mukavemetini artırmaktadır. Literatür taramaları GMAW işleminin ısı girdisiyle oluşan martensit temperlenmesindeki ve ferrit tane boyutundaki artışların çift fazlı çeliklerin çekme mukavemetinde kritik azalmalara neden olabildiğini ortaya koymuştur. Bu çalışmada da DP1000 çeliğinin kaynaklı birleşimde en iyi mekanik özelliklerin sağlanabilmesi için GMAW parametrelerinin optimizasyonu hedeflenmiştir. Bu kapsamda gözle muayeneler, mikroyapısal incelemeler, Vickers sertlik ölçümleri ve çekme testleri uygulanmıştır. Çekme testleri sonucunda numunelerin %100'ü SC bölgesinden kopmuştur. Isı girdisindeki artış martensit temperlemesini artırıp sertliği ve çekme mukavemetini azaltmıştır. Çekme mukavemetindeki minimum azalma %21.85 ile maksimum azalma da %26.55 olarak ölçülmüştür. Kaynak hızının, tel besleme hızının ve voltajın çekme mukavemeti üzerindeki etki ağırlıkları sırası ile %30.41,%26.58 ve %18.30 olarak belirlenmiştir. Çalışmanın sonunda, 1.20mm kalınlıklı DP1000 çeliğin GMAW yöntemiyle alın kaynağında en yüksek mekanik değerleri sağlayan optimum kaynak parametreleri 17.5V kaynak voltajı, 380mm/dakika kaynak hızı, 2.2m/dakika tel besleme hızı ve 45A kaynak akımı olarak belirlenmiştir.

Anahtar Kelimeler: DP1000, GMAW, Isı Girdisi, Martensit Temperlenmesi, Çekme Mukavemeti

EXPANDED SUMMARY

The passenger safety, comfort and the fuel consumption are the most significant commercial factors for bus builders. While the global demand for fuel consumption is increasing, some standards such as Euro-6 norms for reduction of CO_2 emissions and ECE-R66-01 regulation for safer passenger transportation became legislative obligations for bus builders. These two adaptations increase the weight of a bus structure as nearly 600kg which also increases the fuel consumption nearly 1.5-3%. The most effective methods to compensate this increase in fuel consumptions without any loss on passenger safety and comfort can be improved by redesigning bus body aerodynamics, chemical changes on the consumed fuel, engine efficiency improvement, and reduction on the structure weight. Among these applications, reducing the vehicle weight is the most effective and applicable method for fuel economy. Reducing the weight includes redesigning the bus body structure and use of higher strength to weight ratio steels instead of mild carbon steels (such as S235, S275 and S355). Unfortunately, geometrical design changes on bus structure have limited potential to compensate the weight increase which is caused by the legislative obligations. Thus, the best way to compensate the weight increase is decreasing the thickness of the parts by using higher strength structural steels. Therefore, in this study DP steels were investigated because of their good formability and excellent mechanical properties.

The microstructure of DP steels consist of martensite and ferrite phases. The ferrite provides the steel with good formability and martensite increases the hardness and UTS of the steel. On the other hand, increase in heat input decreased the cooling rate of the welding. Increased holding time at high temperature also increased the martensite tempering effect and decreased the hardness distribution measurements throughout the heat effected zone (HAZ). Therefore, the high heat input of GMAW can decompose the martensite islands of DP steels into softer tempered martensite (TM) and increase the ferrite grain size; UTS of the joint

decreases. Thus, this study focused on the optimization of GMAW parameters to provide the highest mechanical properties from 1,20mm DP1000 steel which has the highest weight reduction potential and the highest precision to heat input. In this aim, the examined range of weld heat input was defined between 0.10kj/mm and 0.22kj/mm, due to preliminary studies. Visual and microstructural inspections, Vickers hardness and uniaxial transverse tensile tests were applied to define the effects of arc voltage, welding speed, wire feed rate (WFR), arc current and heat input on weld quality and mechanical properties of DP1000 sheet steel. An automated welding station was designed, built and used to form consistent linear welds at constant welding speeds. ER70S-6 wire electrode was used as filler metal. Minitab-17 statistical analysis software was used to design the generative full factorial experiment and analyze test results.

As a result of visual inspection it was observed that the ideal welding seams without any imperfection were observed mostly between the heat inputs of 0.12kj/mm and 0.15kj/mm. When the heat input increased over 0.18kj, the occurrence frequency of welding defects, such as burning gap and excessive penetration increased. On the other hand, excessive weld metal and the lack of penetration were observed for insufficient heat inputs, especially between 0.10kj/mm and 0.12 kj/mm heat inputs. The increase in the heat input caused an increase in penetration of the welding, sagging of the welding root and width of the welding. In contrary, the height and concavity of the welding decreased due to the increase in the amount of molten metal and its fluidity.

Increase in welding heat input also increased the martensite tempering and grain growth effects. At the same time, the width of the HAZ increased and the decomposition of martensite found further away from the Ac_1 line when compared to the lower heat input welds. Increase in heat input decreased percentage of volume fraction of martensite (VFM) and increased the ferrite grain size. Thus, hardness distribution of the welding cross-section decreased. The highest reduction of VFM was obtained in SC regions due to the highest percentage of tempered martensite. Thus, the lowest hardness values were measured at SC regions. The tempered martensite phases (completely decomposed martensite phase) in the SC regions dispersed more homogeneously at low heat input welds. But, they were clustered at high heat input welds. As a result, the increase in heat input increased the accumulation of the tempered martensites due to high amount of martensite decomposition obtained at the higher temperatures.

As a result of the tensile tests, 100% of welded DP1000 samples fractured in the SC region of HAZ. A certain relation between the VFM of SC region and UTS was proved. When the welding heat input was increased, martensite tempering increased and thus UTS decreased. The minimum decrease in UTS was calculated as 21.85% and the highest decrease in UTS was calculated as 26.55%. Welding speed, WFR and voltage had 30.41%, 26.58% and 18,30% weightiness respectively on the UTS of DP1000 steel welding. Therefore, welding speed had greatest effect on UTS, because it affected almost directly proportional to heat input.

While welding speed was increasing, UTS of welded plates increased due to the decrease in heat input. But, extremely fast welding speeds caused lack of penetration which also decreased the UTS and made weld quality worse. Therefore, highest welding speed was limited as 380mm/min. On the other hand very low welding speeds caused excessive welding caps.

When WFR was increased with arc current, UTS increased until full penetration was achieved. But as the welding current continued to increase, the UTS began to decrease, because higher heat input increased the martensite tempering. At the same time, excessive penetration could be observed. Thus the optimum WFR was defined as 2.2m/min and arc current was limited with 45A.

The limited voltage (17.5V) was sufficient for the full welding penetration to provide higher UTS. But, higher voltage levels increased the heat input and decreased the UTS of the welding joint. Also, increase in voltage increased the surface tension of molten metal so, burning gaps were detected at high voltage levels.

Voltage-wire feed rate interaction had a decreasing effect and welding speed-wire feed rate interactions had an increasing effect on UTS of DP1000 welding. There was no effect of voltage-welding speed interaction.

The compositions of the fusion zones were mostly ER70S-6 electrode material with a small amount of melted BM from the DP1000 steel. The measured VFM in FZ's were 43,73%, 44,18%, 42,63% and 41,14%. Although, there was no big difference among 4 samples, rise in the heat input had an reducing effect on the percentage of VFM and hardness in fusion zones. The average hardness of the FZ was lower than the hardness of DP1000 BM and higher than the hardness of SC region.

As a result of physical tests and statistical analysis of Minitab-17 software, the optimum butt welding parameter combination was defined as 17.5V voltage, 380mm/min welding speed and 2.2m/min WFR and 45A arc current to provide the highest mechanical properties in GMAW of 1.20mm DP1000 plates.

GENİŞLETİLMİŞ ÖZET

Yolcu güvenliği, konforu ve yakıt tüketimi otobüs üreticileri için en önemli ticari faktörler arasında yer almaktadır. Küresel yakıt tüketiminin her geçen gün artıyor olmasının yanında, CO_2 emisyonlarının azaltılması için Euro-6 normları ve yolcu taşımacılığını daha güvenli hale getiren ECE-R66-01 regülasyonları otobüs üreticileri için yasal zorunluluk haline gelmiştir. Bu iki düzenlemenin araç tasarımına uygulanması neticesinde bir uzun yol otobüsünün ağırlığı yaklaşık 600kg artmaktadır ve yakıt tüketimi de buna bağlı olarak yaklaşık %1.5-3 oranında artmaktadır. Yolcu güvenliği ve konforunda herhangi bir kayba neden olmaksızın yakıt tüketimindeki bu artışı telafi etmenin en etkili yöntemleri ise otobüs aerodinamiğinin yeniden tasarlanması, yakıttaki kimyasal değişiklikler, motor verimliliğini arttırılması ve araç ağırlığının azaltılması olarak tanımlanabilir. Bu uygulamalar arasında, araç ağırlığının azaltılması, yakıt ekonomisi açısından en etkili ve uygulanabilir yöntemdir. Ağırlığın azaltılması otobüs gövde tasarımında geometriksel değişikliklerin yapılmasını ve sade karbonlu çeliklerin (S235, S275 ve S355 gibi) yerine daha yüksek mukavemetli çeliklerin kullanılmasını içermektedir. Ama geometriksel tasarım değişiklikleri yasal yükümlülüklerin, yolcu güvenliğinin ve mekanik gereksinimlerin getirdiği sınırlamalar nedeniyle tek başına yeterli ağırlık kazancı sağlayamamaktadır. Bu sebeple ağırlık artışını telafi etmenin en iyi yolu, daha yüksek mukavemetli yapısal çelikler kullanarak parçaların kalınlığını azaltıp en az mevcut yapısal dayanımı sağlamaktır. Bu sebeple, bu çalışmada yüksek mekanik özelliklere ve şekillendirilebilirliğe sahip çift fazlı çelikler araştırılmıştır.

Çift çeliklerin mikroyapısı martensit ve ferrit fazlarından oluşmaktadır. Ferrit çeliğe iyi şekillendirilebilirlik kazandırırken ve martensit çeliğin sertliğini ve çekme mukavemetini artırmaktadır. Öte yandan, çift fazlı çelikler ısı girdisine karşı hassasiyeti bulunmakta ve mukavemetlerinde kayba uğrayabilmektedir. GMAW yöntemiyle yapılan birleştirme sırasında oluşan ısı girdisindeki artış çelin soğuma hızını düşürmektedir. Bu da çift fazlı çeliğin daha uzun süre boyunca yüksek sıcakta temperlenmesine neden olmaktadır. Neticede çift fazlı çeliğin içindeki martensit fazında dekompozisyon meydana gelir ve ferrit tane boyutu artar. Böylece kaynaklı birleşimin çekme mukavemeti daha da azalıp sertlik dağılımı düşmektedir. Bu sebeple, bu çalışmada en yüksek ağırlık kazancı sağlama potansiyeline ve ısı girdisine karşı en yüksek hassasiyete sahip olan 1.20mm DP1000 çeliğinin GMAW yöntemiyle en yüksek mekanik değerleri sağlayacak parametrelerin optimizasyonuna odaklanılmıştır. Isı girdisinin mekanik özelliklere etkisini imcelemek amacıyla yapılan ön çalışmaları neticesinde ısı girdisi aralığı 0.10kj/mm ile 0.22kj/mm olarak belirlenmiş ve sonraki çalışmalarda kullanılmıştır. Kaynakçı hatalarının ortadan kaldırılmasının yanında kaynak hızı ve torç ile plaka arasındaki mesafelerinin sabit tutulabilmesi için doğrusal kaynak otomasyonu tasarlanmış, üretilmiş ve çalışmadaki tüm kaynak işlemlerinde uygulanmıştır. Dolgu metali olarak ER70S-6 tel elektrotu kullanılmıştır. Kaynak ısı girdisini etkileyen kaynak voltajı, kaynak hızı, tel besleme hızı ve kaynak akımının etkileri belirlemek için görsel muayeneler, mikroyapısal incelemeler, Vickers sertlik ölçümleri ve çekme testleri uygulanmıştır. Deney tasarımını sağlamak ve test sonuçlarını analiz edebilmek için Minitab-17 istatistiksel analiz programı kullanılmıştır.

Görsel muayeneler ideal kaynak dikişi kalitelerinin 0.12kj/mm ve 0.15kj/mm ısı girdileri arasında sağlandığını ortaya koymuştur. Isı girdisi 0.18kj/mm'nin üzerine çıktıkça yanma deliklerinin ve kaynak kökü sarkmasının meydana gelme sıklığı artmıştır. Öte yandan 0.12kj/mm ısı girdisinin altındaki bazı uygulamalarda da yetersiz nufuziyet ve aşırı dış bükey kep formu gözlemlenmiştir. Genel anlamda kaynak ısısını artmasının kaynak nufuziyetini artırdığı ve kaynak kep yüksekliğini azalıp genişliğini artırdığı gözlemlenmiştir.

Yapılan mikro muayenelerde ısı girdisindeki artışın temperlenmiş martensit yüzdesini ve ferrit tane boyutunu artırdığı gözlemlenmiştir. Aynı zamanda ısıdan etkilenen bölgenin (IEB) genişliğinin arttığı, en düşük sertliklerinde Ac_1 çizgisinden daha uzakta bulunduğu tespit edilmiştir. Böylelikle kaynak sonrası geriye kalan orijinal martensit yüzdesi, malzemenin çekme mukavemeti ve sertlik dağılımı ısı girdisinin artmasıyla azalmıştır.

Kaynak sonrası yapılan mikro muayenelerde en düşük orijinal martensit yüzdesi ve en düşük Vickers sertlik ölçümleri IEB'de bulunanan SC bölgesinde tespit edilmiştir. Düşük ısı girdili kaynaklarda SC bölgesindeki temperlenmiş martensit fazları, yüksek ısı girdili kaynaklara göre daha homojen bir şekilde dağılmıştır. Isı girdisi arttıkça temperlenmiş martensit oluşumunda kümelenmenin arttığı gözlemlenmiştir.

Bu sebeplerden dolayı, çekme testlerinde numunelerin %100'ü SC bölgesinden kopmuştur. Yapılan gözlemler ve ölçümler kaynaklı numunenin çekme mukavemeti ile SC bölgesindeki orijinal martensit yüzdesi arasında kesin bir ilişki olduğunu ortaya koymuştur.Temperlenmiş martensit yüzdesindeki arttıkça kaynaklı numunelerin çekme mukavemetinde düşüş gözlemlenmiştir. Çekme dayanımındaki en düşük seviyedeki azalma %21.85 ve en yüksek azalma %26.55 oranlarında gerçekleşmiştir. Bu aralıkta ısı girdisi arttıkça çekme dayanımındaki kayıp artmıştır. İstatistiksel analizler neticesinde kaynak hızının, tel besleme hızının ve voltajın çekme dayanımı üzerindeki yüzdesel ağırlıkları sırası ile %30.41, %26.58 ve %18.30 olarak belirlenmiştir. Nümerik olarak doğrudan ısı girdisi ile ilişkili olduğu için kaynak hızı parametreler arasından çekme mukavemeti üzerinde en yüksek etkiye sahip faktördür. Kaynak hızı artarken ısı girdisi azaldığından çekme mukavemeti artmıştır. Ama yetersiz nufuziyete sebep olacak kadar yüksek kaynak hızları çekme mukavemetinde azalmaya ve aşırı dış bükey kaynak kepine neden olmaktadır. Bu sebeple azami kaynak hızı 380mm/dakika olarak sınırlandırılmıştır. Tel besleme hızının kaynak akımı ile birlikte tam nufuziyet sağlanana kadar artması çekme mukavemetini de artırmıştır.Bunun üstündeki tel besleme hızları ısı girdisini artırdığından çekme mukavemetinde azalmaya neden olmuştur. Bu nedenle ideal tel besleme hızı 2.2m/dakika ve kaynak akımı da 45A olarak belirlenmiştir. Yüksek tel besleme hızı aynı zamanda aşırı dış bükey kaynak kepine neden olmuştur. Nerdeyse tüm 17.5V kaynak gerilimi uygulamalarında tam kaynak nufuziyeti sağlanmıştır. Bu değerin üstündeki kaynak gerilimlerinde yanma delikleri oluşabilmiştir. Aynı zamanda ısı girdisi arttığından dolayı martensit temperleme etkisi artmış ve kaynaklı numunenin çekme mukavemeti azalmıştır. Yapılan fiziksel testler, muayeneler ve istatistiksel analizler neticesinde 1.20mm DP1000 kalite sacın GMAW yöntemiyle yapılacak alın kaynağı için ideal parametre kombinasyonu 17.5V kaynak gerilimi, 380mm/dakika kaynak hızı ve 2.2m/dakika tel besleme hızı ve 45A kaynak akımı olarak belirlenmiştir.

ACKNOWLEDGEMENT

First of all, I would like to express that I was very lucky during my MSc. survey. I had great moments and crucial experiences with brilliant people. I cannot find the appropriate words to express my gratitude to my advisor, Prof. Dr. Melih BAYRAMOĞLU, who supported and motivated me to enroll in new fields of manufacturing. His encouragement and guidance in starting my academic life would like to be pronounced forever. I learned lots of things from him and so many are left to be learnt.

I am grateful for helps of Res. Assist Ahmet ÇETİN and Res. Assist. Mete Han BOZTEPE on my laboratory studies.

I also thank to Sevda AVCI for her help on my microstructural inspection at Gedik Welding Company’s Research and Development Laboratory.

I could not finish my Msc thesis without support and encouragement of my family, my beloved wife Eda KARATAŞ, my mother Gülderen KARATAŞ and absolutely my father Hacı KARATAŞ. I dedicate this difficult work to them in remembrance of their love, patience and trust.

CONTENTS **PAGE**

LIST OF TABLES **PAGE**

LIST OF FIGURES **PAGE**

LIST OF ABBREVIATONS

AC	: Alternating Current
AGB	: Austenite Grain Boundary
AHSS	: Advanced High Strength Steels
Ar	: Argon
B.C.C	: Body Centered Cubic
B.C.T	: Body Centered Tetragonal
BM	: Base Metal
C_0	: Steel Mean Carbon Content
CE	: Carbon Equivalent
C_f	: Carbon Content Of Ferrite
C_m	: Carbon Content Of Martensite
CO_2	: Carbon Di Oxide
CTWD	: Contact-Tip-To-Workpiece Distance
DC	: Direct Current
DCEN	: Direct Current Electrode Negative
DCEP	: Direct Current Electrode Positive
DOE	: Design of Experiment
DP	: Dual Phase
E	: The Generated Energy By The Power Source
F.C.C	: Face Centered Cubic
Fe	: Iron
Fe_3C	: Carbur
FEM	: Finite Element Method
FL	: Fusion Layer
FZ	: Fusion Zone
GG	: Grain Growth

GMAW : Gas Metal Arc Welding
GR : Grain Refined
H_2 : Hydrogen
HAZ: : Heat Affected Zone
He : Helium
HI : Heat Input
SLA : High Strength Low Alloy
HV : Hardness Vickers
I : Current (A)
IC : Intercritical
LBW : Laser Beam Welding
Mn : Manganese
N_2 : Nitrogen
Nb : Niobium
O_2 : Oxygen
R : Current Resistance
RSW : Resistance Spot Welding
SAW : Submerged Arc Welding
SC : Subcritical
SEM : Scanning Electron Microscopy
SMAW : Shielded Metal Arc Welding
TIG : Tungsten Inert Gas
TM : Tempered Martensite
U : Voltage (V)
UTS : Ultimate Tensile Strength
UTS_{BM} : Ultimate Tensile Strength of Base Metal
$UTS_{weld\ joint}$: Ultimate Tensile Strength of Welded Joint
VFF : Volume Fraction Ferrite

VFM : Volume Fraction Martensite

WFR : Wire Feed Rate

α : Ferrite Phase

γ : Austenite Phase

η : Arc Efficiency

V : Welding Speed (mm/min)

1. INTRODUCTION

The passenger safety, comfort and the fuel consumption are the most significant commercial factors for bus builders. While the global demand for fuel consumption is increasing, some standards such as Euro-6 norms for reduction of CO_2 emissions and ECE-R66-01 regulation for safer passenger transportation become legislative obligations for bus builders. These two adaptations increase the weight of a bus structure as nearly 600kg which also increases the fuel consumption nearly 1.5-3%.The most effective methods to compensate this increase in fuel consumptions without any loss on passenger safety and comfort can be improved by redesigning bus body aerodynamics, chemical changes on the consumed fuel, engine efficiency improvement, and reduction on the structure weight. Among these applications, reducing the vehicle weight is the most effective and applicable method for fuel economy.

Reducing the weight includes redesigning the bus body structure and use of higher strength to weight ratio steels. Unfortunately, geometrical design changes on bus structure have limited potential to compensate the weight increase which is caused by the legislative obligations. Thus, the best way to compensate the weight increase is decreasing the thickness of the parts by using higher strength structural steels. Therefore, DP steels, which is the most effective grade of advanced high strength steels (AHSS) were investigated in this study. As shown in Figure 1.1, the tensile strength and formability of DP steels are better than conventional high strength low alloy (HSLA) steels. The thinner gauge DP steel can be used to provide the same design requirements. Due to their high strength and ductility, DP steels are the best choice to use instead of mild structural steels such as S235 (St37), S275 (St44) and S355 (St52). It is anticipated that, the weight of the bus can be decreased nearly 25% (750kg) without any loose on structural strength of the bus by utilizing DP steels on bus structure in a high percentage.

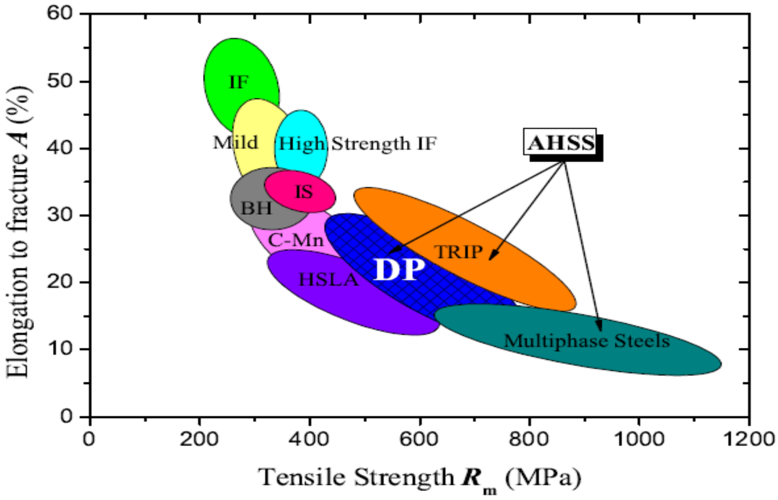

Figure 1.1. Relationship between yield strength and total elongation for various types of steels (Tsipouridis, 2016)

DP steels are defined by their high UTS, e.g., DP steel that has a UTS of 600 MPa is referred to DP600.The high performance mechanical properties of DP steels are obtained from their microstructures which consist of martensite and ferrite phases. The ferrite phase provides the steel with good formability. Martensite phase increases the hardness and tensile strength of the steel. Thus, while the volume fraction of martensite within the ferrite matrix is increasing, the strength of DP steel also increases. The VFM for the DP600, DP780, and DP980 were approximately 7.5%, 20%, and 46%, respectively (Burns, 2009). Also, the finer grain size of ferrite and banding of the martensite islands increase the strength of the DP steels. Higher carbon content of individual martensite phase also increases the hardness of the martensite islands and so DP steel. On the other hand, reductions in ductility and elongation are observed, while VFM is increasing.

DP steels have been recently used for automotive industry to reduce the vehicle weight, the fuel consumption and to improve the passenger safety. It is critical from the technical and economical point of view to choose the appropriate method for DP steel welding during automotive manufacturing. Resistance spot welding (RSW), laser beam welding (LBW), tungsten inert gas (TIG) welding and GMAW methods are mainly used for permanent joining processes in the automotive industry.

Nowadays, a bus structure is constructed by using mostly mild carbon steels such as S235, S275 and S355. Thicknesses and sizes of the bus structure components are mostly greater than automobile components. Hence, higher welding heat input is needed for sufficient welding penetration than automotive manufacturing applications. On the other hand, high heat input decreases the performance DP steels. Because, the high heat input of GMAW can decompose the martensite islands of DP steels into softer islands of tempered martensite. Also, the ferrite grain size increases, when temperature is higher than 1100^{o}C. Both can reduce UTS of the DP steel with the lower joint efficiency and cause premature localized necking in the region where tempered martensite forms. Lee et al. (2014) investigated the effect of LBW, TIG welding and GMAW on microstructure and UTS of DP780. They defined that, higher heat input weld (GMAW>TIG>LBW), also increased the size of the fusion zone (FZ) and HAZ. VFM and hardness's of the FZ and HAZ increased with higher cooling rate (LBW>TIG>GMAW).Thus, the highest decrease in UTS was observed on GMAW method.

Base metal (BM) fracture is desired from the DP steel weldings to guarantee original UTS of the steel which is used in the structure design of the bus. It can be provided at low strength grade of DP steels by using just sufficient heat input. But, while the UTS grade of DP steel is increasing from DP450 to DP600, DP780 and DP1000; the joint efficiency decrease under the same welding parameters. Especially, high heat input welds of DP1000 mostly fracture in SC region. Rocha et al. (2015) studied the microstructure and tensile test results of laser beam welded DP600 and DP980 steels. It is defined that, tempered martensite percentage and drop in hardness were higher at the SC region of the DP980 side than that of DP600 side. Because, DP980 base metal had higher VFM. Thus, this study focused optimization of GMAW process parameters for improving the mechanical properties of 1.20mm DP1000 steel which has the highest weight reduction potential and the highest precision to heat input. In this aim, visual and microstructural inspections, Vickers hardness and uniaxial transverse tensile tests were applied to define the effects of voltage, welding speed, wire feed rate and heat input on welding quality and mechanical properties of DP1000 sheet steel. The relations between the results of inspections and tests were correlated.

1.1. Dual Phase Steels

Dual phase steels were developed in the 1970's to provide higher tensile strength, elongation and formability for upgraded fatigue resistance and crash resistance demands of automotive industry. Also, DP steels have been using to decrease the weight of vehicles for fuel saving. The microstructure of DP steels consist of martensite and ferrite phases. The ferrite phase provides the steel with good formability and martensite phase increases the hardness and tensile strength of the steel. The original scanning electron microscopy (SEM) microstructures of DP600 and DP980 base metals are shown in Figure 1.2a and Figure 1.2b, respectively. In the images, the ferrite phases appears grey and martensite phases appears white (In optical microscopy, ferrite will appear white and martensite will appears grey).

The VFM islands within the ferrite matrix and the ferrite grain size are the main factors that affect the UTS of DP steel; as the VFM increases or as the ferrite grain size decreases, UTS and hardness of the DP steel will also increase. The shape and orientation of the martensite islands can also affect the UTS and cause the steel to exhibit anisotropic mechanical properties; elongated bands of martensite can be formed during processing (Guo et al., 2015).

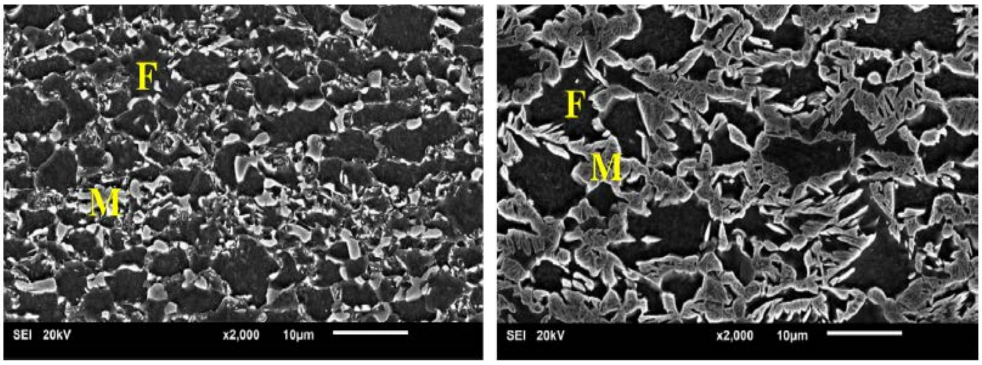

(a) **(b)**

Figure 1.2. SEM microstructures of base metals. “M” shows martensite and “F” shows ferrite. (a)DP600 and (b)DP980 (Guo et al., 2015)

DP steels are produced by intercritical (IC) annealing. In this process, the temperature of the steel is elevated to the required temperature where body centered cubic (B.C.C) ferrite (α) phase transforms to an face centered cubic (F.C.C.) austenite (γ) phase. As shown in Figure 1.3, ferrite phase is labeled as ‘α’, austenite phase is labeled as ‘γ’ and IC region is labeled as ‘α+γ’, which includes both phases in Fe-Fe_3C binary phase diagram. The annealing temperature and the IC limits (Ac_1 and Ac_3 lines) of the steel form different volume fractions of austenite and ferrite. Burns (2009) investigated the effect of two different annealing temperature on VFM at process-A and process-B. While the annealing temperature is increasing and approaching to Ac_3 line, the volume fraction of austenite increases. T_A(~750°C) and T_B (~810°C) annealing temperatures of the same steel samples are shown in the Figure 1.3. Volume fraction of austenite is approximately 20% at T_A (~750°C). While annealing temperature is increasing to T_B (~810°C), volume fraction of austenite also increases to 50%. Then, quenching the intercritically annealed steels can transforms all austenite phase to martensite phases. As a result, increase in intercritical annealing temperature also increases the VFM of DP steels (Burns, 2009).

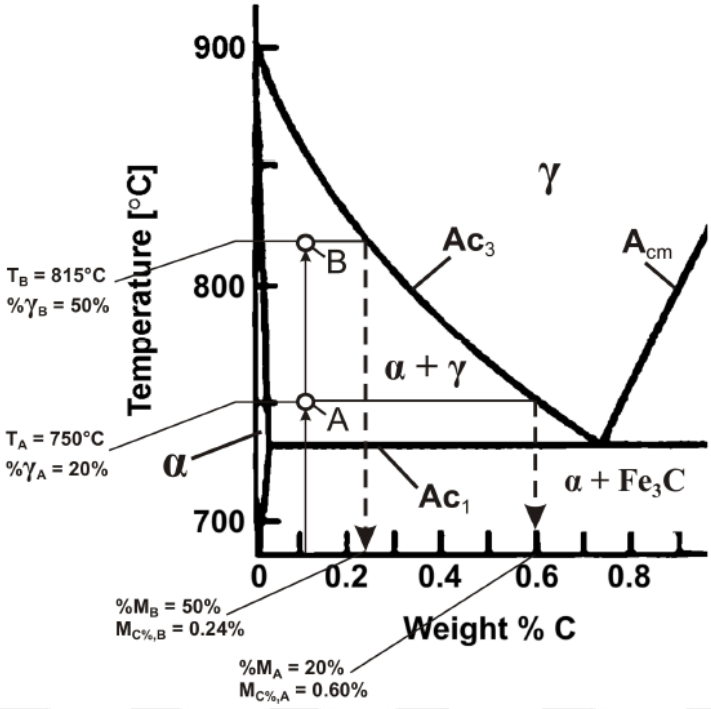

Figure 1.3. The intercritical region of a plain carbon steel Fe-Fe_3C binary phase diagram. Example intercritical annealing processes, A and B, used to make the DP steel microstructure are shown (Burns, 2009)

Carbon content of martensite (C_m) affects the mechanical properties of martensite phase in DP steels. C_m can be calculated by using the equation 1.1. (Burns, 2009)

$$C_0 = C_f \,.VFF + C_m \,.VFM \quad (1.1)$$

Where;

C_0: Steel mean carbon content,

C_f: Carbon content of ferrite,

$C_{m:}$ Carbon content of martensite,

VFF: Volume fraction of ferrite,

VFM: Volume fraction of martensite.

As shown in Figure 1.4, C_m is decreasing with increase in VFM for the same alloy. Carbon solubility of austenite phase is much higher than ferrite phase. During the quenching process, the carbon atoms are trapped in the formed martensite phase. Because, there is no sufficient time for carbon diffusion. Thus, C_m is 60% for process-A which has 20% VFM and C_m of was 24% for process-B, which has 50% VFM.

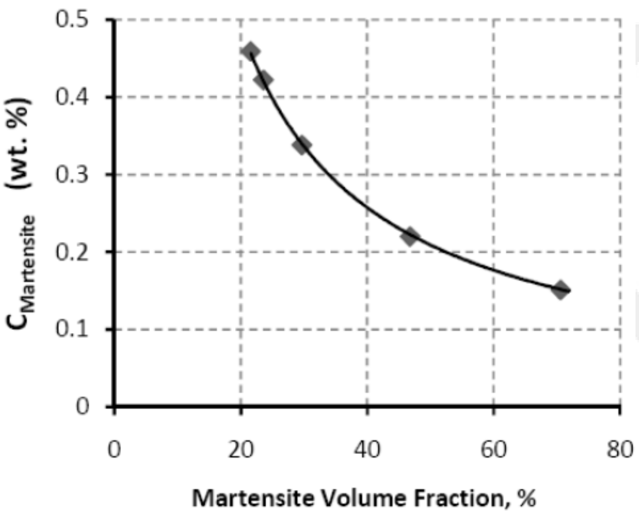

Figure 1.4. The relation between the C_m and VFM (Burns, 2009)

1.2. Martensite Tempering of DP Steels Welding

There are two types of martensite tempering process. One of them is isothermal tempering and another is nonisothermal tempering. Isothermal tempering includes low heating rate, long holding time at peak temperature, and low cooling rate to increase the ductility of the steel. Nonisothermal tempering occurs during the manufacturing processes such as welding process which has rapid heating and cooling.

When martensite is heated, carbon diffuses from the supersaturated martensite and forms a mixture of cementite and ferrite phases (Figure 1.5).

Martensite tempering depends on the carbon content of martensite, tempering temperature and duration. While tempering duration and temperature are increasing, decomposition rate will increase, cementite will coarsen, the width of the softened region will increase and thus hardness of the DP steel will decrease.

At the temperatures between 25-200 ºC, carbon atoms migrate to dislocation sites in the martensite, which has less than 0.2% C. In higher C martensites, these dislocation sites become saturated with carbon and ε-carbides starts to form. Rod shaped carbides, which identified as cementite, start to precipitate in martensite at 200-250^{o}C. These rod shaped carbides and ε-carbides transform into spherical cementite (Fe_3C) at 250ºC. The cementite phase coarsens at temperatures above 600ºC as shown in Figure 1.6. The highest decomposition rate occurs just below the A_1 temperature (approximately 727°C for plain carbon steels). A fully tempered martensite island includes cementite in a ferrite matrix. There is no remainder martensite (Biro, 2013).

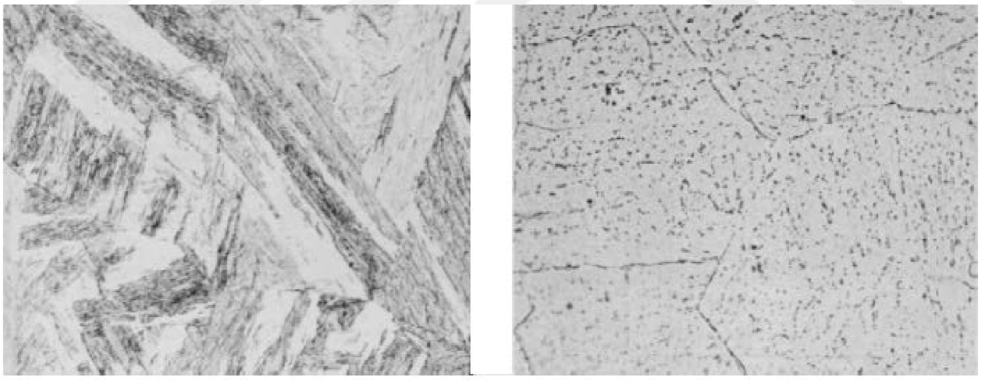

(a) **(b)**

Figure 1.5. Microstructure of (a) martensite and (b) tempered martensite in a 0.12% C steel (Biro, 2013)

In this study, DP1000 steel welding, that is a nonisothermal tempering process, was investigated. When a DP steel is welded, the martensite tempering occurs. Thus, the hardness and UTS of the steel decrease. As an example, Lee et al.

(2014) investigated effect of the TIG welding heat input on mechanical properties of DP780 steel which has 270HV hardness. They measured the hardness of the SC region as 220HV and UTS of the joint as 94.6% of the base metal. They also inspected the microstructure of SC region by using SEM. As shown in Figure 1.7, large tempered martensite islands were observed in the SC region of DP780 welding.

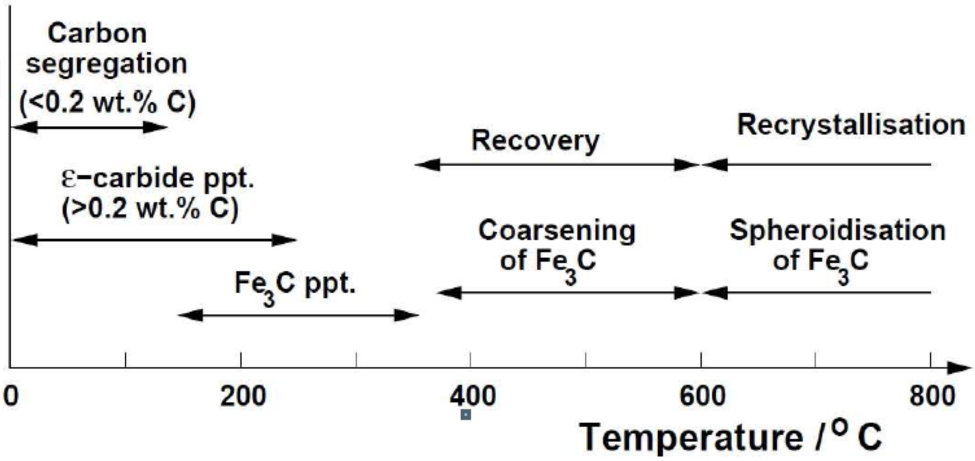

Figure 1.6. Summary of Fe-C martensite decomposition processes as a function of temperature during a one hour heat treatment (Biro, 2013)

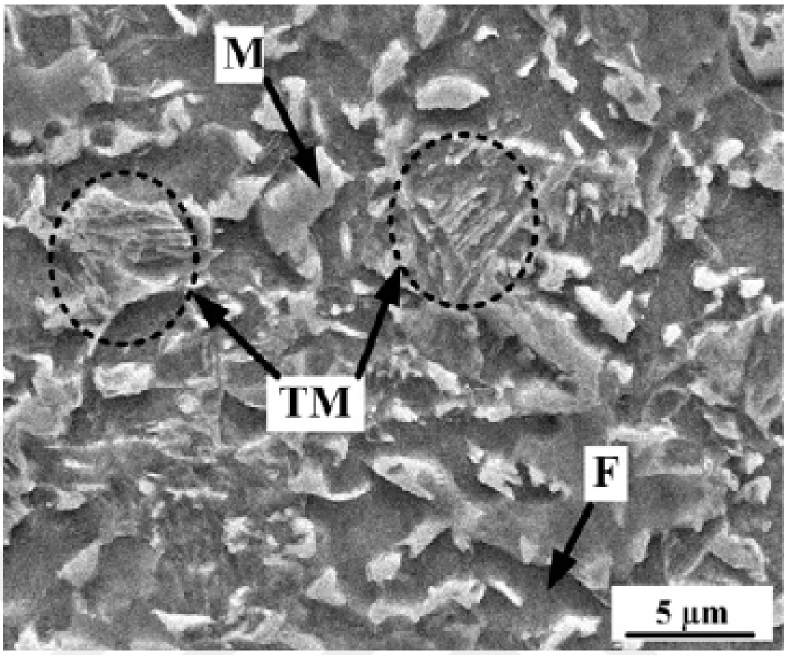

Figure 1.7. SC region microstructure of TIG welded DP780 steel (Lee et al, 2014)

1.3. Microstructural Regions of DP Steels Welding

In the welding of DP steels, different microstructural regions are occurred depending on the chemical composition of the BM and thermal cycles of welding process. These regions are shown in Figure 1.8. The chart in Figure 1.8a is the Fe-Fe_3C steel phase diagram. The microstructural regions in the HAZ are relatable to the phase diagram and occur at different temperature and carbon weight percentage. The important microstructural regions are marked on the phase diagram, which include: the FZ, the grain growth (GG) region and grain refined (GR) region, the IC region, SC region, and BM.

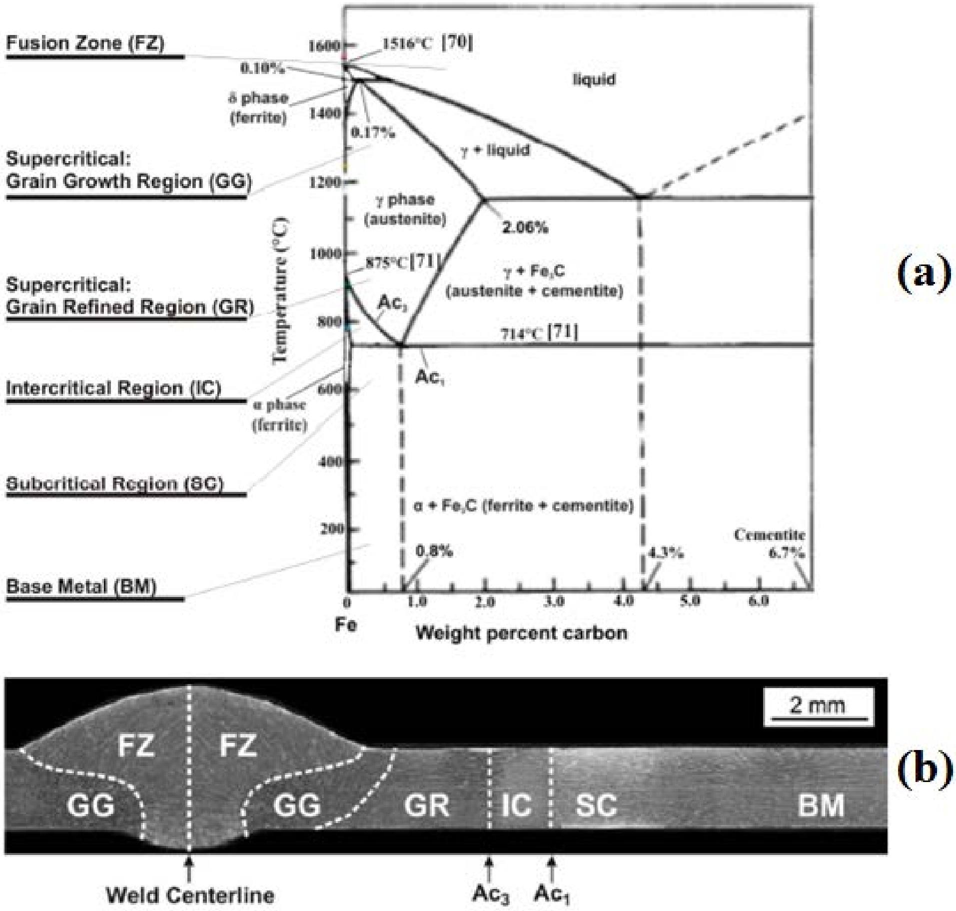

Figure 1.8. Overview of the DP weld HAZ (a) A typical Fe-Fe_3C binary phase diagram (b) A typical cross-section from a GMAW DP600 weld (Burns, 2009)

As an example, DP600 weld cross-section, that has been labeled with the microstructural regions in Figure 1.8b. Carbide nucleation and carbide coarsening caused the highest softening in SC region, immediately adjacent to the Ac_1 line. Thus, the lowest hardness is measured in SC region. The Ac_1 and Ac_3 lines, which are the boundaries for the IC region are defined on the image of the cross section. In IC region, the martensite and carbide phases in the base metal partially reform to austenite and then re-quench to martensite. IC region has a significant spike in hardness compared to the adjacent SC region, because of the renucleated martensite in IC region.

In GR region, the steel is fully transformed to austenite. Then, austenite phase transforms to massive martensite at the end of the cooling. The largest grains are observed immediately adjacent to the fusion layer (FL) in GG region. Because, above a certain peak temperature the inoculants dissolves in the austenite mix and the grains grow much larger than the grains in the GR region. These largest grains transforms to massive martensite. Hence, the hardness increases further upon entering the GR region and then reaches the maximum hardness in the GG region.

1.4. Gas Metal Arc Welding

Welding is a process, which two materials are joined permanently with or without a filler material under suitable combination of temperature, pressure and metallurgical conditions. There are different methods of welding, such as shielded metal arc welding (SMAW), GMAW, TIG welding, submerged arc welding (SAW), RSW and LBW for different joining requirements. Among these welding methods, GMAW is the mostly applied industrial welding process because it has high joining speed and adoptions to semi or fully automated systems.

Weldability can be defined as the ease of producing a sufficiently penetrated weld without defects such as crack, impurities and porosities. Also, welding characterizes the final mechanical properties of the steel. As described in previous chapters, welding heat input has a harmful effect on the mechanical properties and microstructure of DP steels. Especially, the thermal cycle of a welding process execute the percentage of DP steel martensite tempering. The different welding processes, which are used in automotive industry, have different heat inputs. They have also different heating and cooling rates. Rise in welding heat input decreases the cooling rate. In this case, martensite tempering increases and hardness decreases. For example, cooling rates of the RSW is nearly 2.000°C/s-100.000°C/s, for a laser welding, the range is a nearly 500°C/s-

5.000°C/s, and for a GMAW, the range is approximately 10°C/s-100°C/s. Therefore, the highest martensite tempering can mostly occur on GMAW applied DP steels (Gould et al., 2004)

The GMAW process is mostly performed on lower grades of DP steels such as DP480 and DP600, however, it can be used to weld higher strength grades (DP780, DP1000). But, martensite tempering percentage and decrease in UTS increase with higher grade DP steel usage at the same heat input. On the other hand, GMAW is the mostly applied technique in bus building industry, because it is the fastest and most applicable welding method for joining of rectangular cross-sectional profiles. Thus, the focus of this study is GMAW process optimization of DP1000 steel to provide the highest joining performance.

1.4.1. Components of GMAW System

GMAW process creates an electric arc between a consumable wire electrode and the workpieces to melt and join base materials. The filler metal is fed automatically from the wire feeder mechanism, through a liner, then out of a contact tip in the torch. In this process, CO_2 or mixture gas (combinations of Ar, He, CO_2 and O_2) are used to prevent oxidation and diffusion of H_2 and N_2 to the molten metal. GMAW process can be applied semi-automatic or fully automatic. Because of the horizontal current characteristic of the process, arc voltage is kept constant, direct current or alternating current are used by depending on the type of base metal and welding position. There are four metal transfer modes of GMAW. These are short circuit, globular, spray, and pulsed spray transfer modes which have different characteristics with advantages and limitations.

Figure 1.9 shows a general schematic of a GMAW system. The welding arc is created between the tip of the filler metal and the workpiece. The filler metal is continuously fed by a wire feeding rollers. A molten metal pool is created on the workpiece by the heat inputs of welding arc and the metal droplets transferred from the tip of the electrode into the molten base metal. When the FZ solidifies, a permanent joint is provided, as the welding torch travel along the weld joint. GMAW is a electrical process which is horizontal characteristic. Thus, while the distance between the workpiece and welding torch is changing, a constant voltage and a constant arc gap can be provided.

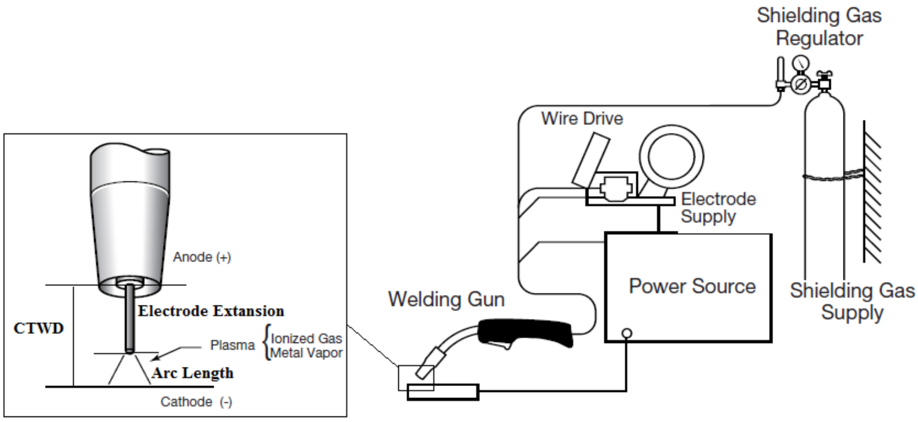

Figure 1.9. A general schematic for the setup of a GMAW system (Lincoln, 2014)

Also, current can be fluctuated during GMAW process. There are three electrical current types in GMAW applications. These are direct current electrode positive (DCEP), direct current electrode negative (DCEN) and alternating current (AC). AC current causes arc instability and electrode melting rate during the welding, so it generally not used. In direct current (DC) applications, electrons move from the cathode (negative polarity) to anode (positive polarity), therefore at anode (+) exposed a higher heat input. In DCEP application, wire electrode is connected to positive polarity and workpiece is connected to negative polarity of the welding machine. Thus, higher heat input occurs at the tip of the electrode and melting rate of the electrode increases. Also, better penetration and better arc stability are provided. In DCEN application, the negative polarity of the power supply is connected to wire electrode and positive polarity is connected to workpiece. Hence, higher heat input occurred on the workpiece and wire melting rate decreases, arc stability is less than DCEP system. Therefore in this study, DCEP is used for its heat input to workpiece.

The melting rate of the filler metal depends on arc voltage, electrode polarity, electrode diameter, contact-tip-to-workpiece (CTWD) distance, WFR and electrode chemical composition. While the wire electrode is extending, the electrical resistance and so temperature of the electrode tip increase. When sufficient temperature is reached, a molten bead will form at the tip. Then, this molten metal can be stripped off the end of the electrode and enter the weld pool by the electromagnetic force (Lorentz force) and the force of gravity.

1.4.2. Modes of Metal Transfer

In the GMAW process, different modes of metal transfer can be generated by depending on the current, voltage and shielding gas. These are short circuit metal transfer, globular metal transfer, spray metal transfer and pulsed spray metal transfer. Among these, short circuit metal transfer and spray metal transfer are the mostly applied modes.

Short circuit metal transfer occurs at low voltages when the electrode tip makes contact with the molten weld pool. As an example of a single cycle of the short circuiting metal transfer process is shown in Figure 1.10. The electrode melting rate is not sufficient to create and tear a molten bead from the electrode tip before contact with molten weld pool. Because, the electromagnetic pinch force is not sufficient at low voltage to separate the molten droplet. When the molten metal contact with the weld pool, a short circuit occurs and welding current shows a spike. In this way, the necessary pinch force is provided. Increase in the currents also increases Lorentz forces which cause pinching and necking of the molten metal. Thus, the surface tension forces decrease and the molten bead detaches. As the electrode makes contact, it causes the electrical path short and the arc to extinguish (step H, I, and A in Figure 1.10). Because, the electrical resistance decreases and the welding current rapidly increases (step B, C, and D in the image).

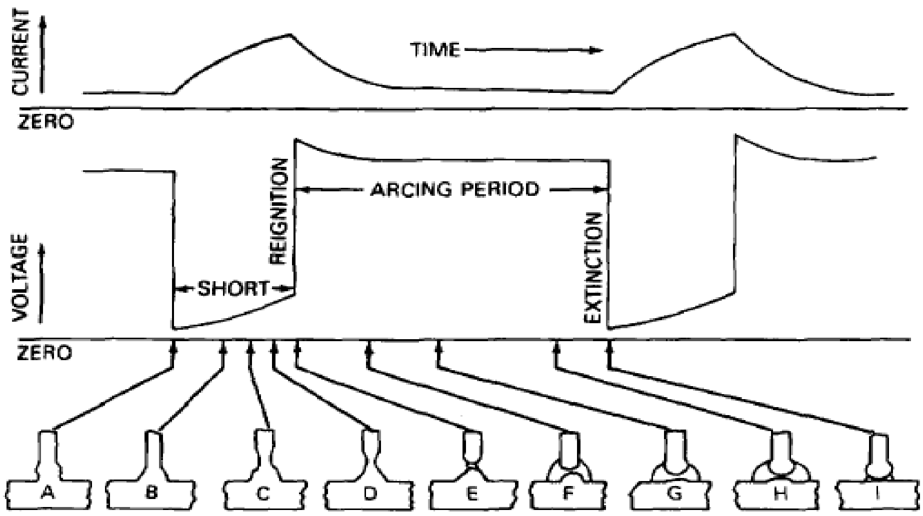

Figure 1.10. GMAW short circuit metal transfer (Park et al., 1981)

This spike in current increases the melting rate of the electrode significantly. This situation causes the ejection of molten metal; this is known as spatter. The solidified spatter on the workpiece has to be removed to prevent the decrease in fatigue strength of the structure. After the molten bead detaches and the electrode is no longer in contact with the weld pool the arc re-ignites and the process is repeated. Short circuit welds typically have low heat input and low welding penetration. Thus, it can be insufficient for providing the fully penetration of thicker workpiece. It is applied on the thin plates (0.60mm-5.00mm). The low heat input also helps to limit HAZ softening of DP steels and welding distortion of the structure. CO_2 shielding gas is mostly used because it is cheaper than Argon (Ar) mixed gas.

In globular metal transfer, short circuit current occurs. The molten filler metal is transferred to the weld pool as larger droplets than the diameter of filler metal. These irregularly shaped molten droplets don't follow an axial detachment from the filler metal, instead they can fall out of the path of the weld or move towards the contact tip. Therefore, the arc current is controlled difficultly and as a result, large amount spatter occurs. Thus, high spatter increases need for costly cleanup and decreases efficiency of electrode to the range of 87 – 93% (Park et al., 1981). Also, cold lapping of molten metal causes insufficient penetration which results in costly repairs. Globular metal transfer produces extremely convex weld bead due to the poor wetting at the weld toes. Therefore, globular metal transfer is applied rarely.

Spray metal transfer occurs when higher welding voltages and Ar rich shielding gases are used. This creates a larger arc gap, so the electrode tip to melt off before making contact with the molten weld pool. A molten bead at the electrode tip is stripped off and projected towards the weld pool, as shown in Figure 1.11. In this mode, the arc is continuous and does not extinguish. The diameter of the molten bead droplet in projected spray transfer and the diameter of the wire electrode are similar. In streaming spray transfer, the bead becomes smaller in diameter than the electrode. Molten droplets melt off at a frequency of approximately 100 Hz in projected spray transfer and up to approximately 1000 Hz in streaming spray transfer (Belinga et al, 2012). Spray metal transfer produces higher heat input and higher deposition rate than short circuiting transfer mode. Thus, the weld penetration and torch travel speed of spray metal transfer are also higher than short circuit mode. Penetration is also increased because in spray transfer the molten beads are being propelled towards the weld pool at high velocities causing ‘finger’ weld penetration geometry, as shown in Figure 1.11. The diameters of the beads are smaller than the electrode diameter, hence this schematic is for streaming spray transfer. Ar+CO_2 mixture gases are used as shielding gas in spay transfer mode applications.

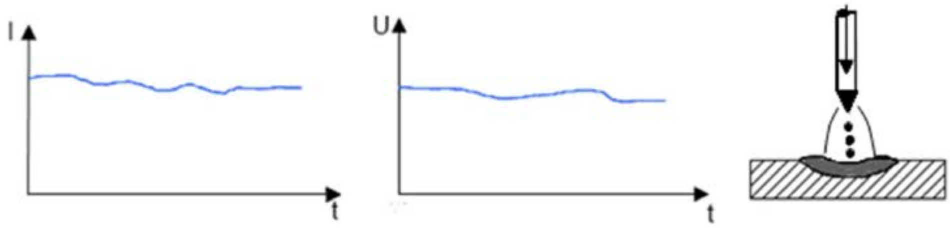

Figure 1.11. Transfer of spray arc (Belinga et al, 2012)

In pulsed spray metal transfer, the welding current is fluctuated between a high and low current levels. Metal transfer occurs as a single molten droplet during the high energy peak level. Pulsed spray metal transfer mode minimizes the spatter and eliminate the incomplete penetration. At the sametime, the efficiency of the filler metal is high and heat input is low. Therefore, pulsed spray metal transfer is often applied during the welding of HSLA base metal. Argon based shielding gas (CO_2 max:18%) which has high cost is used in pulsed spray metal transfer for the mild steels. On the other hand, initial investment cost of the system is higher than the systems which provides other 3 metal transfer modes.

The higher heat input rates associated with spray transfer can be detrimental for welding of DP sheet steels in automotive applications. Because it causes greater softening in the HAZ and weld joint quality issues such as burn through become problematic (Tiziani et al., 2011). Therefore, the short circuiting metal transfer is utilized in the welding of DP steel sheets. Because it has a lower heat input and lower weld root penetration; this helps to avoid burning through the sheet steel. The low heat input of the short cut transfer mode also helps to limit DP HAZ softening and welding distortion. Therefore in this study, short circuit transfer mode, which has lowest heat input among others was used. Also, 1,2mm plate thickness limited the maximum voltage and current to prevent burning gap.

1.4.3. The Effects of GMAW Parameters on Welding

Welding parameters define the mechanical properties, weld metal deposition rate, spatter creation, arc characteristics, weld geometry and welding quality. These main welding parameters are arc current, voltage, welding speed, wire feed rate, electrode diameter, electrode composition and shielding gas.

1.4.3.1. Electrode Diameter

If the thickness of the workpiece increases, the diameter of the electrode should be also increased for required deposition rate and penetration. 0.80, 0.90, 1.00, 1.20 and 1.60mm are the mostly used commercial diameters of the GMAW electrode. The diameter of the electrode is chosen by depending on the required heat input, deposition rate and mode of metal transfer (short cut or spray arc). While the diameter of electrode is increasing for thicker base metal welding, higher arc current should be increased to increase the electrode melting and weld deposition rates and weld penetration. Thus, electrode diameter influences the weld geometry and surface quality. On the other hand, extremely high electrode diameter can increase the martensite tempering of DP steels due to high heat input. Therefore, in this study 0.8mm wire which is minimum commercial diameter, is selected for 1.2mm thickness of base metal.

1.4.3.2. Arc Current

Electrode size, wire feed rate, mode of metal transfer, thickness of the workpiece and required heat input determine the magnitude of welding current. When the wire feed rate increases, the arc current should be increased, proportionally. Insufficient welding current can cause, lack of penetration and rough weld surface. Whereas excessive weld current can cause porosity, spatter and poor weld bead shape. In the GMAW application of automotive industry, DCEP current is mostly utilized due to its high welding penetration and weld quality with a stable electric arc and low spatter.

1.4.3.3. Arc Voltage

The mode of metal transfer, thickness of the workpiece, diameter of the electrode, desired weld geometry and shielding gas composition define the suitable welding voltage. Since the arc voltage increases, the amount of wire melt closer to the nozzle and free arc length increase. Hence, metal drops spread over a larger area and surface tension of molten metal increases and width of the welding enlarges as depicted in Figure 1.12. Therefore, the weld bead widen and flatten with increase in welding voltage. On the other hand, extremely high voltages can cause arc instability, undercut, spatter and porosity. Decrease in voltages increases the height of the weld cap and decreases the width of the weld bead.

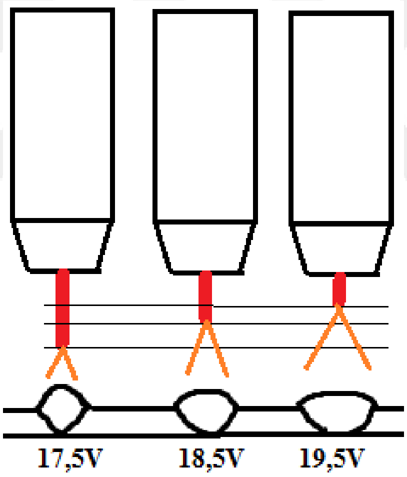

Figure 1.12. Effect of the welding voltage on free arc length and welding width

1.4.2.4. Free Wire Length

Free wire length is the distance between the last point of electrical contact on nozzle and the tip of the electrode. The increase in free wire length also increases the electrical resistance (I^2xR) where I is the arc current and R is the current resistance. In this case, electrode melting rate and heat input to workpiece increase. Thus, the martensite tempering of DP steels increase. The free wire length can be calculated 10 times of the electrode diameter for short circuiting transfer mode. Thus, in this study, 8mm free wire length was applied and fixed by using the automated GMAW system

.

1.4.2.5. Welding Speed

Increasing the welding speed increases the production rate of welded structures. On the other hand, heat input and dimensions of the weld bead decrease when the other parameters are constant. Increase in welding speed increases the welding penetration, initially. Because, the welding arc affects the base metal more directly. As the welding speed continues to increase, the weld penetration decreases and undercut can be occurred. Also, the heat input decreases and the cooling rate increases. Thus, HAZ becomes smaller and martensite tempering effect on DP steel decreases (Burns, 2009).

2. LITERATURE REVIEW

The following literature review focuses on the effects of GMAW process parameters, thermal cycles and filler metal on the high strength DP steels to provide the highest mechanical properties.

2.1. Microstructures and Mechanical Properties of Dual Phase Steels

Dual Phase steels contains a soft ferrite and hard martensite phases to obtain high strength and good formability together. Therefore, DP steels have an increasing application in automobile industry. As seen in Table 2.1, the yield strength of martensite phase is higher than ferrite phase, thus increase in the martensite phase percentage also increases the yield strength and UTS of the DP steel.

Table 2.1. Mechanical properties of the ferrite and martensite phases (Van, 2007)

PHASE	E-Modulus (GPa)	Poisson Ratio	Initial Yields Stress (MPa)
Ferrite	220	0.3	380
Martensite	195	0.3	1800

By interpreting different models, Lawson et al. (1981) suggested that, during early stages of DP steel plastic deformation and strain only accumulate in the soft ferrite matrix. After martensite decomposition starts, thus the strain accumulation becomes comparable within both phases. They defined that, the start of martensite decomposition depended on the carbon content and morphology of the martensite structure. During their tensile test, crack formation in martensite was more prevalent when the carbon content was high and the VFM of DP steel was high enough so that banding occurred.

Sodjit and Uthaisangsuk (2012) investigated the effect of VFM on tensile strength of DP600 and DP800 steels. They defined that, increase in the martensite percentage increased the tensile strength and decreased the ductility of the DP steels. Also, the martensite phases which had lower carbon content was thus weaker. The tensile strength and ductility of the dual phase steels were affected by the morphology of the martensite phase. At the sametime, the finer the grain size and the higher VFM principally increased the tensile strength of the DP steels.

Pouranvari (2010) correlated mechanical properties of DP steels with their VFM values. Figure 2.1 which shows the relation between the carbon content and VFM, was obtained as a result of the study. The carbon content of the martensite phase decreased with increase in VFM. It was defined that, the carbon content of martensite phase also determined the UTS of the martensite phase. Because, increase in the carbon content of martensite phase increased the UTS of the martensite phase.

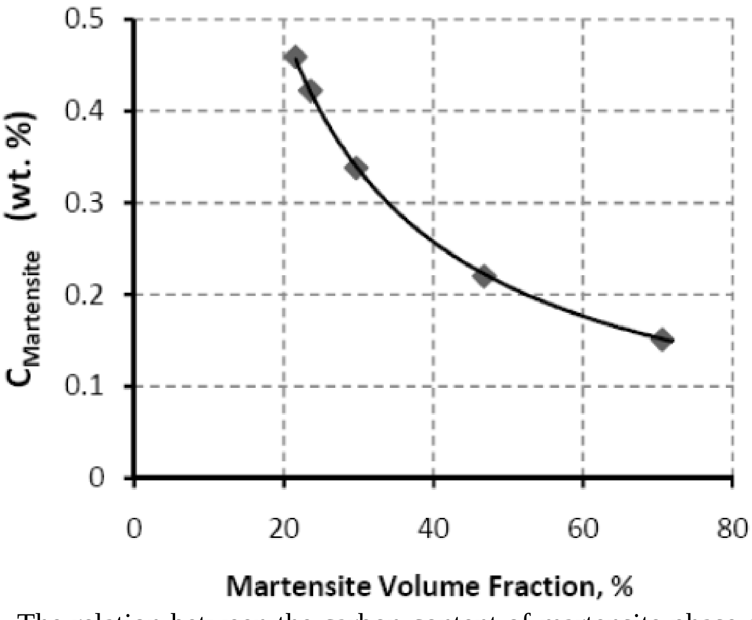

Figure 2.1. The relation between the carbon content of martensite phase and VFM (Pouranvari, 2010)

Biro (2013) investigated martensite tempering of DP steels. In the scope of this study, it was defined that increase in carbon content of martensite decreased the required welding heat input for HAZ softening. Also, increase in VFM increased the yield strength of the DP steels as shown in Figure 2.2.a. While the VFM was increasing, the UTS firstly increased and then decreased due to the decrease in carbon content of martensite (Figure 2.2.b). As a result, the highest UTS was obtained at 50% VFM.

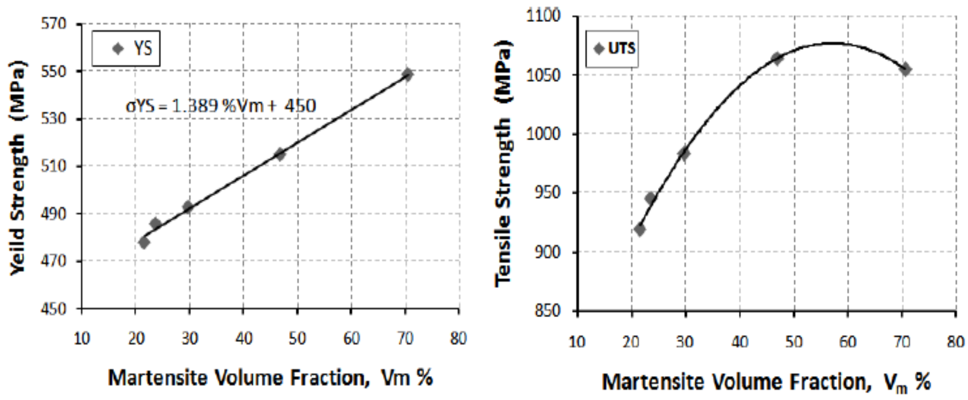

(a) **(b)**

Figure 2.2. Effect of VFM on the mechanical properties (a) yield strength (b) tensile strength (Pouranvari, 2010)

Burns (2009) reported the result of Brooks (1996) investigation. It was determined that increase in the carbon content also increases the hardness of DP steels as shown in Figure 2.3. The hardness of martensite reaches a limit at approximately 0.6%C.

Sodjit and Uthaisangsuk (2012) produced DP microstructures exhibited the VFM of 25, 35, 45, 60, and 90% with regard to the intercritical annealing temperatures of 750, 770, 790, 810, and 830°C, respectively. The obtained microstructures which had different VFM are shown in Figure 2.4. The bright gray regions are ferrite and the dark gray regions are martensite in the optical micrograph.

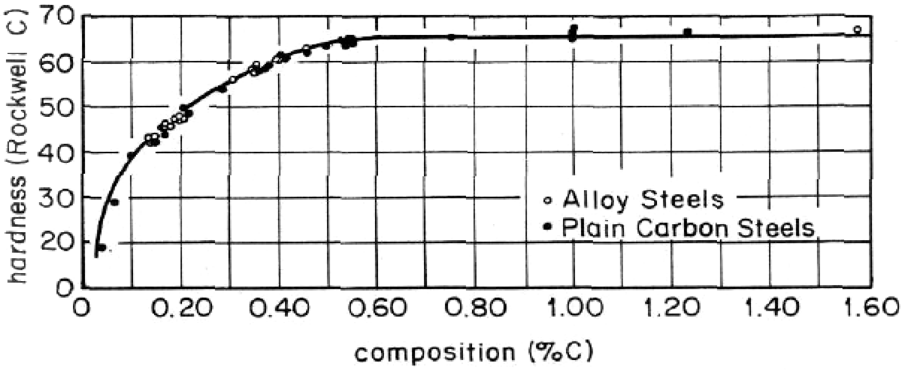

Figure 2.3. The hardness of martensite as a function of the carbon composition (Burns, 2009: taken from Brooks 1996)

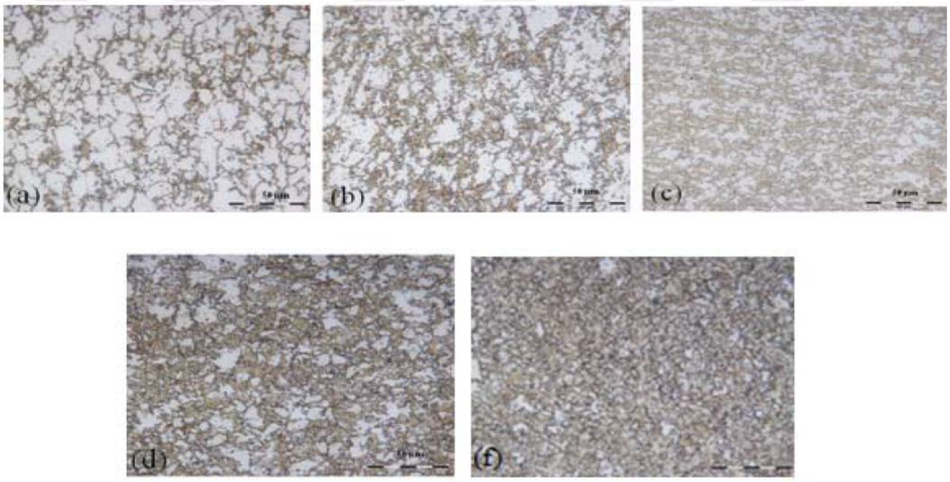

Figure 2.4. Optical micrographs (x1000) of the investigated DP steels with the VFM of (a) 25%, (b) 35%, (c) 45%, (d) 60%, and (f) 90% (Sodjit and Uthaisangsuk ,2012)

Okamoto et al. (1981) and Lawson et al.(1981), all found that UTS of DP steels were directly proportional to the VFM. They also defined that, differences in UTS of DP steel which had similar VFM were caused by their ferrite hardness. Davies (1978) went further to suggest that UTS of DP steel was dependent on the VFM and the ferrite grain size.

2.2. Mechanical Properties of Welded Dual Phase Steel

In this section, the previous studies on the factors which affect the mechanical properties and microstructure of welded DP steel, are presented.

2.2.1. The Effect of Base Metal Chemical Compositions on the Mechanical Properties of DP Steel Welding

Kapustka et al. (2008) investigated the effects of base metal chemistry, thermal cycle and filler metal composition on the microstructure and hardness of HAZ and FZ for DP steels welding. When the FZ characterization values of DP780 and DP1000 lap joints were compared, similar microstructures and hardness values were detected. Hence, it was defined that, the base metal chemical composition didn't significantly affect the mechanical properties and microstructure of FZ of two different DP steel. Because, weld metal mostly consisted of filler metal and a small amount of DP steel base metal.

Biro and Lee (2004) investigated the effect of material chemistry, weld heat input, and welding method on HAZ softening of rich and lean alloy DP600 steels. As a result of the experiments, the effect of welding heat input of different welding methods on the softening characterization of rich and lean chemistry DP600 steels were occurred on Figure 2.5. It was defined that, the rich DP600 steel chemistry had higher peak HAZ hardness, decreased the degree of softening, and increased the distance to maximum softening under the same heat input. This study had shown that, material chemistry could create martensite tempering kinetics at different locations in the HAZ; it also affected austenitization and hardenability in the hardened HAZ. The FZ had similar hardness for both lean and rich alloy DP steels, which suggested that the composition of the GMAW filler metal was the dominant factor for determining FZ hardenability. At the same time, Hernandez et al. (2011) studied the martensite tempering of DP steels. They defined that, the rich chemistry DP steel which had fine cementite and less decomposed tempered structure had also higher resistance to softening than the lean chemistry DP steel with coarser cementite.

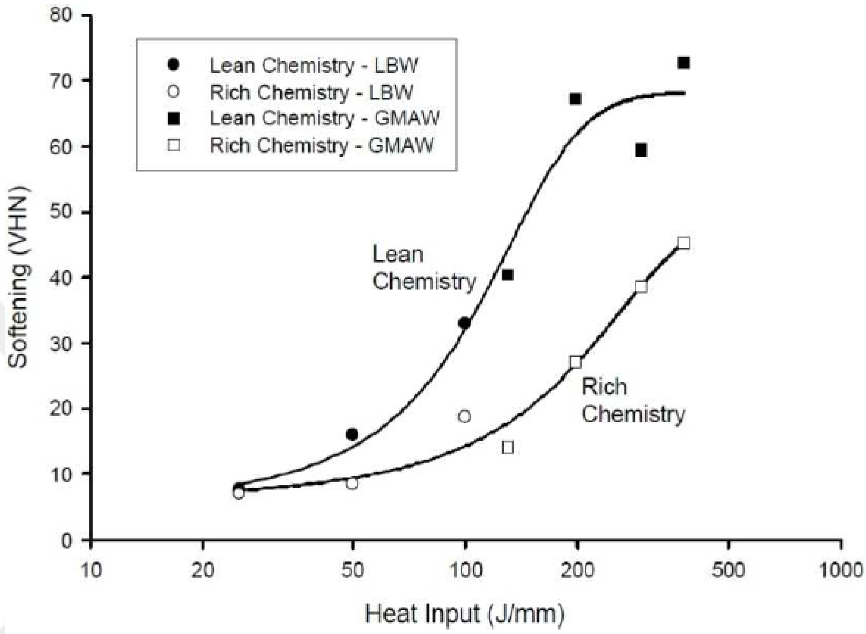

Figure 2.5. The effect of material chemistry and welding method on HAZ softening of DP600 steel (Biro and Lee, 2004)

Conrardy et al. (2006) examined the effect of GMAW heat input on 1,54mm DP780 and DP1000 plates. They found that, GG regions of both welded steel had higher hardness than their own BM hardness's. They observed more increase in degree of softening of approximately 30–40 VHN for the DP1000 steel when compared to the DP780 and attributed this to the higher percentage of martensite in the DP1000 BM. Also, Burns (2009) was found that, the GMAW welded uniaxial transverse weld tensile specimens that were 1.20 mm DP980 sheet steel were observed to fracture in the HAZ failure location through 100% of uniaxial tensile testing and had a significant decrease (~28%) in UTS when compared to the unwelded BM UTS. On the other hand, the failures in welded DP600 samples occurred in BM or HAZ by depending on the heat input.

Guo et al. (2015) studied on the microstructure and tensile test results of laser welded DP600 and DP980 steels. They identified that, because of the higher VFM on DP980 side, tempered martensite percentage and magnitude of the drop in hardness were higher at the SC region of the DP980 side than that of DP600 side.

2.2.2.The Effects Of Heat Input On The Mechanical Properties Of DP Steel

Kang et al. (2010) examined on the suitable GMAW parameters to provide sufficient weld quality of DP780 for the automobile body. They defined that when there was low heat input (high weld speed, low weld current and low voltage), lack of penetration was observed. Also, UTS decreased as welding speed increased extremely. On the other hand, burning gaps occurred at high welding heat input (low weld speed, high weld current and high voltage).

Koganti et al. (2010) analyzed the GMAW of 1,40mm DP980 to determine the effect of heat input, WFR and welding speed on the UTS by using a full factorial DOE (Design of Experiment) method. They defined that welding speed, WFR and their interaction had significant effects on the UTS of the DP980 GMAW joint. The investigated parameter combinations which had high heat input, reduced UTS of DP980 welded joint. Also, 40% drop in the hardness was detected in the SC region by comparing the BM.

Lee et al. (2014) investigated the effect of LBW, TIG welding and GMAW on microstructure and UTS of 3.2 mm DP780 whose original WFM was 39%. They defined that higher heat input weld (GMAW>TIG>LBW), also increases the size of the weld and HAZ. VFM and hardness of the FZ and HAZ increased with higher cooling rate (LBW>TIG>GMAW). Therefore, the highest decrease in strength was observed on gas metal arc welded samples. LBW and TIG welded samples had higher VFM due to the low heat input and higher cooling rate than GMAW welded samples.

Tiziani et al. (2011) studied the effect of different welding methods on DP600 steel in terms of both metallurgical and mechanical properties. They found that the widths of FZ and HAZ increased with the rise in the heat input. At the same time grain coarsening effect became more effective on mechanical properties. When heat input increased, the cooling rate decreased for a given BM thickness. The cooling rate under the same heat input could be designated with others such as material thickness; specify heat, density and thermal conductivity.

Wang et al. (2016) examined the effect of heat input on the microstructure of the laser beam welded DP1000 steel. They defined that decrease in the heat input also decreased the width of the softened region and improved the mechanical properties of the joint. During the ultimate tensile tests, the UTS of the laser beam welded DP1000 samples were measured as 86–91% of the BM. The mean hardness of the SC region was 75% of the BM. Rise in the heat input increased the grain size of the softened region and mechanical properties got worsen. On the other hand, the hardness of the GG region was 125% of the BM.

Mukherjee et al. (2011) investigated mechanical properties of gas metal arc welded DP600 steels by using the ER70S-6 as filler metal. They measured that the UTS of the welded sample was 100MPa lower than the DP600 BM.

Burns (2009) investigated the tempering effect of GMAW heat input in the SC region of 1.65 mm DP600 sheet steel. In the study, the transition of failure location from the HAZ to the BM during uniaxial transverse weld tensile was examined in detail. 100% of the samples which had low heat input, fractured in the BM. Because, the adjacent harder IC and BM regions supported the narrow SC region. This support limited diffuse necking in the SC, therefore the critical strain to induce localized necking did not occur. By limiting diffuse necking in the SC, the BM region incurred greater reduction in cross sectional area and thus the BM entered a state of higher stress than the SC and fractured once it reached the UTS of BM. On the other hand, the high heat input weld had a greater decrease in VFM and which tempering/decomposition was found further away from the Ac_1 line when compared to the low heat input weld. 100% of the high heat input welds of the same steel fractured in the HAZ. Mixed failure during tensile testing occurred within this low and high range of heat input. This showed that, a sufficiently low heat input could be achieved with GMAW welding, therefore that welds made in DP600 sheet steel attain 100% joint efficiency.

Li et al. (2014) investigated the heat input effect of TIG welding on microstructure and mechanical properties of DP780 steel which had 270HV hardness. They defined that the hardness of the SC region was measured as 220HV due to the martensite tempering. Also, UTS of the joint was measured as 94.6% of the BM. They also inspected the microstructure of SC region where the hardness was minimum by using SEM. They showed the martensite, ferrite and tempered martensite phases in Figure 2.6. Ashrafi et al. (2016) also examined the effect of TIG welding heat input on the DP700 steel. They defined that, UTS of the sample was 81% of the BM and it fractured at the SC region, during the tensile test.

Ramazani et al. (2012) investigated the martensite tempering of gas metal arc welded DP600 steel. They observed that martensite and ferrite phases transformed into austenite phase. After nucleation, the austenite grains grew. In the cooling cycle, the austenite phase transformed into bainite phase or bainite and ferrite phases by depending on the welding heat input.

Biro and Lee (2004) found that the degree of softening increased, distance to maximum softening increased and so hardness decreased, as weld heat input was increased. Because, higher heat input increased the time for carbon diffusion and the width of the softened zone increased as a larger portion of the steel was elevated to a temperature that was sufficient for carbon diffusion to occur. At the sametime, the type of GMAW metal transfer mode did not appear to have an effect on welded DP steel HAZ hardness.

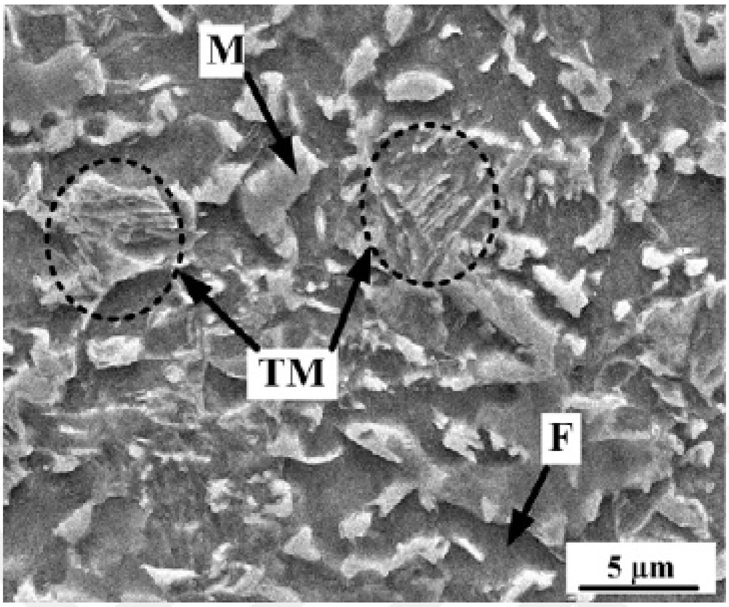

Figure 2.6. The SC region microstructure of TIG welded DP780 steel (Lee et al., 2014)

Rocha et al. (2015) studied on the influence of heat input on mechanical and metallurgical properties of butt welded joints of 1.8 mm DP1000 sheets. Volume fraction of the phases were measured following as 51% of ferrite and 49% martensite (error of ± 4% for both phases). They also measured the weld metal cross-section areas of the joints and the average results plotted as a function of heat input in Figure 2.7. They defined that, the highest values of hardness were developed in the GR region and the lowest occur in the SC region. In every application of DP1000 welding, weld metal minimum hardness was always greater than the minimum value found in the SC regions. In all uniaxial tensile tests, in all conditions, fractures of the samples always occurred in SC region where hardness values were very low and decomposition of martensite was quite severe. As heat input was increased, elongation also increased almost in a linear fashion. They suggested that, this could be related to the increase of new ferrite due to martensite tempering in HAZ. In addition, they defined that, austenite recrystallization and grain refining occurred in IC region.

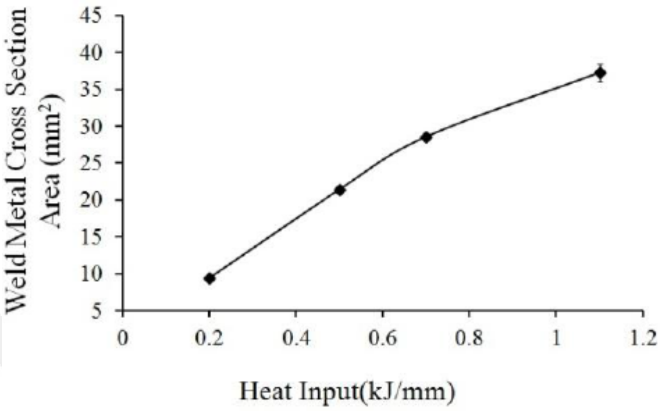

Figure 2.7. The relation between the heat input and welding cross-section of 1.80mm DP1000 steel (Rocha et al., 2015)

Aghakhani et al. (2011)studied on the effect of heat input on the GMAW penetration. They defined that, increasing the welding voltage and WFR increased the heat input and thus weld penetration. On the other hand, increasing the welding speed or nozzle-to-plate distance decreased the heat input to the workpiece and decreased the penetration. In addition, the WFR was defined as the most significant welding parameter for welding penetration.

Na et al. (2011) examined the interaction between welding heat input and bead geometry of fillet GMAW to provide the optimal bead geometry. They found that increase in welding current also increased the weld bead dimensions. The bead height and reinforcement height decreased with welding speed increase.

Elliott (2014) examined lap welding of DP600 steels for improved weld quality and increased fatigue life. In this study, it was defined that, decreasing WFR, increasing torch angle or increasing nozzle-to-plate distance decreased the weld penetration. On the other hand, fatigue life of lap welded joint increased by decreasing WFR, decreasing welding speed, increasing nozzle-to-plate distance.

Sudersanan and Kempaiah (2012) studied the effect of VFM in the DP steel on the residual stress introduced after welding. The results showed no significant influence of VFM on the residual stress. The finite element method (FEM) simulation and consequent thermomechanical analysis carried out had shown the residual stress increased with heat input. It was also observed that the residual stress considerably decreased with travel speed.

2.2.3. Effect of Cooling Rate on HAZ Softening of DP Steels

The cooling rate of the metal is related with the thermal conductivity and the thickness of the BM. The higher thermal conductivity metals have higher welding cooling rate and smaller HAZ (Chu, 2007).

Burns (2009) defined that the welding HAZ of 1.65 mm DP600 sheet steel consistently had an increase in hardness of the IC, GR, GG, and FZ regions during the cooling. The increase in hardness of IC microstructural region was consistently associated with an increase in VFM of this region that was caused by the formation of renucleated martensite during the cooling cycle. The renucleated martensite had formed when that region of microstructure had been elevated to temperatures above the Ac_1 line and below the Ac_3 line.

Conrardy et al. (2006) analyzed cooling rate of GMAW process to observe different effects on HAZ softening of DP steels. They established a high cooling rate by making butt welds with GMAW welding short circuit transfer and a copper backing. On the other hand, they obtained a low cooling rate by using a GMAW pulsed spray transfer without a copper backing bar. They determined that a lower cooling rate produced a wider softened HAZ region, lower peak HAZ hardness and slightly increased the degree of softening for both DP780 and DP1000. They attributed higher peak hardness to a higher VFM for welds made with higher cooling rate. The peak HAZ hardness was 260 VHN for low cooling rate and the peak HAZ hardness was 370 VHN for high cooling rate.

Ghosh (1990) investigated the effect of different welding cooling rates with the normal machine cooling and forced air cooling on the microstructure changes in the HAZ of 3.7 mm Mn-C-Mo DP steel. The original hardness of the BM was measured as 252 HV. As a summary of the study results, the softest region in the HAZ occurred approximately 6 – 7 mm from the weld centerline. After welding with forced water cooling the softened zone hardness was 245 HV, and after welding without forced cooling the softened zone hardness was 220 HV. Therefore, increase in the cooling rate decreased the martensite tempering and HAZ softening.

Salamci et al. (2011) examined the influence of cooling rate on intercritical annealed DP steel. Therefore, the annealed samples were cooled in water, oil and furnace. As a result, the highest VFM was observed in the water cooled sample and the lowest VFM was observed in the furnace cooled sample. Hence, they defined that, decrease in cooling rate decreased the VFM.

Kapustka et al. (2008) examined the effect of cooling rate on mechanical properties of welded DP780 steel. They introduced that, higher cooling rates decreased the width of the HAZ and increased the peak hardness. At high cooling rate, the peak hardness of HAZ of DP780 was approximately 80% higher than the BM. On the other hand, it was 25% higher than the BM at low cooling rate. Because decrease in cooling rate increased the martensite tempering and softening effects. Therefore the hardness of the low and high cooling rated DP780 welds were measured as 260HV and 375HV respectively. Also, they investigated the effect of cooling rate on static and dynamic tensile strength. During static tensile testing, the butt joint efficiencies ($UTS_{weld\ joint} \div UTS_{BM}$) of DP780 plate were higher than 90% at high cooling rate, but the joint efficiencies were between 85% and 90% at low cooling rate. On the other hand, during dynamic tensile testing, there was not a distinguishable effect on the UTS of the DP780 butt joint welds.

Biro et al.(2008) found that increase in heat input decreased the cooling rate and thus UTS of the welded DP780 steel during the analyzing the FZ/HAZ boundary fractures. Because higher martensite tempering percentage caused a softer microstructure. They also detected that, BM failures occurred at the high cooling rates of low BM hardness DP steels and HAZ failures occurred at the low cooling rates of high BM hardness DP steels.

2.2.4. Effect of Filler Metal on Mechanical Properties Of DP Steels

The UTS of the filler metal in GMAW has a significant effect on the welded HSLA steel structures. The filler metal can be classified as undermatched, matched and overmatched. If the UTS of the filler metal is lower than the BM, it is defined as undermatched. If the UTS are the same, it is matched and overmatched filler metal has higher UTS than the BM. This part of the literature review focuses on that, overmatched filler metal is really needed or not for DP steels.

The effect of GMAW filler metal on the efficiency of the welded joint was studied by Hsu et al. (2004). They made butt welds with 4 mm thick DP600 steel using ER70S-6 (UTS: 500MPa) or ER100S-G (UTS:760MPa) filler metal and Ar-CO_2 blends of shielding gas with a backing bar. They found that, the ER70S-6 filler metal achieved similar hardness in the weld FZ when compared to the DP600 BM hardness. ER100S-G filler metal did not increase the transverse weld tensile strength of GMAW made in DP600 sheet. Because, the weld joint efficiency was based on the weakest point in the HAZ which was the softened zone (SC region).

Rocha et al. (2015) compared the effects of ER80S-G (UTS: 550MPa) and ER120S-G (UTS: 940MPa) filler metals on microhardness distribution of DP1000 welding at the same heat inputs. As seen in Figure 2.8, similar hardness values were measured on GG regions and minimal HAZ's within themselves for both low and high grade filler metal at the same heat input values; although weldings with stronger filler metals always had weld metals with higher microhardness. Also, all tensile test specimens were fractured from the SC region. As a result of the study, it was defined that UTS of DP1000 weld joint could not be improved by using higher strength filler metal, since fracture always occurred at the HAZ.

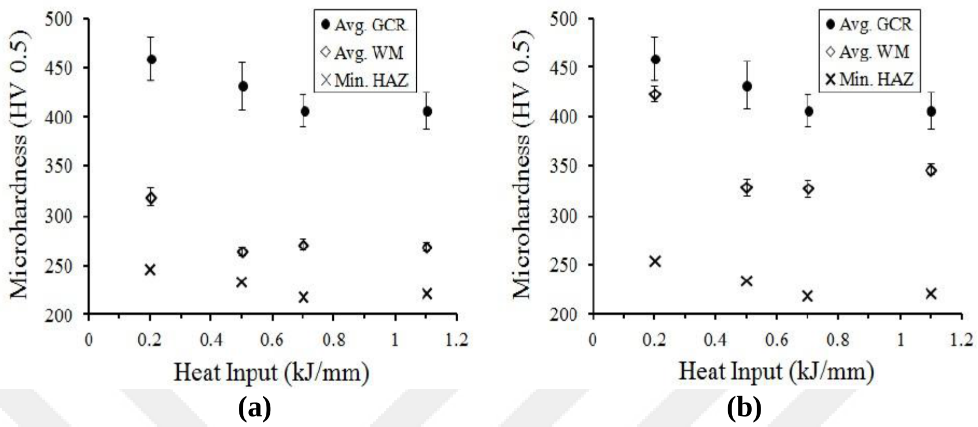

Figure 2.8. Minimum microhardness in HAZ and average microhardness both weld metal and GG region as function of heat input (a) Weldments with AWS ER80S-G and (b) Weldments with AWS ER120S-G (Rocha et al., 2015)

Conrardy et al. (2006) determined that, an ER70S-6 filler metal was sufficient for a DP780 weld, but that higher grade (ER100S-G) filler was also examined for tests on a DP1000 weld. The ER100S-G filler did not have any discernible effect on the UTS of the DP780 welds. On the other hand, by using an ER70S-6, they observed similar hardness (~260 VHN) and microstructure in the weld FZ for DP780 and DP1000. They expected that this might have been too soft for the DP1000 sheet steel. By switching to the higher grade ER100S-G , the weld metal hardness increased (~300 VHN) and the microstructure was observed to have greater amounts of harder constituents (bainite and martensite). As a result, they defined that the strength grade of the filler metal did not appear to be a significant factor for determining joint UTS, because the welds fracture in either the softened HAZ for DP1000.

Kapustka et al. (2008) examined the effect of ER70S-6 filler metal characteristics on the DP780 welding. The minimum hardness was defined in the SC region of HAZ. This softening was caused by the martensite tempering. The SC region limited the UTS of the DP780 joint. Therefore, it was defined that, higher strength consumable could not increase the static or dynamic tensile strength of the joint.

Rodrigues et al. (2004) analyzed the numerical model of the relation between the HAZ mechanism and the fracture crack formation. They identified that, the SC region defined the UTS of the welded joint for matched and undermatched filler metal selection. Also, the width of HAZ defined the efficiency of the DP steel welding. If the width of the HAZ was less than 1/3 of the sheet thickness, the loss of the strength was less than 10% for undermatched filler metal. As a result, the UTS of the DP welding decreased with increase in HAZ width.

3. MATERIALS AND METHODS

The goal of this study is optimization of GMAW process parameters for improving mechanical properties of DP1000 steel joint. For this aim, the effects of GMAW welding parameters on mechanical properties and weld quality of 1.2mm DP1000 plates were investigated. Welding voltage, travel speed, wire feed rate were selected as experimental parameters, and ER70S-6 wire electrode was used as filler metal. An automated welding station was designed, built and used to form consistent linear welds at constant welding speeds. Visual inspections and microstructural analyses, Vickers hardness distribution and tensile tests were applied in order to define the optimum parameters, which provide the highest UTS with acceptable weld quality according to EN ISO 3834. Moreover, the relations among the microstructural changes, hardness distribution and UTS were presented. Minitab-17 statistical analysis software was used to design the generative full factorial experiment and analyze test results.

All criteria's were defined to create the acceptable weld beat geometry. All used equipments for weld preparation were listed and respective setup procedures were given. All procedures for weld testing are explained with a brief description along with their intended purpose.

3.1. Experimental Materials

In this chapter, an outline of DP1000 basemetal, GMAW welding consumable, shielding gas and experimental apparatus that were utilized in this study, are presented.

3.1.1. DP1000 Base Metal

DP1000 steels have the highest UTS and weight reduction capacity for vehicle structures among all commercial DP steels. On the other hand, they has the highest precision for welding heat input. Their joint efficiency is not retained by

100% after welding process. Therefore, the study mainly focused on the metallurgical and mechanical effects of arc voltage, welding speed, wire feed rate and arc current to increase the joint efficiency of DP1000 welding.

The commercial name of base metal is Docol1000, and it is produced by SSAB Steel Company. The DP1000 steel has been produced by using successive operations, such as continuous casting, hot-rolling the billets down to the desired sheet thickness and then intercritically annealed with a rapid quench to form pockets of hardened martensite in a ferrite grain matrix. The volume fraction of martensite is increased for the higher strength grades by holding the sheet steel at a higher temperature during the intercritical annealing step.

In this study, DP1000 steel with a thickness of 1,20mm was used. The mechanical properties and chemical composition of DP1000 steel are shown in Table 3.1 and Table 3.2, respectively. The carbon equivalent (CE) value was calculated as 0,4% using equation-3.1, which resulted lower than 0,5% for current experimental conditions, hence it was suitable for welding.

Table 3.1. Mechanical properties of DP1000 steel (www.ssab.com, 2009)

Base Metal	Yield Strength (N/mm^2)	Tensile Strength (N/mm^2)	% Elongation	Hardness (HV0.5)
DP1000	700	1000	7	320

Table 3.2. Chemical composition of DP1000 steel (www.ssab.com, 2009)

BASE METAL	C%	Si%	Mn%	P%	S%	Al%	Nb%
DP1000	0.15	0.5	1.5	0.01	0.02	0.04	0.015

$$CE = C + Mn/6 + (Cr + Mo + V)/5 + (Cu + Ni)/15 \quad (3.1)$$

$$=0.15+1.5/6$$

$$=0.4\ \%$$

The dimensions of the DP1000 plates and welding design were defined depending on TS 6868-1 EN 287-1 standard. Therefore, 300x150x1.2mm DP1000 steel plates were used for butt welding as shown in Figure 3.1.

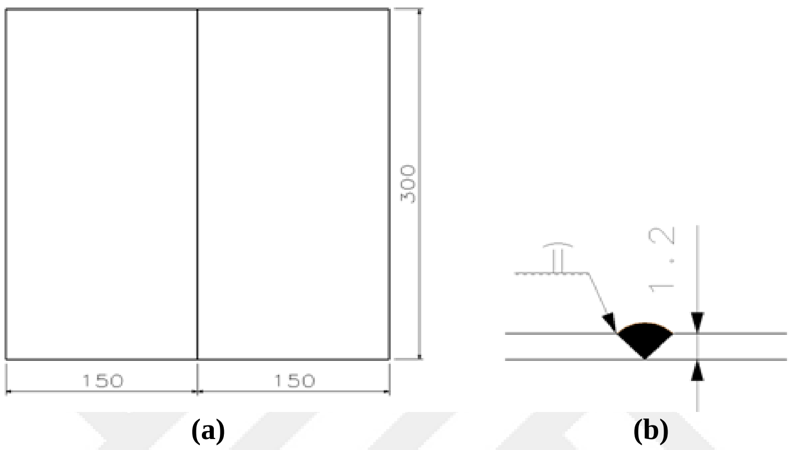

Figure 3.1. The welding design (a) Dimensions of welding samples (b) Cross-section of welding

3.1.2. Welding Filler Metal

The filler metal was selected as ER70S-6 in AWS 5.18 standard (G3Si1 in TS EN ISO 14341-A). The SG2 is the commercial name of the welding wire, which is produced by Gedik Welding Company. The diameter of welding wire was selected as 0.80mm due to the thin workpiece. Because, the required current to melt the wire also increases with increase in the wire diameter. In the present case, heat input could increase dramatically. The mechanical properties and chemical composition of the filler metal are shown in Table 3.3 and Table 3.4, respectively.

Table 3.3. The mechanical properties of ER70S-6(www.gedikkaynak.com.tr, 2016)

Filler Metal	Yield Strength (N/mm^2)	Tensile Strength (N/mm^2)	Impact Toughness (ISO-V/-30^oC)	Min. % Elongation
ER70S-6	420	500-640	47J	22

Table 3.4. The chemical composition of ER70S-6 (www.gedikkaynak.com.tr,2016)

Filler Metal	C	Si	Mn	Fe
ER70S-6	0,08	0,85	1,5	Rest

3.1.3. Welding Shielding Gas

During the welding process, 100% CO_2 shielding gas was used, which is presented as C in EN 439 norm. Low heat input and high penetration rate were aimed by shortcut current transfer using %100 CO_2. Also, its low cost is an advantage for high manufacturing rates. The shielding gas flow rate was defined as 8.00 L/min, which is calculated as 10 times of wire electrode diameter.

3.1.4. Experimental Apparatus

In this study, GMAW method was used to make weld deposits. An automated GMAW system was designed and built to provide consistent linear welds and to eliminate the welding defects, which can be caused by the welder. In this way, free wire length was kept constant. The welding automation system, whose components are shown in Figure 3.2.

Frounius Transpuls Synergic 2700 welding power supply, which had 270A current capacity was employed for welding applications. DCEP polarity was utilized for better penetration, arc stability, higher electrode melting rates and lower heat input to workpiece. Short circuit was also applied to further reduce the heat input transferred to workpiece. The welding current start and stop functions were controlled with an adapted on/off switch panel.

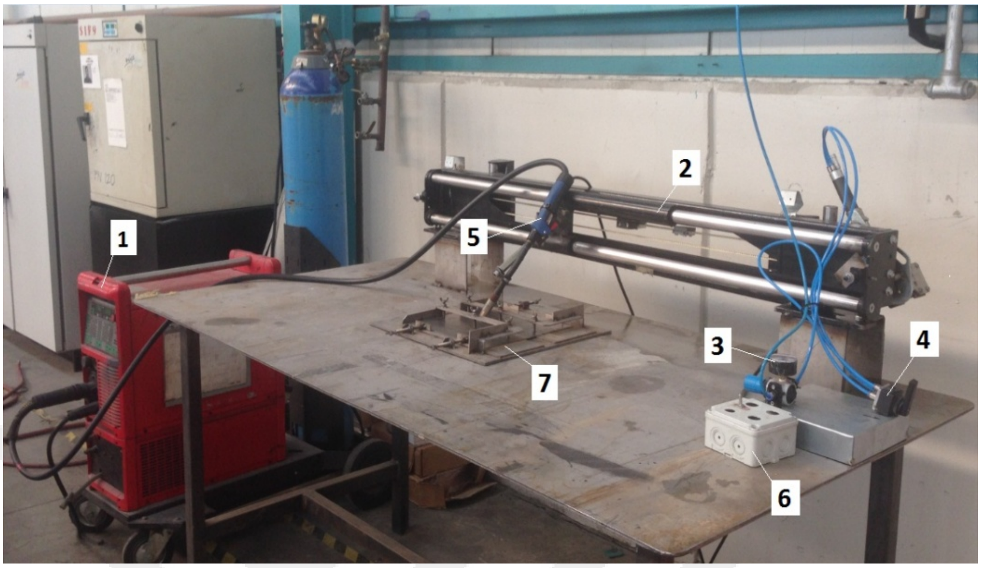

Figure 3.2. Components of the automated welding system used for experimental work. (1) Frounius Transpuls Synergic 2700 Welding Power Supply, (2) Pneumatic Welding Automation Mechanism, (3) Pneumatic Valve To Control Welding Speed, (4) Pneumatic Valve To Control Welding Start/Stop and Direction, (5) GMAW Torch, (6) Welding Arc Start/Stop Control Panel and (7) Welding Fixture

The automation system was propelled using a pneumatic activation system. The welding travel speed and direction were controlled by valve-3 and valve-4 respectively which are shown in Figure 3.2. The welding distortion could be easily occurred on thin plates. In order to prevent lost welding designs due to the welding deformation, a workpiece clamping fixture shown in Figure 3.3 was designed and produced.

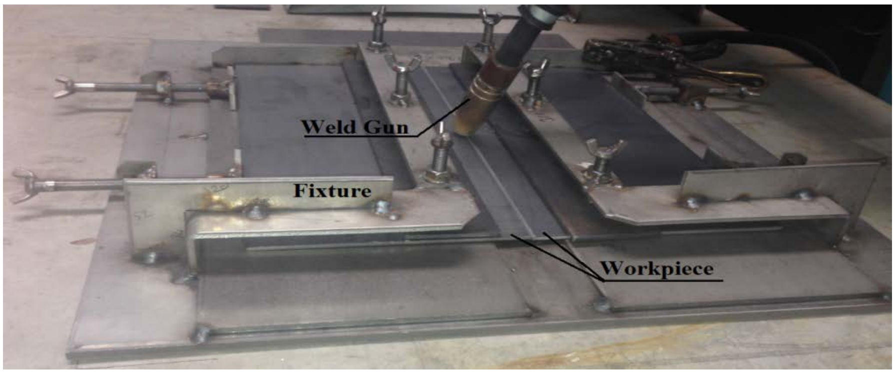

Figure 3.3. The fixture system for welding process

Generally, the distance between workpiece and tip of welding torch is calculated as 10 times of welding wire diameter for short circuit arc applications. The used wire diameter was 0,8mm, thus the distance was calculated as 8mm for current test conditions. There was a 35^{o} pulling angle between the welding torch and workpiece as shown in Figure 3.4.

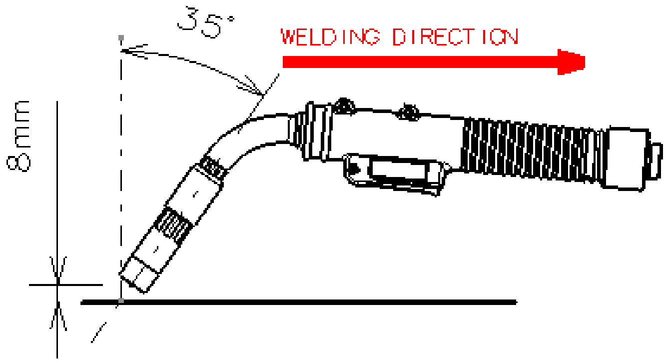

Figure 3.4. The welding direction and pulling angle between workpiece and welding torch

3.2. Experimental Methods

In this section, the test methods, which were used to define the ideal welding parameters to provide the possible highest UTS of gas metal arc welded

DP1000 steel are explained in detail. Also, the related clauses of EN ISO 3834, which were used for visual inspection of the welding are defined.

3.2.1. Heat Input Calculation and Control

The heat input of GMAW process is the amount of heat supplied to the workpiece during the welding. Welding voltage, current and travel speed define the heat input, which mostly affect the microstructural changes and UTS of the DP1000 welding. Extreme heat input causes softening at HAZ and insufficient heat input brings lack of welding penetration. Therefore, effects of heat input on UTS and weld quality were investigated to define the optimum welding parameters for DP1000 steel.

During GMAW process, voltage stays constant, because GMAW has a horizontal characteristic current. If the free wire length changes as uncontrolled manner, the current also changes as shown in Figure 3.5. For example, decrease in free wire length (arc length increases) also increases welding current and heat input produced during welding process. Therefore, the welding automation system and fixtures were installed with dimensional precision to maintain constant free wire length for steady current and heat input.

The equation-3.2 and The equation-3.3 were used to calculate the generated energy by the power source (E) (www.ssab.com, 2009);

$$E = \frac{UxIx60}{Vx1000} kj/mm \tag{3.2}$$

where U = Voltage (V), I = Current (A) and V = Welding Speed (mm/min).

In order to calculate the heat input more accurately, the arc efficiency (η), which is 0,8 for present GMAW welding process was taken into account. Finally, the following formula is used for calculating the welding heat input;

$$HI = \eta \text{ x E} \tag{3.3}$$

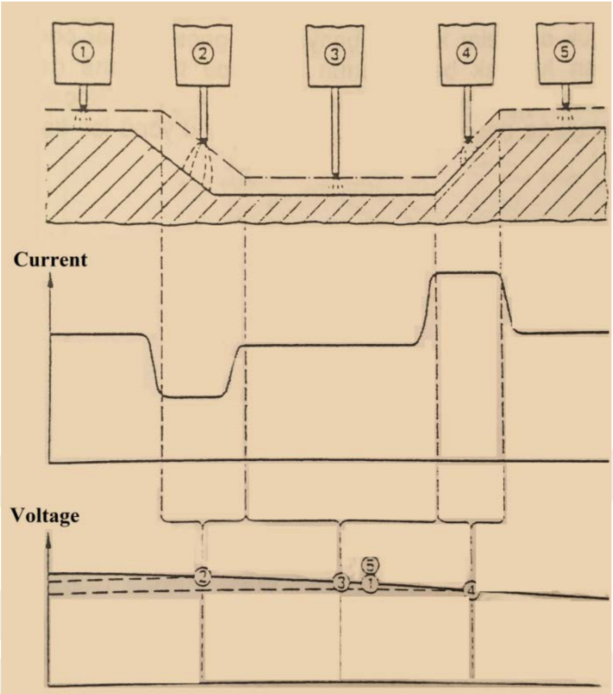

.
Figure 3.5. The internal adjustment mechanism of arc current (Tansal, 2008)

3.2.2. Full Factorial Design With Minitab-17

During the experimental studies, DOE statistical method is applied to maximize the knowledge gained from the experimental data. In this way the experiments are designed and analyzed statistically. Also redundant observations are eliminated, thus waste of time and sources are prevented.

In this study, DOE was used to optimize the welding design and to analyze the effects of multiple factors (arc voltage, welding travel speed, arc current and wire feed rate) on the mechanical properties, microstructural characteristics and quality of DP1000 welding. The influence of individual factors on the mechanical properties were studied to determine which factor had more influence, which one had less. Thus, it was utilized to figure out the factor with tightest tolerance and tolerance which should be relaxed. Therefore, DOE statistical method was especially useful in GMAW welding**.**

The experiment was designed as a full factorial design method by using Minitab-17 software. Therefore, responses were measured at all combinations of the levels of experimental factors. The combinations of factor levels represented the conditions at which responses were measured. When the experiments were completed, the responses were analyzed and main effects of each factor were plotted by the software. At the same time, the interactions between the factor couples were also defined and plotted.

While designing the full factorial experiment, the following steps were applied;

1. Before using Minitab-17, pre-experimental studies were completed. In this case, the welding voltage, welding speed and wire feed rates were applied and analyzed within wide ranges. Then, the welds were visually inspected and mechanically tested to define the suitable lowest and highest levels of the parameters. As a result, 3 levels were defined for each factors as shown in Table 3.6.

Table 3.5. The welding parameters and their levels

VOLTAGE (V)	WELDING SPEED (mm/min)	WIRE FEED RATE (m/min)
17.5	260	2.2
18.5	320	2.4
19.5	380	2.6

By using clamp meter, the applied mean welding currents were measured on the torch cables for each wire feed rates. The measurements were listed in Table 3.7 and used to calculate the heat input for each welding parameter combinations.

Table 3.6. Wire feed rates and related welding currents

WIRE FEED RATE (m/min)	CURRENT (A)
2.2	45
2.4	53
2.6	60

2. By Minitab-17, a full factorial design was created. Each combination was replicated two times, hence 54 (3x3x3x2) runs were obtained. The experimental design is shown in Table 3.8.
3. The experimental design was applied. The responses were recorded and then loaded into Minitab-17 software.
4. "Analyze Factorial Design" function was utilized to analyze the responses.
5. Main effect and interaction plots were displayed to evaluate the design.
6. In order to optimize responses, "Response Optimizer Function" was employed to obtain a numerical and graphical analysis.

3.2.3. Experimental Studies

In this study, visual and microstructural inspections, Vicker's hardness and tensile tests were applied to reveal the influences of arc voltage, welding speed and arc wire feed rate (current) on mechanical properties and quality of DP1000 GMAW process. Thus, the applied procedures and aim of the inspections and mechanical tests are explained.

Table 3.7. Experimental design of DP1000 GMAW

RUN	VOLTAGE (V)	WELDING SPEED (mm/min)	WIRE FEED RATE (m/min)	CURRENT (A)	HEAT INPUT (KJ/mm)
1	18,5	380	2,6	60	0,14
2	17,5	320	2,2	45	0,118
3	17,5	260	2,2	45	0,145
4	19,5	320	2,6	60	0,176
5	18,5	320	2,6	60	0,167
6	18,5	380	2,2	45	0,105
7	18,5	260	2,6	60	0,205
8	19,5	320	2,4	53	0,155
9	17,5	320	2,4	53	0,139
10	19,5	260	2,2	45	0,162
11	18,5	260	2,4	53	0,181
12	19,5	260	2,6	60	0,216
13	17,5	260	2,4	53	0,171
14	18,5	260	2,2	45	0,154
15	17,5	320	2,6	60	0,158
16	17,5	260	2,6	60	0,194
17	19,5	260	2,4	53	0,191
18	19,5	380	2,4	53	0,131
19	18,5	380	2,4	53	0,124
20	18,5	320	2,2	45	0,125
21	17,5	380	2,6	60	0,133
22	17,5	380	2,4	53	0,117
23	17,5	380	2,2	45	0,099
24	19,5	320	2,2	45	0,132
25	18,5	320	2,4	53	0,147
26	19,5	380	2,2	45	0,111
27	19,5	380	2,6	60	0,148
28	18,5	380	2,6	60	0,14
29	17,5	320	2,2	45	0,118
30	17,5	260	2,2	45	0,145
31	19,5	320	2,6	60	0,176
32	18,5	320	2,6	60	0,167
33	18,5	380	2,2	45	0,105
34	18,5	260	2,6	60	0,205
35	19,5	320	2,4	53	0,155
36	17,5	320	2,4	53	0,139
37	19,5	260	2,2	45	0,162
38	18,5	260	2,4	53	0,181
39	19,5	260	2,6	60	0,216
40	17,5	260	2,4	53	0,171
41	18,5	260	2,2	45	0,154
42	17,5	320	2,6	60	0,158
43	17,5	260	2,6	60	0,194
44	19,5	260	2,4	53	0,191
45	19,5	380	2,4	53	0,131
46	18,5	380	2,4	53	0,124
47	18,5	320	2,2	45	0,125
48	17,5	380	2,6	60	0,133
49	17,5	380	2,4	53	0,117
50	17,5	380	2,2	45	0,099
51	19,5	320	2,2	45	0,132
52	18,5	320	2,4	53	0,147
53	19,5	380	2,2	45	0,111
54	19,5	380	2,6	60	0,148

3.2.3.1. Sample Preparation for Visual Inspection, Microstructural Inspection and Vickers Hardness Measurement

The welding cross-sections were prepared carefully before the visual inspections and hardness measurements. For this purpose, a circular saw, Struers Citopress-1 bakelite forming device and an automated grinding device were used (Figure 3.6). After cutting the welding sections precisely, the following steps were pursued to improve the surface quality.

1. First of all, the sectioned weld specimens were mounted in black bakelite.

(a) **(b)** **(c)**

Figure 3.6. The devices which were used to prepare the samples (a) Circular saw, (b) Bakelite forming device and (c) Automated grinding machine

2. The automated grinding machine was utilized to extinguish roughness of the surface. The weld specimens were grinded until completely planar using 180 grit at force level-3 of the machine and then with 320, 600, 800, 1200 coarse grits, and finally 1200 fine grit at force level-5 for 1 minute. The cleaning operation was performed between the 800 to 1200 coarse grit paper step and between the 1200 coarse to 1200 fine grit step. The samples were cleaned by flushing with methanol and immediately after dried with an air blower. All steps were performed at 300 rpm and each the specimen

was positioned at grinding direction, which was perpendicular to the previous step.

3. Before the microstructural inspection, the samples were subjected to the bath containing 2% nital etchant for 6 to 8 seconds according to TS CR 12361 norm; then flushed with water following with cleaning using methanol and finally air blown was used for drying operation.

3.2.3.2. Visual Inspection (EN ISO 3834)

Visual inspection applied for performing comparison among the samples to reveal the effects of different welding parameters on bead geometry and weld quality of 1.20 mm thick DP1000 steel plates. The Level-C of EN ISO 3834, which has medium tolerance, was selected as a guidance standard on quality levels of the butt welding for imperfections. The related imperfection limits are listed in Table 3.8.

3.2.3.3. Microstructure Inspection (TS EN 1321)

The volume fraction of martensite islands within the ferrite matrix and the ferrite grain size are the main factors that affect the DP1000 steel strength. When DP1000 steels are welded, VFM decreases and the ferrite grain size increases at released welding regions depending on heat inputs. This causes decrease in the hardness and UTS of the DP1000 joints (Rocha et al., 2015).

In this study, the microstructures of FZ, GG region, GR region, IC region, SC region and BM were inspected according to TS EN 1321. Especially, SC regions were investigated more precisely. Because, as defined in literature review section, the lowest hardness and local UTS were measured in the SC regions immediately adjacent to the Ac_1 line (Burns, 2009).

Table 3.8. Guidance on quality levels of butt welding for imperfections (EN ISO 3834)

IMPERFECTION DESIGNATION	**EN ISO 3834 REFERENCE**	**REMARKS**	**Limits For Imperfections For Quality Level-C**
LACK OF PENETRATION	402	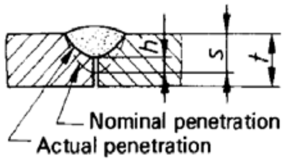	h< 0,1 s, max. 1,5 mm
UNDER CUT	5011	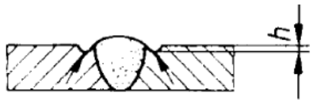	h < 1,0 mm
EXCESS WELD METAL	502	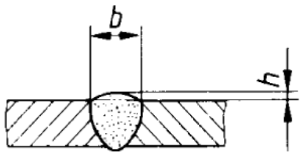	h < 1 mm +0,15b, max. 7 mm
EXCESS PENETRATION	504	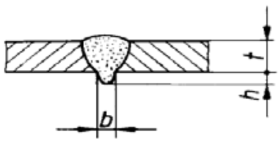	h< 1 mm + 0,6b, max. 4 mm
OVERLAP	506	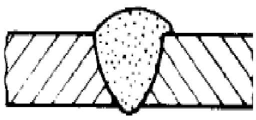	Not permitted
ROOT CONCAVITY	515	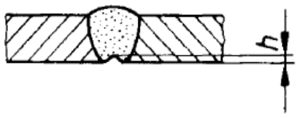	h < 1 mm
LINEAR MISALIGNMENT	507	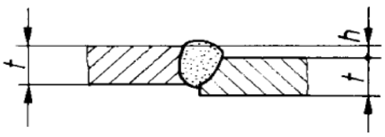	h< 0,15 t, max. 4 mm

The microstructure of all welded samples were correlated with tensile strength measurements and hardness distributions of the same samples. At the same time, the shape and orientation of the martensite islands can also affect the UTS of the DP1000 steel and can cause the steel to exhibit anisotropic mechanical properties. The elongated bands of martensite can be formed during processing, which is known as banding. The banding formation at HAZ increases the hardness. Therefore, it was inspected precisely on the GG and GR regions of DP1000 welding.

The percentages of martensite, ferrite phases and martensite banding on the samples were inspected using Olympus PME-3 scientific microscope equipped with a 500x magnification objective by visualizing microstructure of the welding zone. Images captured using CMOS-5 camera were sent to “My Camera” software for the analysis of welding microstructure. The devices are shown in Figure 3.7.

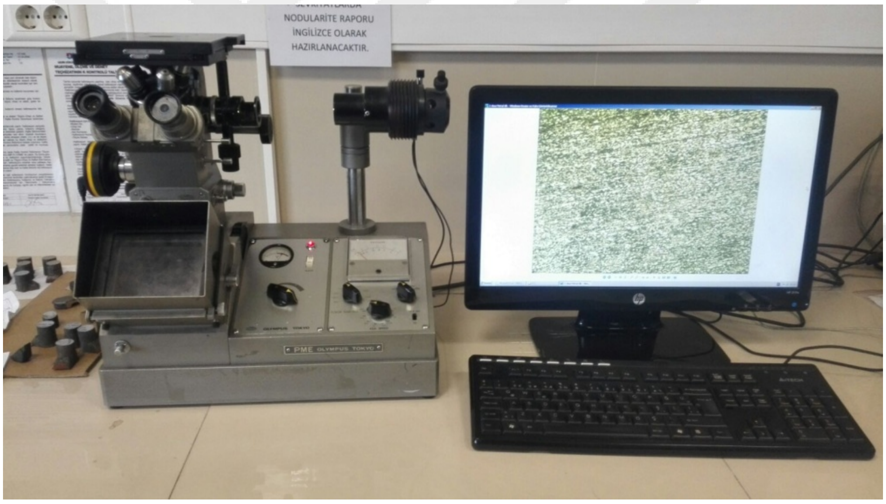

Figure 3.7. Olympus PME-3 scientific microscope and CMOS-5 camera which were used for microstructure analyzing of DP1000 welding

In this study, the microstructures of the samples under the conditions of 23rd, 9th, 11th and 12th Runs, which provided 0.10 kj/mm(minimum), 0.14 kj/mm, 0.18 kj/mm and 0.22 kj/mm (maximum) heat inputs respectively were analyzed. The martensite, ferrite percentages and grain sizes, shapes of each welding regions were revealed with the UTS, fraction regions and hardness distributions.

3.2.3.4. Vickers Hardness Distribution Measurement (TS EN ISO 6507-1)

Vickers hardness is a mechanical property used to quantify the relative effects of weld heat input and each welding factor on the DP1000 sheet steel microstructure. The measurements were implemented according to TS EN ISO 6507-1 norm. A 200kg load was applied for 15 seconds in this study.

For the Vickers hardness profiles, it is important that the single line of indentations is made in a similar location on each weld cross-section. Therefore, the indents were performed on a linear line with interval of 0.75 mm from right base metal to left base metal as shown in Figure 3.8.

Vickers hardness profiles the samples under the conditions of 23rd, 9th, 11th and 12thRuns were examined to observe the relative hardness of each weld in HAZs. In this test, one cross-section of the weld was used in Vickers hardness profiles for each weld. Once hardness values were measured, then they were evaluated together with the microstructure to determine why different weld strengths were occurred during uniaxial tensile testing.

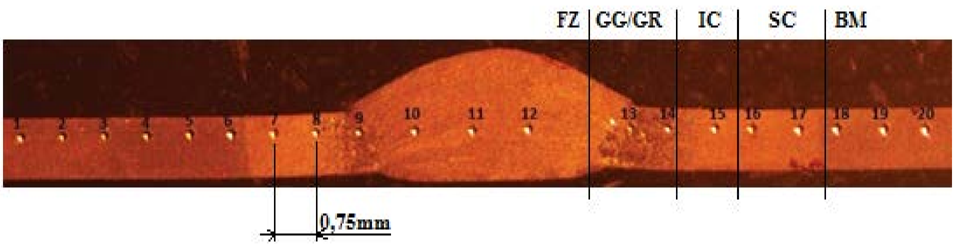

Figure 3.8. The application of Vickers hardness indentations on DP1000 welding

3.2.3.5. Ultimate Tensile Tests (TS 287 EN 895)

Ultimate tensile strength is the main mechanical property to design a bus structure. Higher UTS as possible at each point in the structure makes the vehicle lighter and safer. The main aim of the study was optimizing the welding parameters to provide highest UTS from DP1000 GMAW welding. Therefore, tensile tests were applied to observe the effects of welding voltage, welding speed, wire feed rate and heat input on the UTS of welded DP1000 specimens. These tests confirm that, both the softening phenomenon and grain coarsening are the most important factors which affect the mechanical behavior of DP1000 steel welded joints (Kang et. al, 2010).

For tensile test, 300mm (length) x 30mm (width) welded plates were prepared according to TS 287 EN 895 standard. Figure 3.9 shows the design of test samples. A tensile tests machine (Alsa) with a maximum load of 40 tons was used to measure the UTS and fracture locations of welded samples.

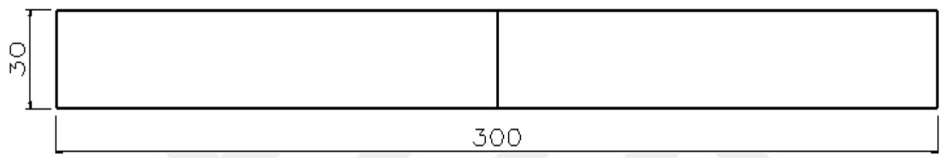

Figure 3.9. Geometry and dimensions of the tensile test specimens used after GMAW

When the tensile tests were completed, responses were analyzed with the aid of Minitab-17 software. The measured UTS values were evaluated in ANOVA to prove the effect of each welding parameter on UTS of the welding. Main effects of each factor and the interactions between the factors were plotted. The relations between the tensile test results with the variation in microstructure and Vickers hardness distribution of weld cross-section were determined.

Figure 3.10. Alsa, 40 tons tensile test machine

4. RESULTS AND DISCUSSIONS

In this study a fully automated GMAW system was utilized for the experiments including total of 54 runs. Visual and microstructural inspections, Vickers hardness and tensile tests were employed to determine the effects of voltage, welding speed, wire feed rate, current and heat input on weld quality, microstructure and mechanical properties of DP1000 steel butt welding. The welding parameters and experimental results of 54 welded seams are given in Table 4.1. The relations between the results of inspections and testing conditions were correlated and the effect of each parameter were discussed in the following sections.

4.1. Visual Inspection

The welding samples of DP1000 steel were visually inspected according to EN ISO 3834 standard. The 27 combinations of welding parameters applied 2 times, which in turn yields totally 54 experimental runs. For this purpose, Level-C which has medium tolerances for imperfections was used as a guide on the quality levels of butt welding. It was observed that the welding qualities obtained for the same parameters were similar, thus the welding applications were accepted stable within themselves. The ideal welding seams without any imperfection were observed mostly between the heat inputs of 0.12kj/mm and 0.15kj/mm. For example, one of the acceptable welding seam was obtained under the welding condition of 20th (HI:0.125kj/mm), as shown in Figure 4.1.

When the heat input increased over 0.18kj, the occurrence frequency of welding defects, such as burning gap and excessive penetration increased. On the other hand, excessive weld metal and the lack of penetration were observed for insufficient heat inputs, especially between 0.10 kj/mm and 0.12 kj/mm heat inputs.

Table 4.1. The welding parameters and experimental results of 54 welded seams

RUN	V (V)	WS (mm/min)	WFR (m/min)	I (A)	HEAT INPUT (KJ/mm)	Mean Tensile Strength (MPa)	Welding Cap Quality	Welding Root Quality
1	18.5	380	2.6	60	0.14	802.50	OK	OK
2	17.5	320	2.2	45	0.12	810.54	OK	Lack Of Penetration
3	17.5	260	2.2	45	0.15	795.50	OK	OK
4	19.5	320	2.6	60	0.18	774.46	Burning Gap	Excessive Penetrations
5	18.5	320	2.6	60	0.17	789.27	OK	OK
6	18.5	380	2.2	45	0.11	810.62	OK	OK
7	18.5	260	2.6	60	0.20	786.73	Burning Gap	Excessive Penetrations
8	19.5	320	2.4	53	0.16	793.85	Burning Gap	OK
9	17.5	320	2.4	53	0.14	800.69	Excess Weld Metal	Lack Of Penetration
10	19.5	260	2.2	45	0.16	783.47	OK	OK
11	18.5	260	2.4	53	0.18	771.22	OK	OK
12	19.5	260	2.6	60	0.22	773.59	Burning Gap	Excessive Penetrations
13	17.5	260	2.4	53	0.17	792.45	OK	OK
14	18.5	260	2.2	45	0.15	792.91	OK	OK
15	17.5	320	2.6	60	0.16	784.98	OK	OK
16	17.5	260	2.6	60	0.19	791.44	OK	OK
17	19.5	260	2.4	53	0.19	775.93	Burning Gap	Excessive Penetrations
18	19.5	380	2.4	53	0.13	798.87	Burning Gap	Excessive Penetrations
19	18.5	380	2.4	53	0.12	801.66	OK	Lack Of Penetration
20	18.5	320	2.2	45	0.12	812.07	OK	OK
21	17.5	380	2.6	60	0.13	796.98	OK	OK
22	17.5	380	2.4	53	0.12	801.83	OK	OK
23	17.5	380	2.2	45	0.10	820.61	Excess Weld Metal	Lack Of Penetration
24	19.5	320	2.2	45	0.13	792.14	OK	OK
25	18.5	320	2.4	53	0.15	795.26	OK	OK
26	19.5	380	2.2	45	0.11	802.51	OK	OK
27	19.5	380	2.6	60	0.15	779.30	Burning Gap	Lack Of Penetration
28	18.5	380	2.6	60	0.14	795.13	OK	OK
29	17.5	320	2.2	45	0.12	809.08	OK	OK
30	17.5	260	2.2	45	0.15	792.75	OK	OK
31	19.5	320	2.6	60	0.18	778.38	Burning Gap	Excessive Penetrations
32	18.5	320	2.6	60	0.17	783.20	OK	OK
33	18.5	380	2.2	45	0.11	805.46	OK	Lack Of Penetration
34	18.5	260	2.6	60	0.2	791.00	OK	OK
35	19.5	320	2.4	53	0.16	792.78	Burning Gap	Excessive Penetrations
36	17.5	320	2.4	53	0.14	790.88	Burning Gap	OK
37	19.5	260	2.2	45	0.16	790.37	OK	OK
38	18.5	260	2.4	53	0.18	774.77	Burning Gap	Excessive Penetrations
39	19.5	260	2.6	60	0.22	772.22	Burning Gap	Excessive Penetrations
40	17.5	260	2.4	53	0.17	794.92	OK	OK
41	18.5	260	2.2	45	0.15	790.65	OK	OK
42	17.5	320	2.6	60	0.16	793.04	Burning Gap	Excessive Penetrations
43	17.5	260	2.6	60	0.19	794.00	OK	OK
44	19.5	260	2.4	53	0.19	777.10	Burning Gap	OK
45	19.5	380	2.4	53	0.13	803.32	OK	OK
46	18.5	380	2.4	53	0.12	797.12	OK	Burn Gap
47	18.5	320	2.2	45	0.12	802.66	OK	OK
48	17.5	380	2.6	60	0.13	797.45	OK	OK
49	17.5	380	2.4	53	0.12	801.52	OK	OK
50	17.5	380	2.2	45	0.10	811.81	Excess Weld Metal	Lack Of Penetration
51	19.5	320	2.2	45	0.13	801.29	OK	OK
52	18.5	320	2.4	53	0.15	802.77	OK	OK
53	19.5	380	2.2	45	0.11	796.86	OK	OK
54	19.5	380	2.6	60	0.15	786.20	Burning Gap	Excessive Penetrations

Similar observations were also obtained by Kang et al. (2010) during the examination of the weldability of DP780 steels for GMAW process. They also reported that low heat input caused lack of penetration and excessive heat input created burning gaps. Moreover, the present experiments revealed that an independence was present among the effects of voltage, current and welding speed on weld quality. Therefore different welding qualities and weld bead dimensions could be obtained even if heat inputs were same.

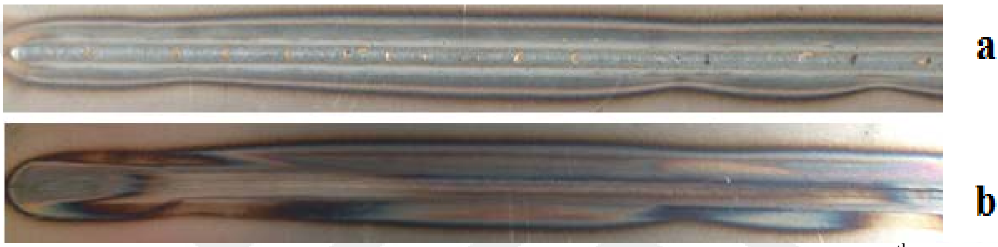

Figure 4.1. Welded specimen under the welding conditions of 20th Run (a) The welding cap, (b) The welding root

4.1.1. Effect of Arc Voltage On Weld Quality

The same welding speed (320mm/min), wire feed rate (2,4m/min) and the current (53A) were used in the experiments conducted under the conditions of 9th, 25th and 35th Runs. Their heat inputs were also close to each other. Therefore, the samples obtained from these runs were selected to analysis the effect of different welding voltages on weld quality. The welding parameters, heat inputs and visual inspection results are tabulated in Table 4.2.

During the visual inspection of the welding seam obtained under the conditions of 9th Run, excessive weld metal and lack of penetration were observed as shown in Figure 4.2a and Figure 4.2b, respectively. The welding seam was narrow and weld cap was high due to the low arc voltage. Aghakhani et al. (2011) also defined that insufficient voltage caused lack of penetration in their study related to the parametric optimization of GMAW process for the necessary weld penetration.

Table 4.2. The welding parameters and visual inspection results under the welding conditions of 9th, 25th and 35th Runs

RUN	V (V)	WS (mm/min)	WFR (m/min)	I (A)	HI (KJ/mm)	Welding Cap Quality	Welding Root Quality
9	17.5	320	2.4	53	0.14	Excess Weld Metal	Lack Of Penetration
25	18.5	320	2.4	53	0.15	OK	OK
35	19.5	320	2.4	53	0.16	Burning Gap	Excess Penetrations

Generally, lack of penetration and excessive weld metal create notch effect and stress concentration under dynamic loading. These defects could not be accepted according to 502th reference of EN ISO 3834. As a result, an increase in voltage was needed to widen the weld cap and improve the weld quality.

In order to define the significance of applied voltage, it increased up to 18.5V under the conditions of 25th Run. The excessive weld metal was prevented and width of the weld increased obviously in this run, as shown in Figure 4.2c. At the same time, sufficient penetration and a fixed dimensional weld bead were obtained as shown in Figure 4.2d. The rise in voltage increased the penetration slightly and resulted acceptable welding quality according to EN ISO 3834.

In the third case, the welding seam under the conditions of 35th Run (19.5V) was inspected. Because of the higher arc voltage, a larger welding seam which had lower welding cap height observed as shown in Figure 4.2e. Lots of burning gaps were occurred because of higher surface tension of molten metal resulted by high voltage. This situation was critical especially for thin plate weldings. Na et. al (2011) conducted a study on the optimization of fillet welding parameters for ideal welding bead. They also reported that, welding voltage and welding speed had a significant effect on the weld geometry.

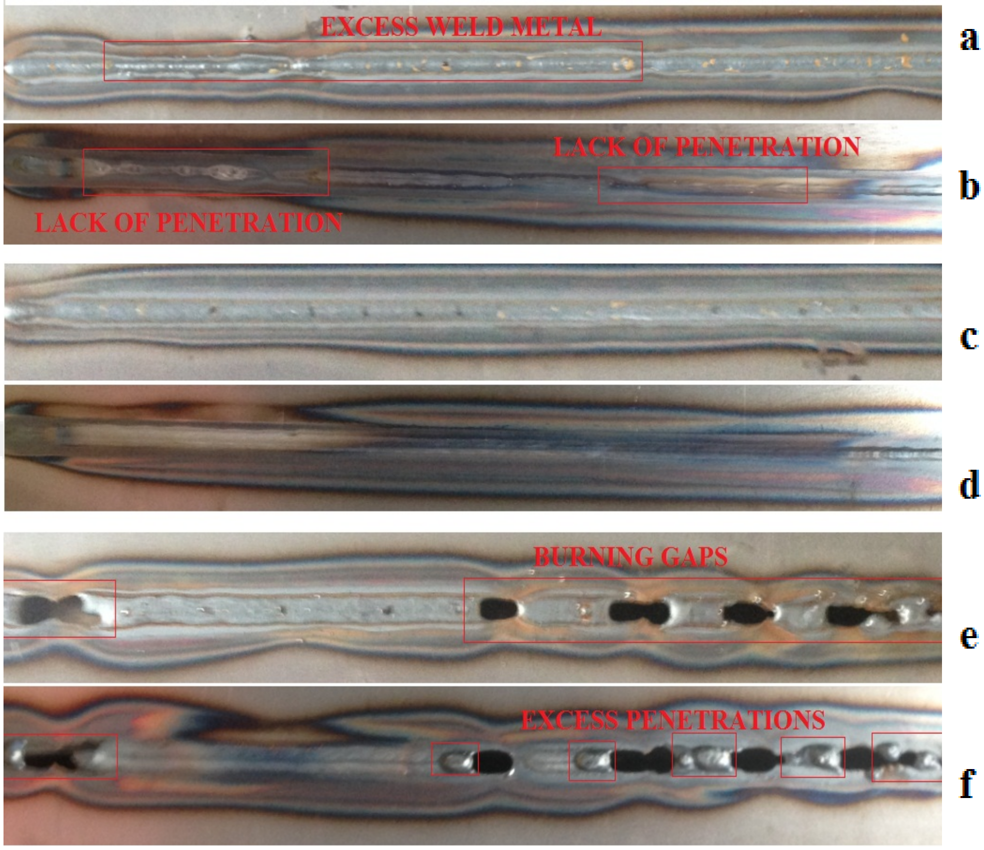

Figure 4.2. Samples obtained under the different welding conditions (a)Welding cap of 9th Run, (b) Welding root of 9th Run, (c)Welding cap of 25th Run, (d) Welding root of 25th Run, (e)Welding cap of 35th Run, (f) Welding root of 35th Run

This experimental work demonstrated that color changes were also occurred, which were indicated with brown color as shown in Figure 4.2e. Because, high heat input burned the chemical elements in HAZ, which in turn creates high amount of smoke. In addition, an excessive penetration was observed as shown in Figure 4.2f. As a result, variation in applied voltage had profound effect on quality and width of the weld; however, its effect on welding penetration was low.

4.1.2. Effects of Wire Feed Rate on the Weld Quality

Wire feed rate is directly proportional to electrode melting speed. Hence, nearly a constant fraction is present between the arc current and WFR due to automatic power source (Chu, 2007). Constant voltage level (17,5V) and welding speed (320mm/min) were used in 2th, 36th and 42th Runs. Therefore the welded plates obtained from these runs were visually inspected in order to discuss the effect of WFR and current on welding cross-section and quality.

Initially, the welding seam under the conditions of 2th Run (45A) was inspected and a tight welding seam was detected, as shown in Figure 4.3a. The ability of penetration was difficult due to low current and low heat input, hence lack of penetrations were detected (Figure 4.3b). This observation also agreed with the results of Kang et al. (2010). When the welding seam under the conditions of 36th Run (53A) was visually inspected, a little bit wider welding seam than the welding under the condition of 2th Run was observed (Figure 4.3c). Consequently, the heat input and weld penetration increased. Elliott (2009) reported that, rise in the WFR with current increased the weld penetration. Similarly, Aghakhani et al. (2011) presented that rise in the WFR increased welding penetration. Particularly, Na et al. (2011) found that bead geometry enlarged with increased WFR.

Table 4.3. The welding parameters and visual inspection results of the weldings under the conditions of 2th, 36th and 42th Runs

RUN	**V (V)**	**WS (mm/min)**	**WFR (m/min)**	**I (A)**	**HI (KJ/mm)**	**Welding Cap Quality**	**Welding Root Quality**
2	17.5	320	2.2	45	0.12	OK	Lack of Penetration
36	17.5	320	2.4	53	0.14	Burning Gap	OK
42	17.5	320	2.6	60	0.16	Burning Gap	Excessive Penetrations

The highest WFR (2,6m/min) and current (60A)were employed under the conditions of 42th Run. Higher WFR and low voltage, which produced short arc length caused excessive spatter and gaps, as seen in Figure 4.3e and f, respectively. Burns (2009) reported that, Park et al. (1981) found the high current and WFR at low voltage caused spatter and lack of fusion.

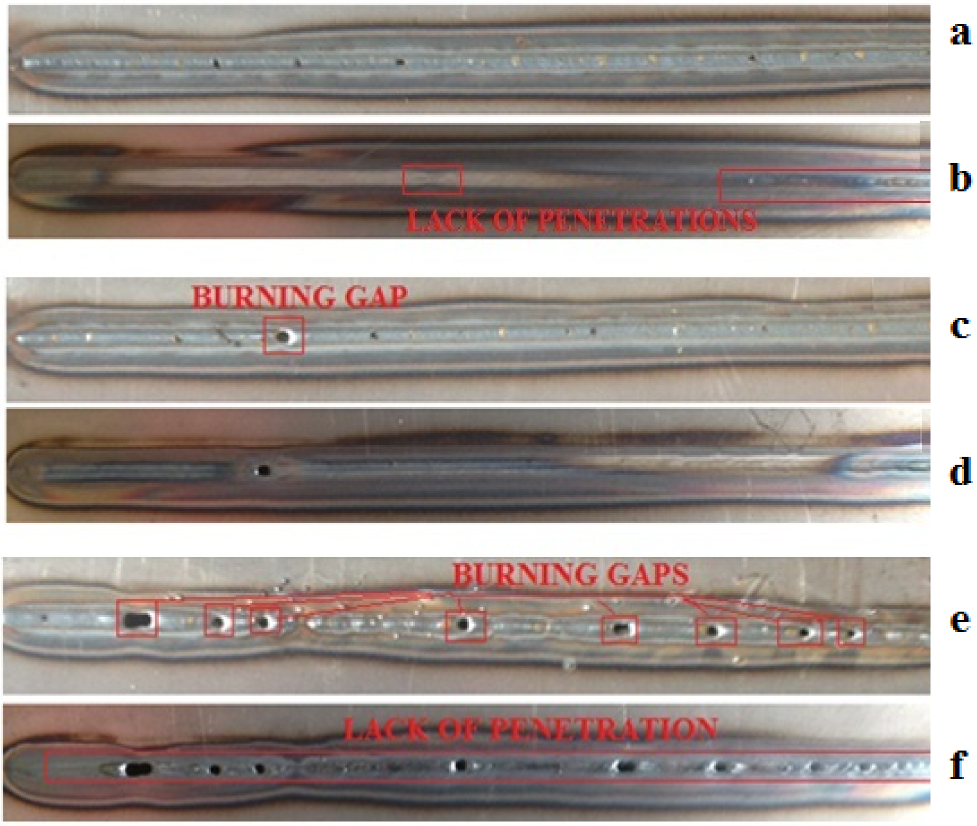

Figure 4.3. Samples obtained under the different welding conditions (a)Welding cap of 2th Run, (b) Welding root of 2th Run, (c)Welding cap of 36th Run, (d) Welding root of 36th Run, (e)Welding cap of 42th Run, (f) Welding root of 42th Run

As a result, increase in the welding current affected the welding penetration significantly. Sufficient welding current had to be provided for full welding penetration. It could be also indicated that the voltage should be increased for preventing the metal spatter, when high current was present. Belinga (2012) stated that the use of low WFR and current resulted a rough weld surface and incomplete fusion. Whereas when the current was extremely high it caused porosity, spatter and poor bead shape.

4.1.3. Effect of Welding Speed on the Welding Quality

The welding seams under the conditions of 19th, 25th and 38th Runs, which had the same arc voltage (18,5V) and WFR (2,4m/min) were visually inspected to determine the effect of welding speed on weld quality and bead dimensions. The related parameters and inspection results are listed in Table 4.4. The conditions of 19th Run, which had the highest welding speed (380mm/min), caused a tight weld seam as shown in Figure 4.4a and local lack of penetrations were detected (Figure 4.4b). Because, the high welding speed resulted insufficient heat input and the filler metal deposition rate per unit of length. The lower welding speed under the condition of 25th Run created higher heat input, better penetration and wider weld cap (Figure 4.4c) than the welding under the conditions of 19th Run. Similarly, Aghakhani et al. (2011) indicated that decreasing the welding speed increased the weld penetration.

Table 4.4. The welding parameters and visual inspection results under the welding conditions of 19th , 25th and 38th Runs

RUN	V (V)	WS (mm/min)	WFR (m/min)	I (A)	Heat Input (KJ/mm)	Welding Cap Quality	Welding Root Quality
19	18.5	380	2.4	53	0.12	OK	Lack Of Penetration
25	18.5	320	2.4	53	0.15	OK	OK
38	18.5	260	2.4	53	0.18	Burning Gap	Excessive Penetrations

The detailed research performed by Belinga (2012) showed that, the penetration increased while the welding speed was increasing initially. Because the arc was applied more directly in the workpiece; but, further increase in welding speed decreased the penetration and caused undercut due to insufficient material to fill the cavity produced by the arc. The welding seam under the condition of 38^{th} Run was inspected to determine the effect of lowest welding speed at same voltage and WFR. Due to the extremely low welding speed, the heat input increased and burning gaps were occurred as shown in Figure 4.4e. Kang et al. (2010) also confirmed that, when low weld speed was applied, burning gap occurred at thin DP steel welding.

The visual inspection results showed that the welding quality of DP1000 sheet was very sensitive to changes in heat input, voltage, wire feed rate (current) and welding speed particularly for the thin thickness (1,20mm) used in the experimental work. During the visual inspections, it has been observed that burning gaps and lack of penetration were the most critical welding defects which were affected mostly by changes in voltage and current respectively.

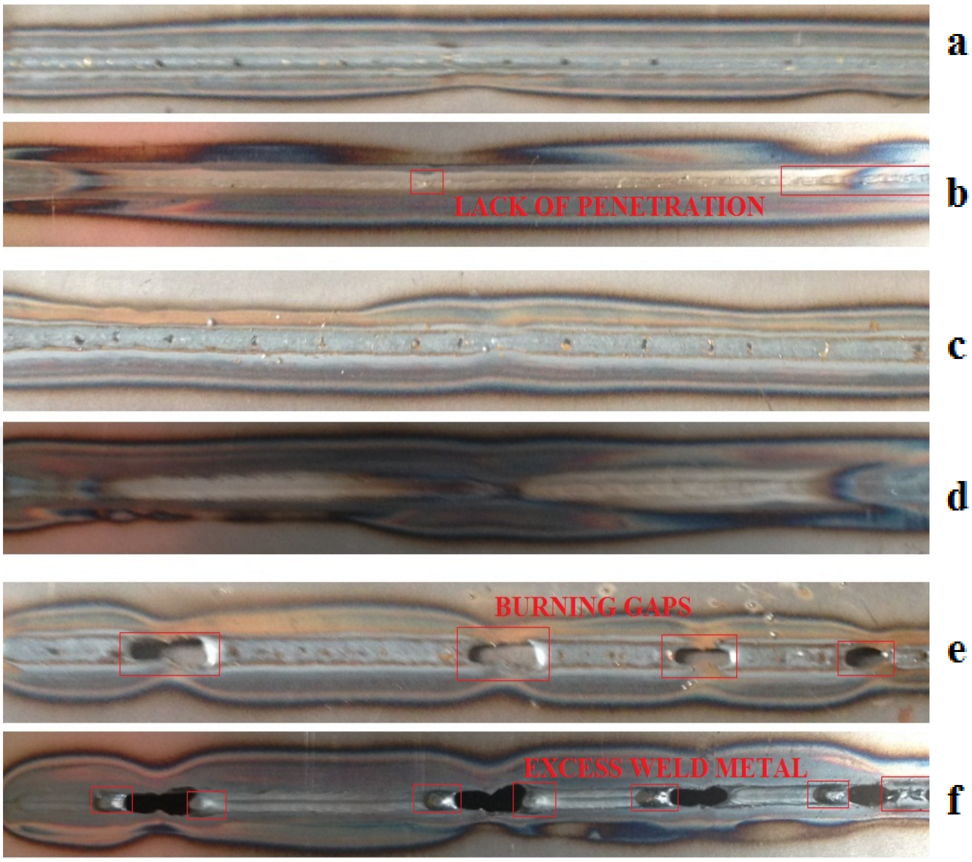

Figure 4.4. Samples obtained under the different welding conditions (a)Welding cap of 19th Run, (b) Welding root of 19th Run, (c)Welding cap of 25th Run, (d) Welding root of 25th Run, (e)Welding cap of 38th Run, (f) Welding root of 38th Run

4.2. Microstructure Analyses

Martensite tempering, orientation of the martensite islands, VFM islands within the ferrite matrix, and the ferrite grain size are the main factors, which affect the strength and hardness of DP steels (Okamoto et al. (1981) and Lawson et al. (1981)). The characteristics features of these factors depend on the welding parameters which defines the heat input. Therefore, the effect of heat input on these factors were examined by studying the microstructural changes obtained for different parameter combinations of DP1000 GMAW used in this study. For this purpose, the different microstructural regions were inspected in the HAZ and FZ. The original microstructure of DP1000 steel was also analyzed for comparison purposes. It was defined that base metal consists of 51% martensite and 49% ferrite phases. The martensit (black color) and ferrite (light color) formations were dispersed homogeneously as shown in Figure 4.5. Rocha et al. (2015) also measured the volume fraction of phases as 51% of ferrite and 49% martensite (error of ± 4% for both phases) for DP1000 steel.

23th Run, 9th Run, 11th Run, 12th Run with 0,10kj/mm (minimum), 0,14kj/mm, 0,18kj/mm and 0,22kj/mm (maximum) heat inputs respectively were examined to identify the effect of heat input on the dimensions of weld cross-section and microstructural changes. H_{23}, H_9, H_{11} and H_{12} are the heights of welding caps and W_{23}, W_9, W_{11} and W_{12} are the widths of the welding caps. As shown in Figure 4.6, the comparison among the dimensions of welding cross-sections presented that, $H_{23}>H_9>H_{11}>H_{12}$ and $W_{23}<W_9<W_{11}<W_{12}$. Therefore, the highest height and tightest weld were obtained under the welding conditions of 23th Run, which had lowest heat input. On the other hand, the welding conditions of 12th Run resulted the lowest welding height and widest cross-section. It could be reported that rising the heat input caused an increase in penetration of the welding, sagging of the welding root and width of the welding. In contrary, the height and concavity of the welding decreased due to the increase in the amount of molten metal and its fluidity.

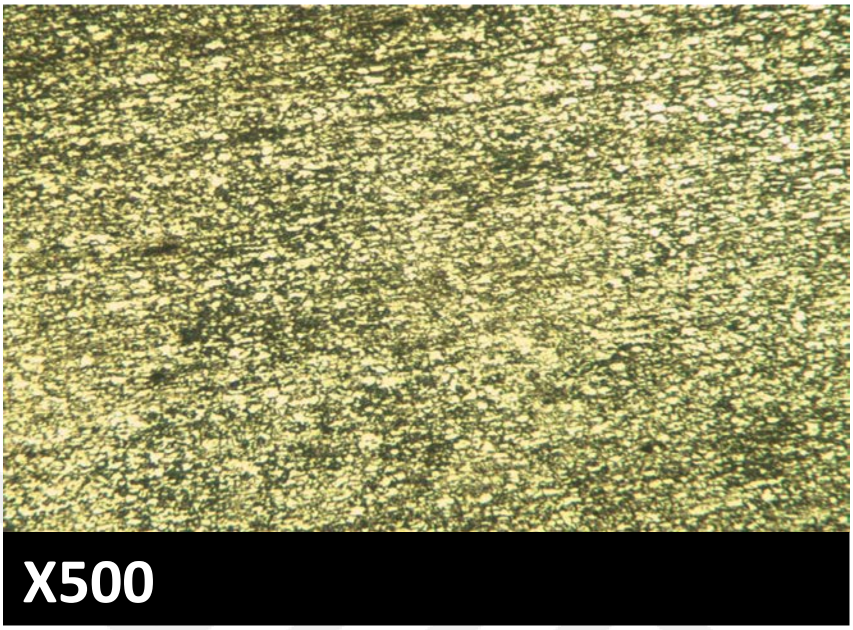

Figure 4.5. The original microstructure of DP1000 base metal which consists of 51% martensite and 49% ferrite

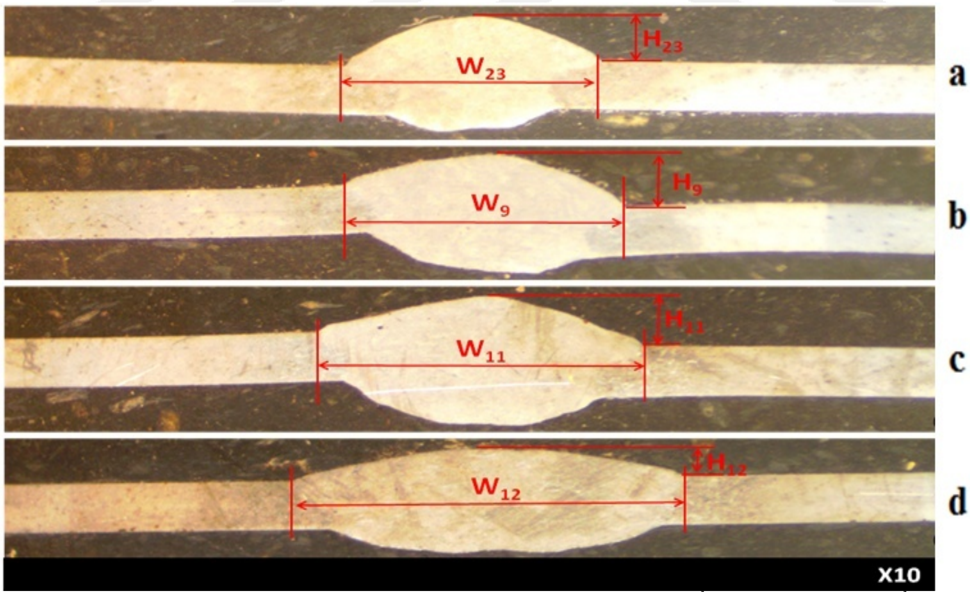

Figure 4.6. Overviews of welding cross-sections. (a) 23th Run, (b) of 9th Run (c) 11th Run, (d) 12th Run

The FZ and GG/GR regions obtained from the experiment conducted under the conditions of 23th Run (HI:0.10kj/mm), 9th Run (HI:0.14kj/mm), 11th Run (HI:0.18kj/mm) and 12th Run (HI:0.22kj/mm) are presented in Figure 4.7. It was seen that higher heat input increased the martensite tempering effect and width of the HAZ. Rocha et al. (2015) also reported that FZ and HAZ widths increased with the rise of heat input. Especially, when 23th Run (Figure 4.7a) and 12th Run (Figure 4.7d) were compared, it was clearly seen that low heat input weld caused higher remaining martensite than higher heat input welds due to increase in the martensite decomposition rate because of high heat input.

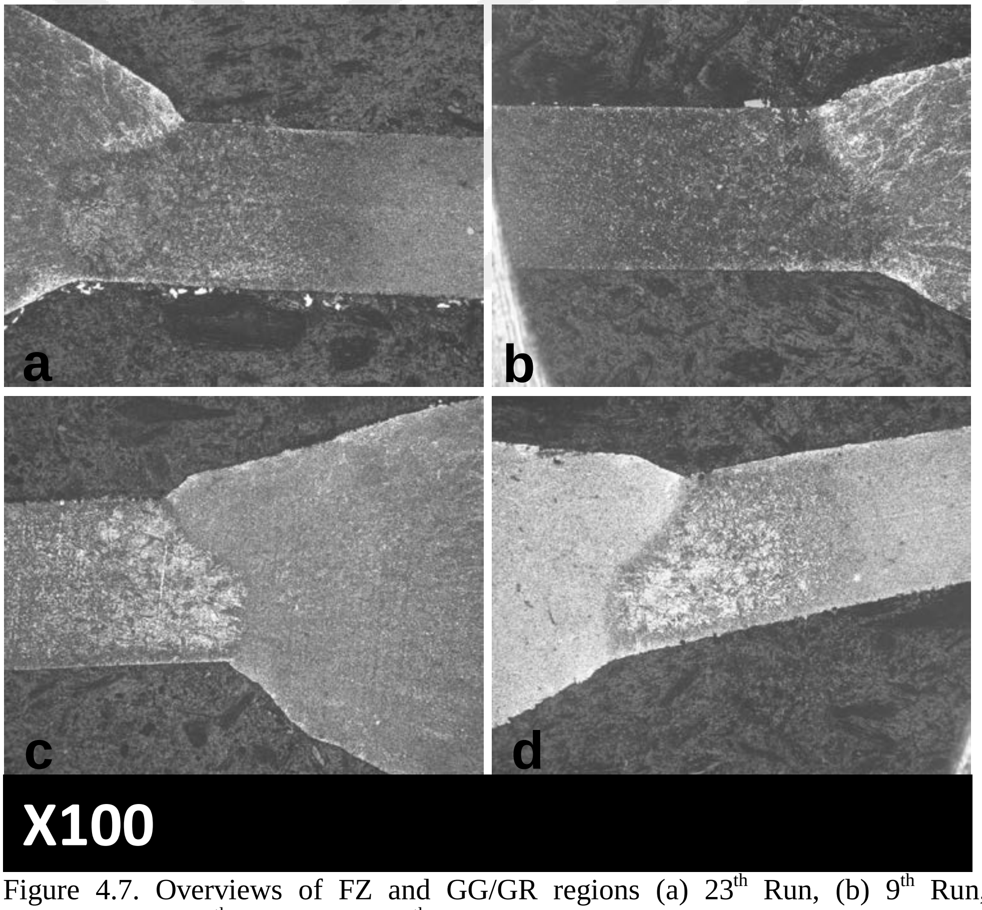

Figure 4.7. Overviews of FZ and GG/GR regions (a) 23th Run, (b) 9th Run, (c) 11th Run and (d) 12th Run

The VFM percentages of each region of 23th Run, 9th Run, 11th Run, 12th Run were also measured (Table 4.5). The highest reduction of VFM in SC regions were obtained because of the highest percentage of tempered martensite resulted from high heat input. Because carbide nucleation caused the highest decrease in VFM of SC region. Rocha et al. (2015) also found that the lowest VFM was obtained in SC region, when 1.80mm DP1000 steel was welded.

Table 4.5. Martensite percentages of microstructural regions and FZ's

RUN	VOLUME FRACTION OF MARTENSITE (%)					Heat Input (KJ/mm)
	FZ	GG	GR	IC	SC	
23	43.73	49.43	49.60	46.84	41.12	0.10
9	44.18	48.32	48.12	45.41	39.80	0.14
11	42.63	47.45	46.92	43.42	38.36	0.18
12	41.14	45.83	44.14	41.83	37.87	0.22

As shown in Figure 4.8, the microstructures of four SC regions resembled the BM, but there were also islands of decomposed (tempered) martensite in the ferrite matrix. Moreover, it was observed that the SC regions in the conditions of 23th Run (HI:0.10kj/mm), 9th Run (HI:0.14kj/mm), 11th Run (HI: 0.18kj/mm), 12th Run (HI:0.22kj/mm) had 41.12%, 39.80%, 38.36% and 37.87% VFM, respectively. The lowest decrease in VFM among four SC regions was detected under the condition of 23th Run. It was calculated as "(51-41.12)/51=19.37%". On the other hand, the highest martensite tempering was observed under the conditions of 12th Run and VFM of BM was decreased from 51% to 37.87%. Thus, martensite tempering percentage was calculated as; "(51–37.87) /51= 25.74%". Another difference between the SC regions was the distribution of tempered martensite. They were dispersed more homogeneously at low heat input weld under the conditions of 23th Run (Figure 4.8a). On the contrary, tempered martensites were clustered at high heat input under the 12th Run as shown in Figure 4.8d. When SC regions of four samples were inspected, it was found that rise in heat input increased the accumulation of the tempered martensites due to high amount of martensite decomposition obtained at the higher temperatures.

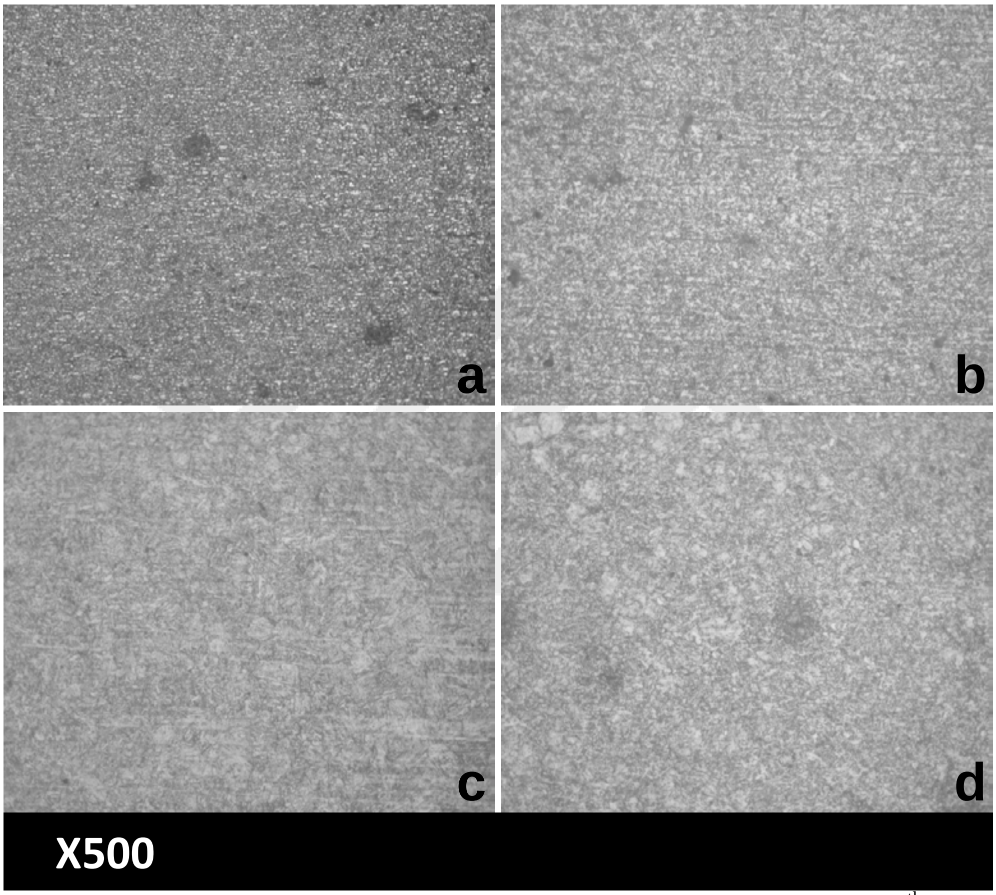

Figure 4.8. SC region microstructures of different welding conditions. (a) 23th Run, (b) 9th Run, (c) 11th Run and (d) 12th Run

Rocha et al. (2015) reported that, austenite recrystallization and grain refining occurred in IC region. In this region, the martensite and carbide phases in the BM partially reformed to austenite and then re-quench to martensite. Thus, the increase in the percent area of martensite in the IC region caused the region to increase in hardness compared to the SC region. As shown in Table 4.5, the percentages of VFM of IC region was higher than SC region for all samples. When heat input was increased, the martensite tempering effect was increased in IC region, too. Therefore, among the IC regions of four samples, the percentage of VFM was found highest (46,84%) with fine grain structure (Figure 4.9a) at 23th Run because of lowest heat input (0,10kj/mm). In addition, the original martensite phase and tempered martensite phase were nearly homogeneously distributed in IC region for low heat input weld (Figure 4.9a). The lowest percentage of VFM was detected in IC region of 12th Run, which had the highest heat input (0.22kj/mm).

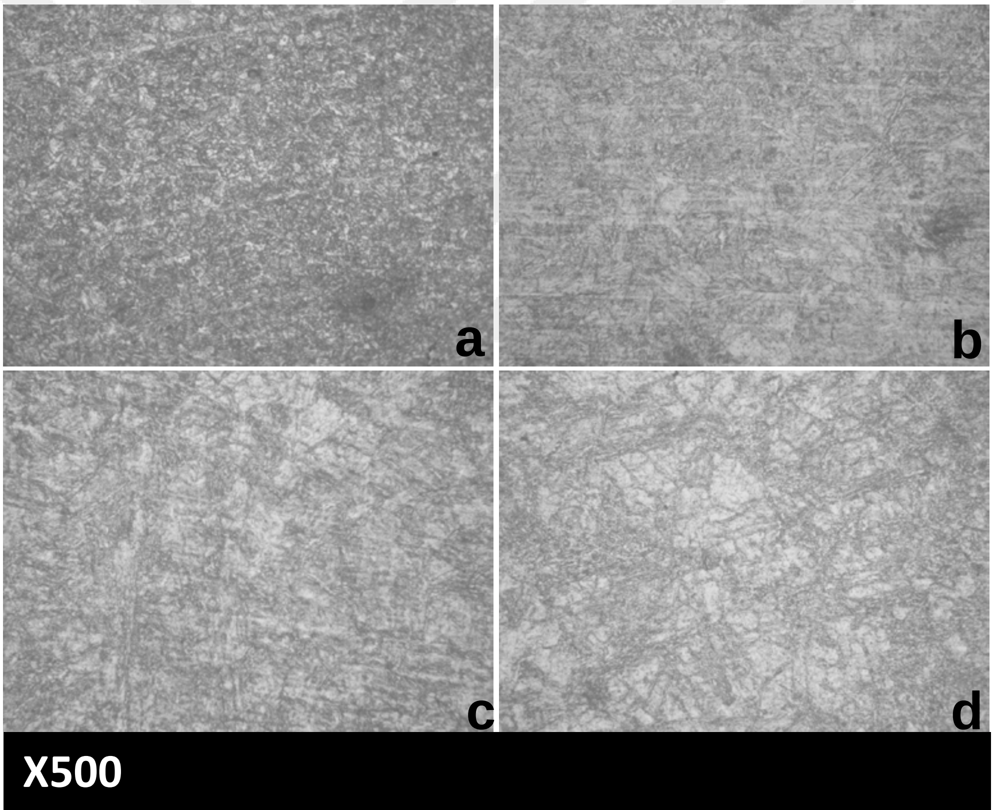

Figure 4.9. IC region microstructures of different welding conditions. (a)23th Run, (b)9th Run, (c)11th Run and (d) 12th Run

The VFM percentages of IC regions in 23th and 9th Runs with 0,10kj/mm and 0,14kj/mm heat inputs respectively, were found higher than 11th and 12th Runs because of the higher percentage of renucleated martensite phases formed at lower heat inputs. As a result, it was identified that the martensite tempering effect also increased in IC region, while heat input was increasing.

The steel was fully transformed to austenite in GR region. After welding, austenite in this region transformed to massive martensite upon cooling. The finest grain structure was observed in GR regions. Among four samples, the finest grain structure was defined at lowest heat input weld under the condition of 23th Run (Figure 4.10a).

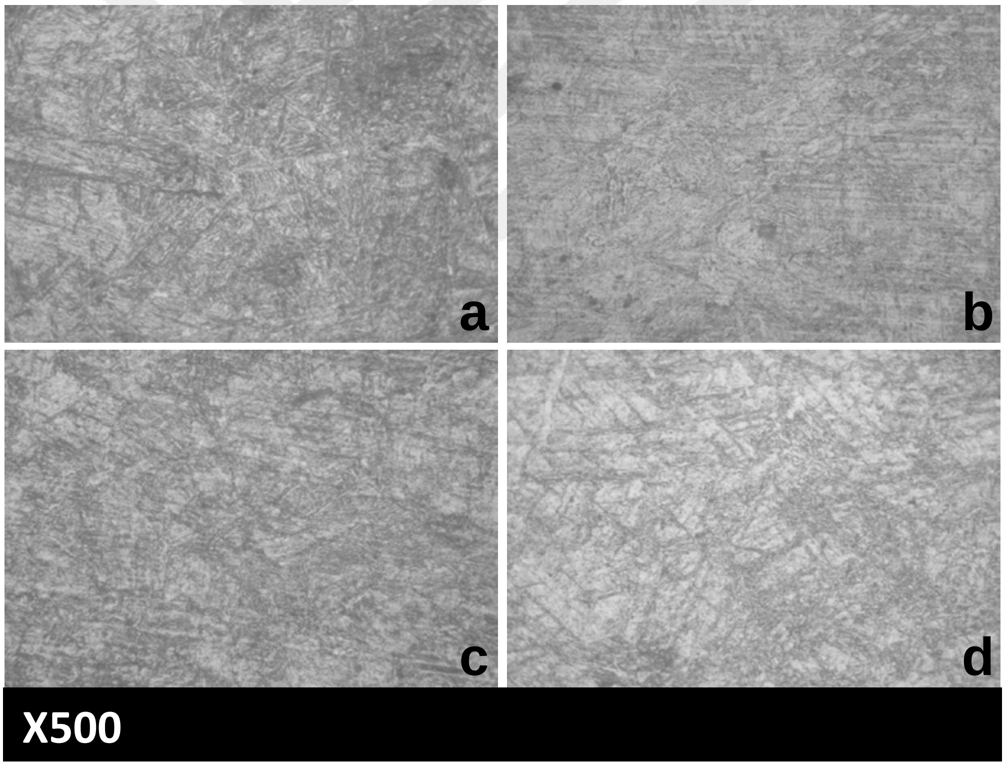

Figure 4.10. GR region microstructures of different welding conditions. (a) 23th Run, (b) 9th Run, (c)11th Run and (d) 12th Run

Because, increase in heat input decreased cooling rate due to quenching effect; also increased the martensite tempering and grain growing effects.

The grains of GG regions were larger than the grains in the GR regions. The largest grains in HAZ's were observed immediately adjacent to the fusion layer. The microstructures which consisted of massive martensite and acicular ferrite phases were detected in the GG regions, as shown in Figure 4.11. GG region under the condition of 23th Run had the lowest heat input and highest VFM (49.43%), which was lower than VFM (51%) of BM.

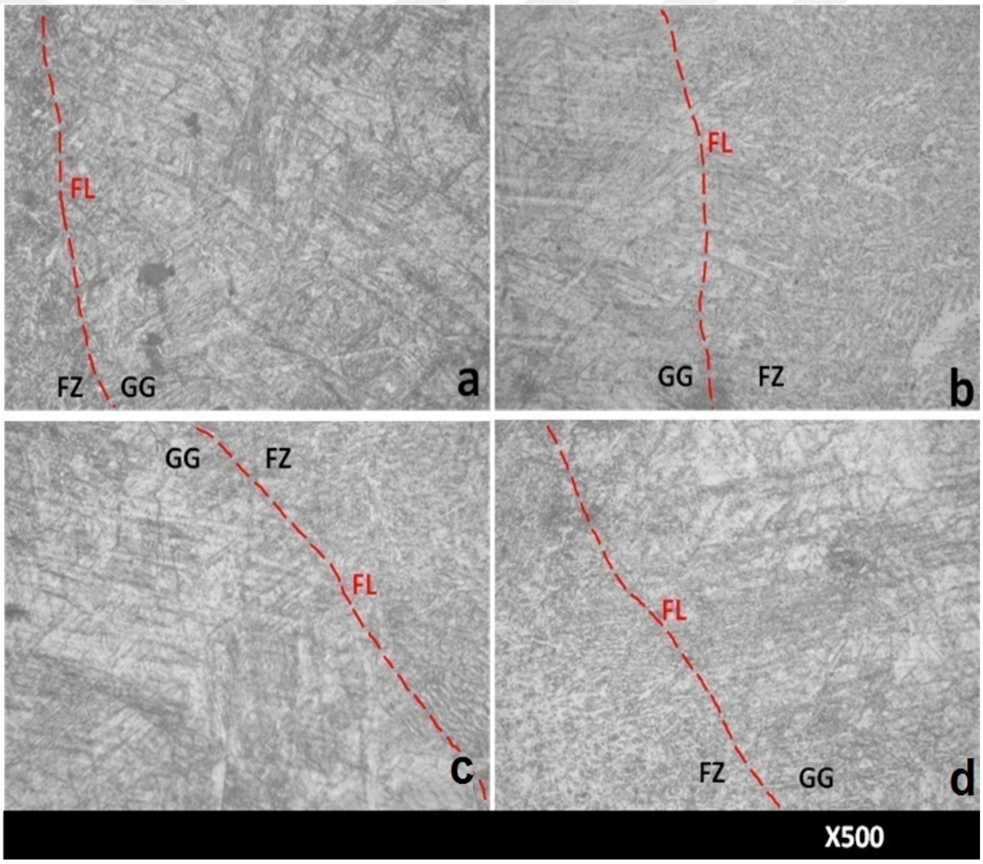

Figure 4.11. Microstructure of GG regions obtained at different welding conditions (a)23th Run (b) 9th Run, (c)11th Run and (d) 12th Run

When the heat input was risen with increments of 0.04kj/mm under the conditions of 9th, ,11thand 12th Runs, the percentages of VFM's continued decreasing in GG regions. They were about 48.32% (Figure 4.11b), 47.45% (Figure 4.11c) and 45.83% (Figure 4.11d), respectively. Hence it was determined that rise in heat input also decreased the VFM of GG region, too. This result was also supported by the insights gained from Rocha et al. (2015), which showed decrease in the VFM and hardness of GG region in the case of increased the heat input.

The compositions of the FZ's were mostly the electrode material and small amount of melted BM. Although there was not any significant difference between the four inspected samples; increase in the heat input reduced the VFM values of FZ's. The percentages of VFM in FZ's were measured as 43.73%, 44.18%, 42.63% and 41.14% as shown in Table 4.5. The microstructure of the FZ compositions were mixtures of martensite and ferrite phases. Conrardy et al. (2006) observed similar hardness magnitudes (~260 VHN) and microstructures in the FZ of DP780 and DP980 steels welded by using ER70S-6 electrode as filler metal. Moreover, Kapustka et al. (2008) who compared the FZ characterization data of the DP780 and DP980 lap joints, also supported these results in their study.

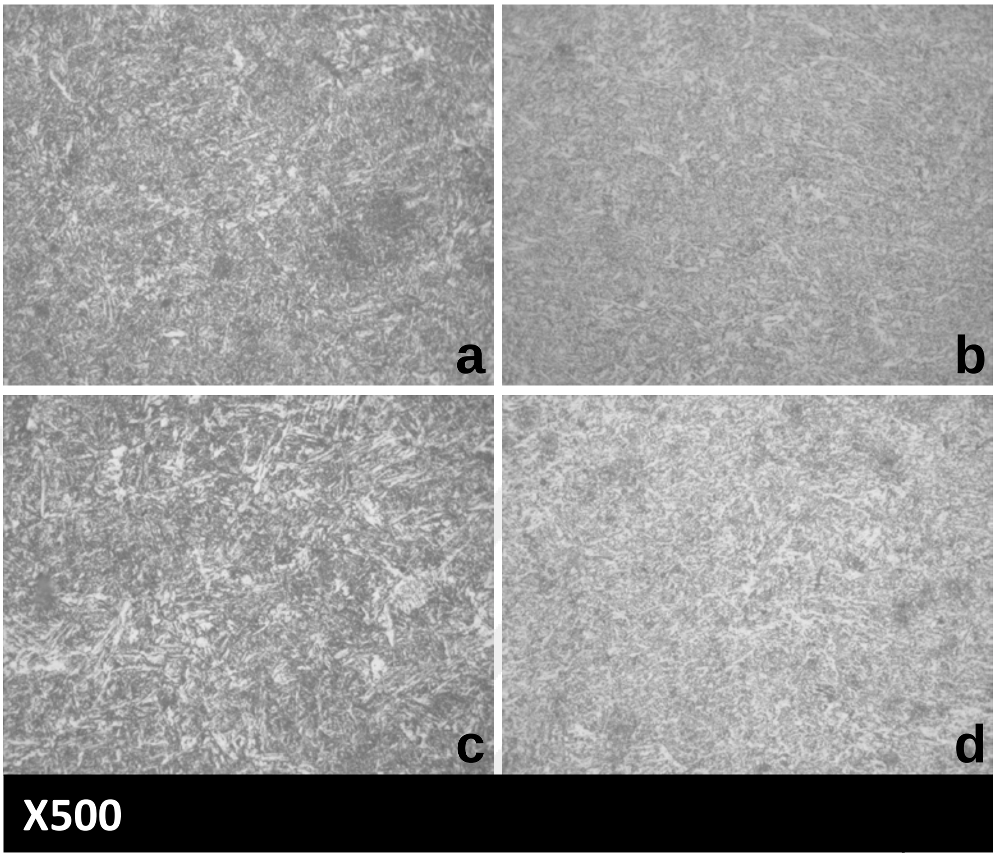

Figure 4.12.FZ microstructures of different welding conditions. (a)23th Run, (b) 9th Run, (c)11th Run and (d) 12th Run

4.3. Weld Vickers Hardness Analyses

Hardness is a mechanical property used to quantify the relative effects of welding heat input on steel microstructure. In this study, the BM hardness was measured as 325HV. SSAB Steel Company, which is the producer of the base metal sheets provided data belonging the hardness of DP1000 as between 320HV and 340HV. In addition, the producer experienced that the hardness of the BM may decrease from nearly 330HV to 220HV, when the DP1000 steel was welded by GMAW method (www.ssab.com, 2009).

The welding operations conducted under the conditions of 23rd, 9th, 11th and 12th Runs were selected to examine the hardness profiles in the HAZs and FZs. The distances between indents on the HAZ and FZ was applied as 0,75mm. The results of hardness measurements related to these runs are given in Table 4.6.

Table 4.6. Vickers hardness measurements of the welded samples under the conditions 23th Run, 9th Run, 11th Run 12th Run

INDENT POINT	VICKERS HARDNESS MEASURMENTS (HV)			
	23th RUN (HI:0.10kj/mm)	9th RUN (HI:0.14kj/mm)	11th RUN (HI:0.18kj/mm)	12th RUN (HI:0.22kj/mm)
1	304	292	288	274
2	294	281	270	237
3	264	221	214	204
4	220	242	234	217
5	252	235	225	241
6	267	241	239	217
7	348	334	324	314
8	247	253	251	262
9	248	244	261	253
10	249	256	232	257
11	336	340	314	322
12	257	263	245	221
13	260	247	234	217
14	225	254	247	257
15	267	218	221	197
16	274	211	206	207
17	267	282	264	234
18	312	300	278	289

The highest Vickers Hardness distribution was observed on the welding cross-section under the conditions of 23th Run, which had the lowest heat input (0.10 kj/mm). In Figure 4.13, the hardness distribution of the related welding seam was illustrated with its FZ, GG, GR, IC, SC regions and A_1, A_3 lines, approximately. The lowest hardness (220HV) was measured in the SC region immediately adjacent to A_1 line on the welding cross-section of 23th Run. The hardness of IC region was measured higher than the SC region, due to the renucleated and elongated martensite phases.

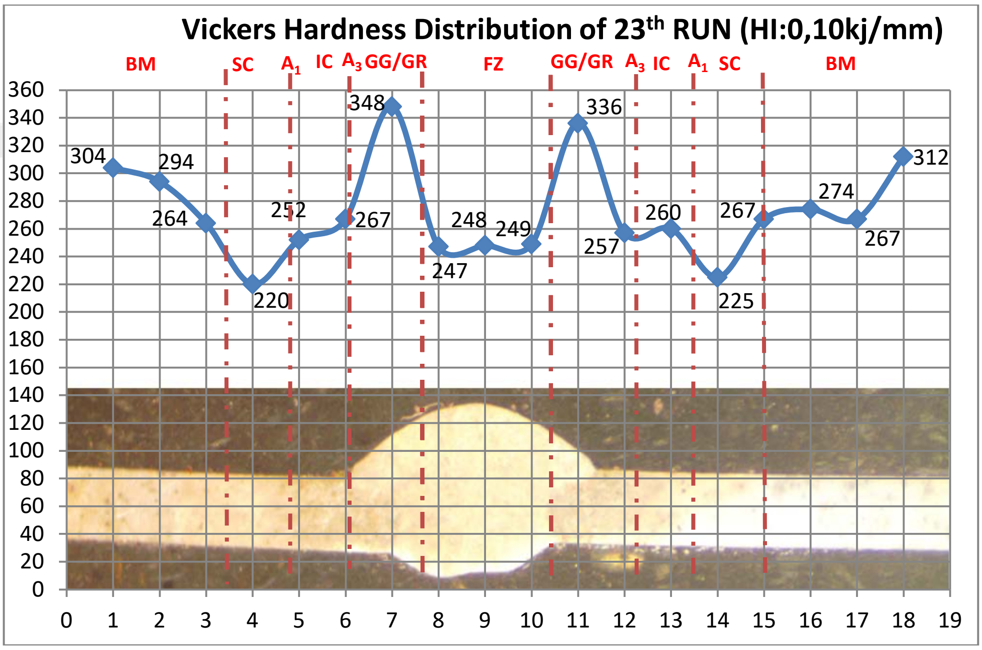

Figure 4.13. The Vickers hardness distribution of the weld cross-section obtained under the welding conditions of 23th Run

In GR region, the steel was fully transformed to austenite during welding. Then austenite phase in this region transformed to fine grained martensite upon cooling. Therefore, the hardness on the cross-section of the 23th Run condition increased further upon entering the GR region and then reached a maximum value (348HV) in the GG region (Figure 4.13). FZ had nearly 248HV mean hardness. It was higher than the hardness of SC region and lower than the hardness of IC region. Rocha et al. (2015) also defined that, the highest values of hardness were developed in the GG region due to transformation of the austenite phase into massive martensite structure under the influence of a high cooling rate.

In Figure 4.14, the hardness distribution on the cross-section of 9th Run condition was illustrated with its FZ, GG, GR, IC, SC regions and A_1, A_3 lines, approximately. The lowest hardness (211HV) was observed in SC region. While passing through IC region, the hardness increased, because of martensite renucleation and elongated martensite band. The increase in the massive martensite percentage and finer grain size also increased the hardness of GR region. The highest hardness (340HV) of the welding was detected on its GG region. However, as the conditions of 9th Run and 23th Run were compared, the higher heat input of 9th Run condition showed itself as the little bite lower hardness distribution throughout the welding cross-section and HAZ.

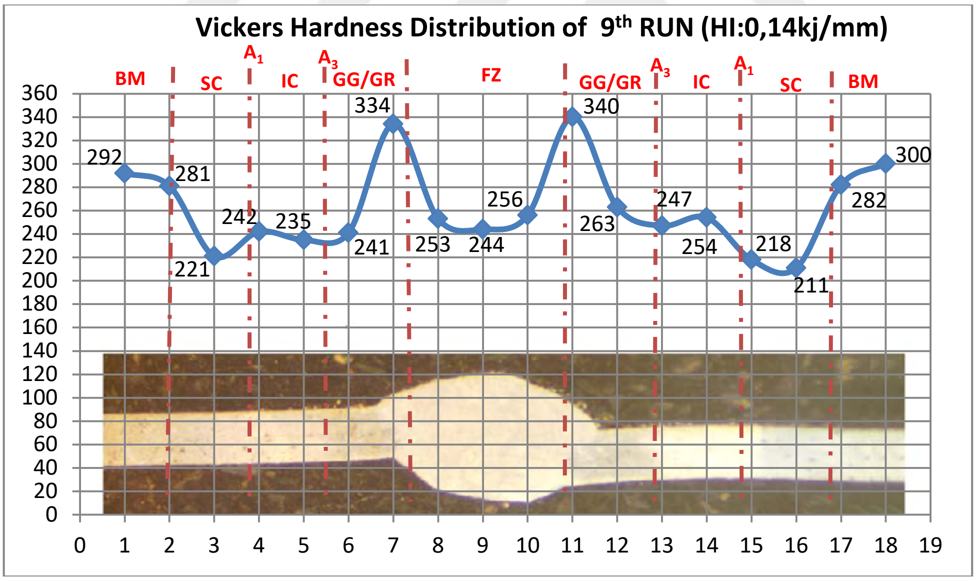

Figure 4.14. The Vickers hardness distribution of the weld cross-section obtained under the welding conditions of 9th Run

The welding conditions of 11th Run had higher welding heat input (0.18kj/mm) than the conditions of 23th Run (0.10kj/mm) and 9thRun (0.14kj/mm).

More martensite tempering and grain coarsening occurred throughout the HAZ and FZ. Thus, the hardness measurements were lower than conditions of 23th Run and 9th Run, generally as shown in see Figure 4.15. SC region had the lowest hardness (206HV) on this cross-section. The hardness of the IC region was measured as 247HV which was higher than SC region of the same sample, however the hardness of the IC region was lower than the same regions of the samples under the conditions of Run 23th Run and 9th Run, because of the tempering and grain coarsening effect of the higher heat input. GR region of the sample under the condition of 11th Run had higher hardness than the IC and SC regions of the same cross-section as shown in Figure 4.15. On the other hand, this GR region had a lower hardness than the samples under the conditions of 23th Run and 9th Run. A similar observation was defined for the hardness of the GG region. Because, higher heat input and lower cooling rate limited the massive martensite formation and martensite banding.

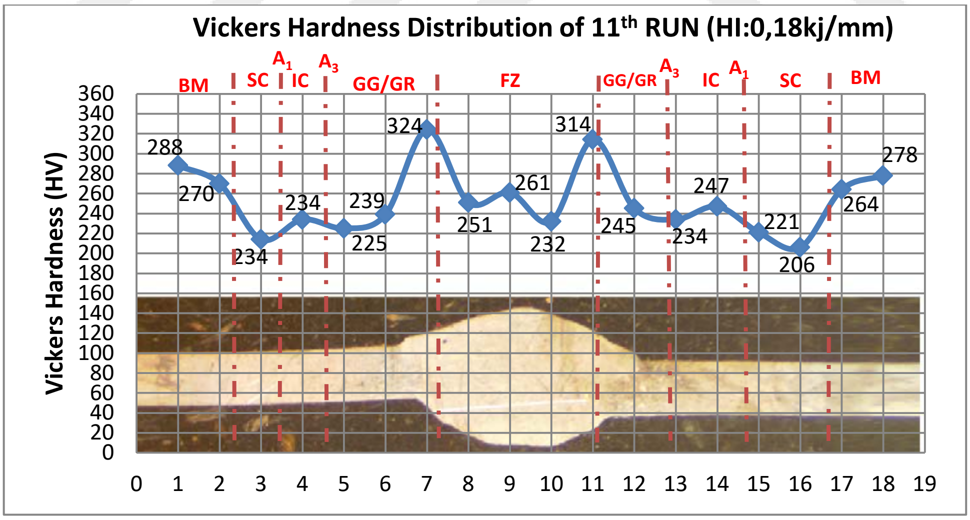

Figure 4.15. The Vickers hardness distribution of the weld cross-section obtained under the welding conditions of 11th Run

The lowest Vickers hardness distribution was observed on the welding cross-section of 12th Run which had the highest heat input (0,22kj/mm). This was due to the highest presence of decomposed martensite islands. The lowest hardness value (197 HV) of this cross-section were measured on the SC region. Also, the martensite tempering found further away from the Ac_1 line than other inspected samples. Thus, it was revealed that the width of the SC region also increased with rise in the heat input. The renucleation of martensite in the IC region was lower than the IC regions of other three welding conditions. Therefore, the lowest mean hardness among all IC regions was defined on the cross-section under the 12th Run condition. The hardness of GR region measured as higher than IC and SC regions on the cross-section of 12th Run. But, the lowest hardness values were obtained for this weld cross-section compared to lower heat input welds in GR region. The highest hardness was measured on the GG region of this sample as shown in Figure 4.16.

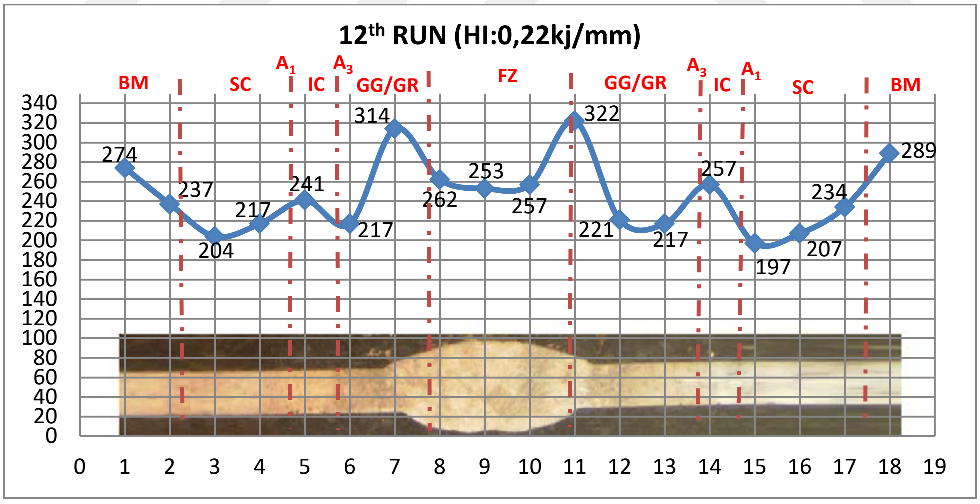

Figure 4.16. The Vickers hardness distribution of the weld cross-section obtained under the welding conditions of 12th Run

The mean FZ hardness magnitudes of the four samples, which had different heat inputs, were also close because of nearly the same percentages of VFM. The increase in the heat input decreased the percentage of VFM and hardness in FZ. The mean hardness values of the FZ's were lower than the base metal hardness substantially. Rocha et al. (2015) also demonstrated that minimum hardness of weld metal was always greater than the minimum value found in the SC regions in all cases of DP1000 welding with various heat inputs.

When hardness distributions of four samples were considered, it was clearly seen that, an increase in the weld heat input decreased the hardness of HAZ and FZ. At the same time, the width of the HAZ was increased when the heat input was increased. Biro (2013) also investigated the effect of welding heat input on the mechanical properties of DP steels. It was defined that, as weld heat input was increased, the peak HAZ hardness decreased, the degree of softening increased, and distance to maximum softening increased.

4.4. Uniaxial Transverse Tensile Test Results

Two tensile test samples were used for each of the 54 welded plates. The samples were chosen on the sections which did not have any welding defect. Hence, UTS of 108 samples were tested according to the TS 287 EN 895 standard. The UTS's of unwelded DP1000 steel were measured as 1050MPa. The UTS's of 54 runs' test specimens were listed in Table 4.1.

During the tensile tests, 100% of welded DP1000 samples fractured at their SC regions which had also the lowest hardness and VFM on the weld cross-sections. Thus, the Vickers hardness measurements and microstructure inspections in this study supported the tensile test results. Because, the failures in welded DP1000 samples were caused by increased material flow in the SC regions; this was due to the presence of decomposed martensite islands. Increased material flow likely caused localized necking to occur in the SC region. At the same time, Rocha et al. (2015) studied the influence of heat input on mechanical properties of butt welded joints of DP1000 sheets. They reported that fractures of the specimens always occurred in SC region, where hardness values were very low and decomposition of martensite was quite severe for all tensile test samples obtained under different welding conditions. The percentage changes in tensile strength depending on the welding parameters were estimated and discussed in the following paragraphs.

In this study, the tensile test samples obtained under the welding conditions of 23th Run (HI:0.10kj/mm), 9th Run (HI:0.14kj/mm), 11th Run (HI:0.18kj/mm) and 12th Run (HI:0.22kj/mm) were analyzed in more detail to investigate the relation between the failure location and heat input. HAZ widths of fractured samples were measured and designated according to run number and arranged as "$H_{23}<H_9<H_{11}<H_{12}$" (Figure 4.17). As a result, the widths of the HAZ and SC regions also increased, when the heat input increased. Biro and Lee (2004) noted that, higher heat input increased the time for carbon diffusion and the width of the softened zone increased, when a larger portion of the steel was elevated to a temperature allowing carbon diffusion. Rodrigues et al. (2004) stated that the joint strength of DP steel decreased linearly with increased HAZ widths.

The minimum decrease in UTS was measured under the welding conditions of 23th Run which had the lowest heat input. This reduction was calculated as "(1050MPa-820.61MPa)/1050MPa=21.85%". On the other hand, the decrease in UTS was calculated as "(1050MPa-773.59MPa)/1050MPa=26.32%" under the conditions of 12th Run which had the highest heat input and martensite tempering percentage. But the highest decrease in UTS was calculated as (1050MPa-771.22MPa)/1050MPa=26.55%" under the welding conditions of 11th Run. Burns (2009) also reported that, the fracture was observed in HAZ of GMAW welded 1.20 mm thick DP980 sheet steel tensile test specimens and a significant decrease (~28%) in UTS when compared to the unwelded BM UTS. In the same study, it was also stated that the failures in welded DP600 samples occurred in BM or HAZ depending on the heat input.

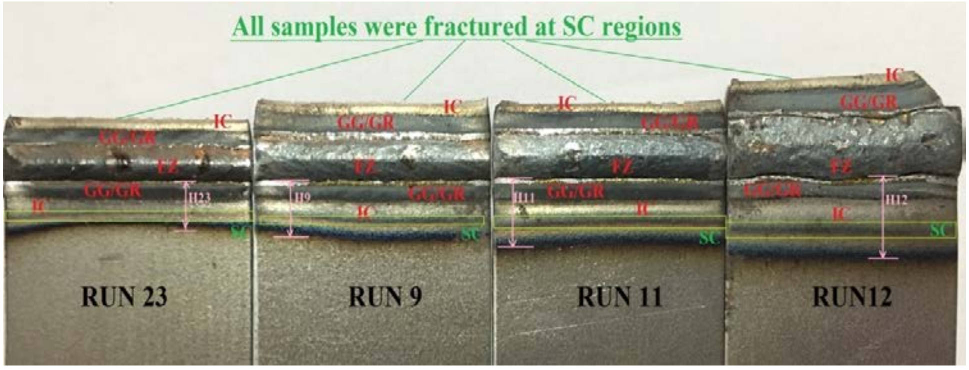

Figure 4.17. FZ, GG/GR, IC and SC regions of the fractured samples whose microstructures were inspected

As shown in Figure 4.18, the relationship between the heat input and UTS was obtained by using the data given in Table 4.1. As a result, when the heat input was increased, the UTS of DP1000 steel decreased. Moreover, the width of SC region increased, which caused even more decrease in UTS. Thus, failures were occurred further away from the welding zone at higher heat inputs. When minimum heat input was applied, the deterioration in mechanical properties was less pronounced, due to less softening in HAZ. Hence higher tensile strength values were observed in the samples obtained under the welding conditions with minimum heat inputs. Therefore, heat input was needed to be kept minimum, while it was providing sufficient welding penetration. On the other hand, heat input was not the only parameter, which affects the UTS. Other welding parameters such as voltage, welding speed, wire feed rate and their binary and trio interactions could have also independent effects on the tensile strength. Therefore, the effect of all defined factors on the UTS were analyzed in detail by using Minitab-17 software.

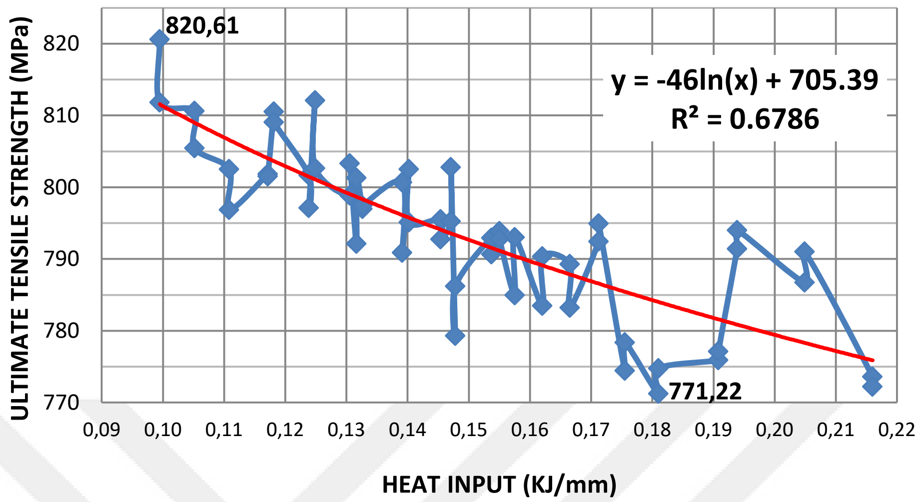

Figure 4.18. Heat input and UTS relation of DP1000 welding

4.4.1. Statistical Analysis of Tensile Test Results

Minitab-17 software was utilized to determine the effects of voltage, welding speed, wire feed rate and their interactions on UTS of DP1000 welding. Satisfactoriness of the experimental design and presence of welding parameters' affecting on the UTS were defined by applying General Factorial Regression Analysis.

In General Factorial Regression Analysis, R-sq value should be minimum 65% to accept experimental design as satisfying. As shown in Figure 4.19, R-sq value was defined as 93.81% in the regression analysis, which was far above the minimum value. Therefore, the experimental design was excellent. The p-values of voltage, welding speed and wire feed rate were 0.000, which were smaller than 0.05. Therefore, three main factors had great effects on UTS of welded DP1000 steels. In addition, voltage-wire feed rate and welding speed-wire feed rate interactions had remarkable effects, because their p-values were smaller than 0.05. But, there was no effect of voltage-welding speed interaction on the UTS, because the p-value of voltage-welding speed interaction was 0.148, which was higher than

0.05. On the other hand, there was a triple effect of interaction between voltage-welding speed-wire feed rate. Therefore, the triple interaction had to be eliminated, thus regression analysis was repeated to eliminate the voltage-welding speed interaction.

As a result of the repeated analysis, R-sq value was defined as 88.76% and it was higher than 65% as shown in Figure 4.20. Hence, the experimental design was still satisfied. But, p-value of voltage-welding speed interaction was 0.281, which was still higher than 0.05. Therefore, it was confirmed that there was no effect of the voltage-welding speed interaction on the tensile strength. This binary interaction was eliminated, than regression analysis was repeated again. As shown in Figure 4.21, the experimental design was accepted as excellent, because R-sq value was 87.06%. On the other hand, a noise factor with 12.7% were identified on the UTS of welded DP1000 steels at the end.

From the regression analysis, equation 4.1 was modeled by the software. By using this equation, UTS of components welded under different combinations of parameters between the lower and upper limits could be estimated approximately.

$$\text{TENSILE STRENGTH (MPa)} = 944{,}5 - 5{,}772\ \text{VOLTAGE (V)} + 0{,}1244\ \text{WELDING SPEED (mm/min)} - 34{,}92\ \text{WIRE FEED RATE (m/min)} \quad (4.1)$$

Factor	Levels	Values
VOLTAGE (V)	3	17,5; 18,5; 19,5
WELDING SPEED (mm/min)	3	260; 320; 380
WIRE FEED RATE (m/min)	3	2,2; 2,4; 2,6

Analysis of Variance

Source	DF	Adj SS	Adj MS	F-Value
Model	26	6304,3	242,47	15,75
Linear	6	5059,7	843,29	54,78
VOLTAGE (V)	2	1229,5	614,76	39,93
WELDING SPEED (mm/min)	2	2043,8	1021,88	66,38
WIRE FEED RATE (m/min)	2	1786,4	893,22	58,02
2-Way Interactions	12	904,9	75,41	4,90
VOLTAGE (V)*WELDING SPEED (mm/min)	4	114,2	28,55	1,85
VOLTAGE (V)*WIRE FEED RATE (m/min)	4	295,7	73,93	4,80
WELDING SPEED (mm/min)*WIRE FEED RATE (m/min)	4	495,0	123,75	8,04
3-Way Interactions	8	339,6	42,45	2,76
VOLTAGE (V)*WELDING SPEED (mm/min)*WIRE FEED RATE (m/min)	8	339,6	42,45	2,76
Error	27	415,7	15,39	
Total	53	6719,9		

Source	P-Value
Model	0,000
Linear	0,000
VOLTAGE (V)	0,000
WELDING SPEED (mm/min)	0,000
WIRE FEED RATE (m/min)	0,000
2-Way Interactions	0,000
VOLTAGE (V)*WELDING SPEED (mm/min)	0,148
VOLTAGE (V)*WIRE FEED RATE (m/min)	0,005
WELDING SPEED (mm/min)*WIRE FEED RATE (m/min)	0,000
3-Way Interactions	0,023
VOLTAGE (V)*WELDING SPEED (mm/min)*WIRE FEED RATE (m/min)	0,023
Error	
Total	

Model Summary

S	R-sq	R-sq(adj)	R-sq(pred)
3,92358	93,81%	87,86%	75,26%

Figure 4.19. The general factorial regression analysis results

Factor	Levels	Values
VOLTAGE (V)	3	17,5; 18,5; 19,5
WELDING SPEED (mm/min)	3	260; 320; 380
WIRE FEED RATE (m/min)	3	2,2; 2,4; 2,6

Analysis of Variance

Source	DF	Adj SS	Adj MS	F-Value	P-Value
Model	18	5964,6	331,37	15,36	0,000
Linear	6	5059,7	843,29	39,08	0,000
VOLTAGE (V)	2	1229,5	614,76	28,49	0,000
WELDING SPEED (mm/min)	2	2043,8	1021,88	47,35	0,000
WIRE FEED RATE (m/min)	2	1786,4	893,22	41,39	0,000
2-Way Interactions	12	904,9	75,41	3,49	0,002
VOLTAGE (V)*WELDING SPEED (mm/min)	4	114,2	28,55	1,32	0,281
VOLTAGE (V)*WIRE FEED RATE (m/min)	4	295,7	73,93	3,43	0,018
WELDING SPEED (mm/min)*WIRE FEED RATE (m/min)	4	495,0	123,75	5,73	0,001
Error	35	755,3	21,58		
Lack-of-Fit	8	339,6	42,45	2,76	0,023
Pure Error	27	415,7	15,39		
Total	53	6719,9			

Model Summary

S	R-sq	R-sq(adj)	R-sq(pred)
4,64540	88,76%	82,98%	73,25%

Figure 4.20. The repeated general factorial regression analysis results

The result of General Factorial Regression Analysis showed that, welding voltage, wire feed rate (current) and welding speed had significant effect on UTS of GMAW welded DP1000 steel. It was seen that voltage-wire feed rate and welding speed-wire feed rate binary interactions had remarkable effects on UTS. There was no effect of voltage-welding speed interaction on UTS. Thus, it was eliminated during the analysis.

Factor	Levels	Values
VOLTAGE (V)	3	17,5; 18,5; 19,5
WELDING SPEED (mm/min)	3	260; 320; 380
WIRE FEED RATE (m/min)	3	2,2; 2,4; 2,6

Analysis of Variance

Source	DF	Adj SS	Adj MS	F-Value	P-Value
Model	14	5850,4	417,89	18,74	0,000
Linear	6	5059,7	843,29	37,83	0,000
VOLTAGE (V)	2	1229,5	614,76	27,57	0,000
WELDING SPEED (mm/min)	2	2043,8	1021,88	45,84	0,000
WIRE FEED RATE (m/min)	2	1786,4	893,22	40,07	0,000
2-Way Interactions	8	790,7	98,84	4,43	0,001
VOLTAGE (V)*WIRE FEED RATE (m/min)	4	295,7	73,93	3,32	0,020
WELDING SPEED (mm/min)*WIRE FEED RATE (m/min)	4	495,0	123,75	5,55	0,001
Error	39	869,5	22,29		
Lack-of-Fit	12	453,8	37,82	2,46	0,026
Pure Error	27	415,7	15,39		
Total	53	6719,9			

Model Summary

S	R-sq	R-sq(adj)	R-sq(pred)
4,72169	87,06%	82,42%	75,19%

Coefficients

Term	Coef	SE Coef	T-Value	P-Value	VIF
Constant	793,669	0,643	1235,20	0,000	
VOLTAGE (V)					
17,5	5,245	0,909	5,77	0,000	1,33
18,5	1,054	0,909	1,16	0,253	1,33
WELDING SPEED (mm/min)					
260	-8,057	0,909	-8,87	0,000	1,33
320	1,184	0,909	1,30	0,200	1,33
WIRE FEED RATE (m/min)					
2,2	7,515	0,909	8,27	0,000	1,33
2,4	-1,060	0,909	-1,17	0,250	1,33
VOLTAGE (V)*WIRE FEED RATE (m/min)					
17,5 2,2	0,28	1,29	0,22	0,826	1,78
17,5 2,4	-0,80	1,29	-0,63	0,535	1,78
18,5 2,2	0,16	1,29	0,12	0,903	1,78
18,5 2,4	-3,19	1,29	-2,49	0,017	1,78
WELDING SPEED (mm/min)*WIRE FEED RATE (m/min)					
260 2,2	-2,18	1,29	-1,70	0,097	1,78
260 2,4	-3,49	1,29	-2,71	0,010	1,78
320 2,2	2,26	1,29	1,76	0,086	1,78
320 2,4	2,25	1,29	1,75	0,088	1,78

Figure 4.21. The lastly repeated general factorial regression analysis results

4.4.2. ANOVA Analysis

ANOVA analysis was applied to define the results in order to investigate the percent weightiness of each parameter and their binary combinations on the UTS of welded DP1000 plates. In ANOVA analysis, the R-Sq value was found as 87.06 %. In addition, importance of the welding parameters on UTS were shown numerically in Figure 4.22 from the SS values. The noise factors with 12.94% could be resulted from selection of impeccable sections on the welded plates, electricity fluctuation, cooling rated differences, difference in ambient temperature and other undefined factors.

Factor	Type	Levels	Values
VOLTAGE (V)	fixed	3	17,5; 18,5; 19,5
WELDING SPEED (mm/min)	fixed	3	260; 320; 380
WIRE FEED RATE (m/min)	fixed	3	2,2; 2,4; 2,6

Analysis of Variance for MEAN TENSILE STRENGTH (MPa)

Source	DF	SS	MS	F	P
VOLTAGE (V)	2	1229,52	614,76	27,57	0,000
WELDING SPEED (mm/min)	2	2043,77	1021,88	45,84	0,000
WIRE FEED RATE (m/min)	2	1786,44	893,22	40,07	0,000
VOLTAGE (V)*WIRE FEED RATE (m/min)	4	295,70	73,93	3,32	0,020
WELDING SPEED (mm/min)* WIRE FEED RATE (m/min)	4	495,00	123,75	5,55	0,001
Error	39	869,48	22,29		
Total	53	6719,90			

S = 4,72169 R-Sq = 87,06% R-Sq(adj) = 82,42%

Figure 4.22. Results of ANOVA for UTS

Figure 4.23 shows the effect of each factor on UTS and interactions. The effect of welding speed, wire feed rate and voltage on the UTS of DP1000 steel welding were found as 30.41%, 26.58% and 18.30%, respectively. These results showed that the welding speed which directly defines heat input had the greatest effect on UTS.

The main effect plots of three factors for UTS are given in Figure 4.24. It was seen that, while increasing welding speed with a weightiness of 30,41% on UTS, had resulted a decrease in heat input and increase in UTS of welded plates. Preliminary welding applications defining the reasonable numerical levels of the factors showed that extremely high welding speed caused lack of penetration, which also caused decrease in the UTS making weld quality the worse. Therefore, highest welding speed was limited as 380mm/min, whose some applications had already lack of fusion in the available design. Also it is already close to the highest manual GMAW speed which is applied by an average welder.

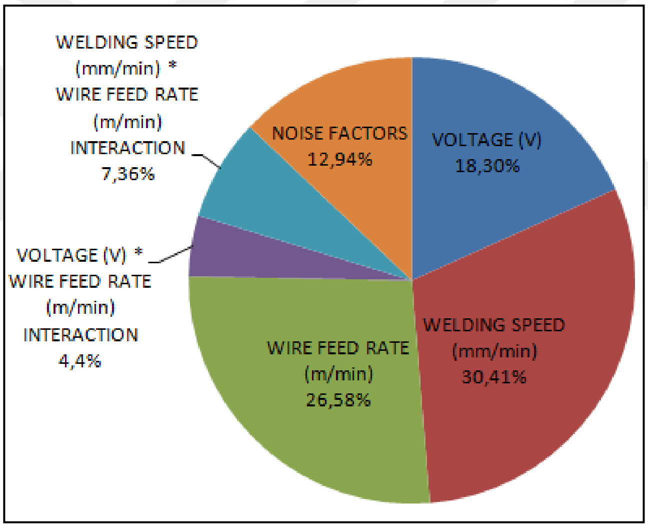

Figure 4.23. Effect percentages of each factor and interaction

Extremely slow welding speeds, lower than 260mm/min, also resulted a reduction in the UTS because of martensite decomposition at high heat input. Furthermore, depending on the voltage and wire feed rate it caused a extreme convex welding cap (at low heat input) or burning gaps (at high input) which was not wanted because of notch effect. It was known that these types of features caused stress concentration and adversely affected the UTS of the welded components.

When the wire feed rate, with a weightiness of 26.58% on UTS was increased; the welding current increased automatically to melt more wire and to get sufficient penetration. Hence, the UTS increased due to enlargement of FZ cross-section area. Therefore minimum wire feed rate was limited to 2.2m/min to obtain sufficient penetration for 1.20mm thick DP1000 plates according to the result of preliminary welding tests. On the other hand, increasing the current over the optimum value caused an increase in the heat input; resulted martensite tempering and grain growth. When wire feed rate was increased to higher values resulted a reduction in UTS of welded DP1000 test specimens as shown in Figure 4.24. Meanwhile, it was observed that, very high wire feed rate caused a very high weld metal spatter during preliminary welding applications.

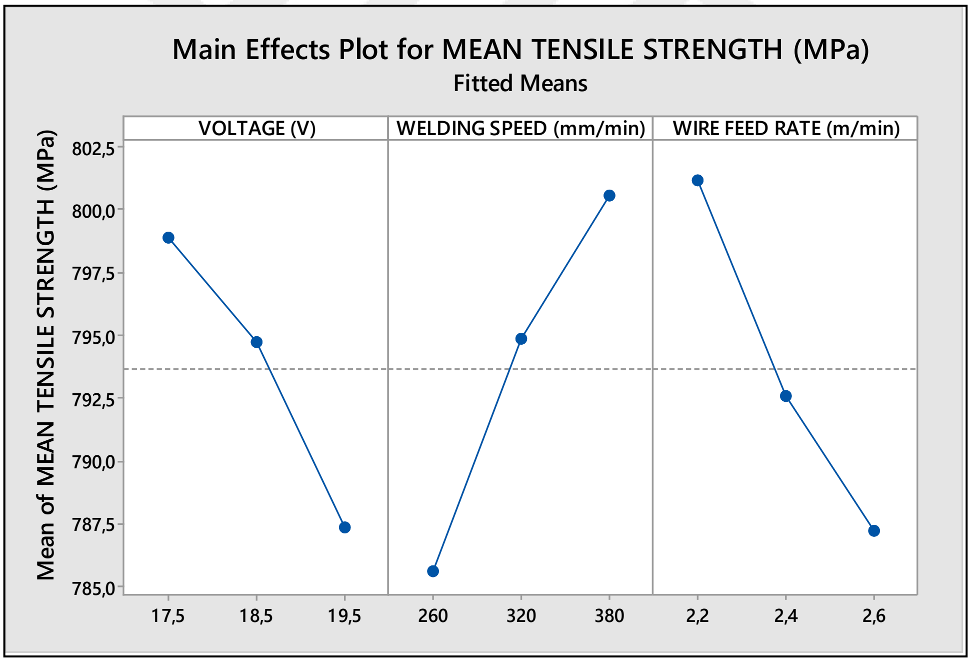

Figure 4.24. Main Effect Plot for UTS of DP1000 welding

This situation was not desired because of its contribution on stress concentration and adverse effect on deposition efficiency. Therefore, highest wire feed rate was limited to 2.6m/min during experimental work.

The limited voltage increased the welding penetration for higher UTS. Also, insufficient voltage caused excessive convex weld metal, which was not accepted according to the Level-C of EN ISO 3834 norm. Therefore, minimum voltage was limited as 17.5V for this experimental study from the preliminary welding applications. When the voltage increased extremely, the heat input also increased the martensite tempering and grain growing effects thus UTS decreased. At the same time, surface tension of melting metal increased by increasing the voltage, which caused burning gaps on the welding seam as shown in Figure 4.24. Therefore, maximum voltage was limited as 19.5V for experimental design by depending on the preliminary welding applications. The result of statistical analyses showed that, if the voltage exceeded the critical level close to especially 18.5 V, UTS decreased.

As shown interaction plots of mean UTS (Figure 4.25), voltage-wire feed rate interaction had a decreasing effect and welding speed-wire feed rate interactions had an increasing effect on UTS of DP1000 welding. The p-value of voltage-welding speed interaction was found as 0.148, which was higher than 0.05 and parallel lines in interaction plot (Figure 4.25) indicated that there was no voltage-welding speed interaction.

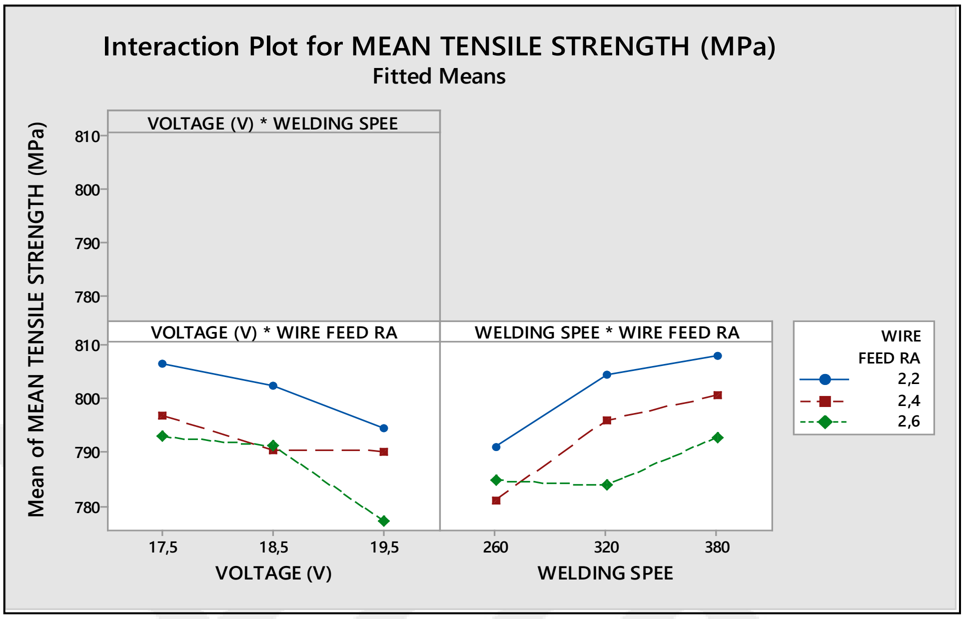

Figure 4.25. Interaction plot for UTS

4.4.2.1. Response Optimization Analysis For Highest Tensile Strength

The measured highest UTS values were 820.61MPa, 812.07MPa and 811.81MPa from the conditions of 23th Run, 20th Run and 50th Run, respectively. In order to increase the gained UTS, Minitab Response Optimization Function was utilized. Although previous studies utilized relatively higher magnitudes, 840MPa was accepted as target UTS during the present analyses. But, the software provided the attainable highest UTS as 813,5MPa. This difference was attributed to 12.94% loss in R-Sq. Therefore, noise factors affected the maximum UTS magnitude.

The software defined the parameters combination of 23th Run (17.5Vvoltage, 380mm/min welding speed and 2.2m/min wire feed rate) as the best for the highest UTS. This combinations produces 0.10kj/mm heat input, which is the lowest in the experimental design.

Figure 4.26. Response optimization plot for maximum tensile strength of DP1000 welding

As a result of physical tests and statistical analysis of Minitab-17 software, the optimum butt welding parameter combination was defined as 17.5V arc voltage, 380mm/min welding speed and 2.2m/min wire feed rate to provide the maximum ultimate tensile strength in GMAW of 1.20mm DP1000 plates.

5. CONCLUSIONS

1. Excessive weld metal and lack of penetration could be emerged at insufficient welding heat inputs (0.10kj/mm-0.12kj/mm). Increasing the heat input increased the penetration and width of the welding. It also decreased the height of the welding cap. Therefore, the ideal welding seams without any imperfection were observed mostly between 0.12kj/mm and 0.15kj/mm heat inputs for 1.20mm DP1000 plates. On the other hand, when the heat input increased over 0.18kj; the occurrence frequency of welding defect creations such as burning gap and excessive penetration also increased obviously. Therefore, heat input was needed to be kept minimum while it was providing full penetration.
2. At low arc voltage (17.5V), narrow and extremely high weld cap observed. Also lack of penetrations were detected. Sufficient voltage (18.5V) increased the width and decreased the height of the weld cap obviously, at the sametime it increased the penetration, slightly. When the arc voltage was overly high (19.5V), very wide weld seams with low weld cap height were observed. The voltage changes affected the width of the welding more than the penetration.
3. The ability of penetration was difficult due to low current (53A) and low WFR (2,2m/min), hence partial lack of penetrations were detected. Increasing the current to 53A (WFR: 2.4m/min), increased the welding penetration, significantly. In this way, continuity of full penetration was mostly provided. On the other hand, excessively high welding current (60A) with short circuit arc could cause extreme spatter and also lack of fusion.
4. In many applications of high welding speed (380mm/min), lack of penetrations and very tight welding seam were detected. Gradually decreasing the welding speed increased in penetration provided the

sufficient penetration. But, very low welding speed (260mm/min) increased the formation of burning gaps and extreme convex welding cap.

5. Increase in heat input increased the martensite tempering and grain growth effects. Therefore, the VFM decreased. At the same time the width of the HAZ increased and the tempering/decomposition found further away from the Ac_1 line when compared to the lower heat input welds.
6. When the VFM increased as the ferrite grain size decreased, the hardness of the DP1000 steel increased. Also the formation of elongated martensite bands increased the hardness of the DP1000 steel.
7. The highest reduction of VFM was obtained in SC regions due to the highest percentage of tempered martensite. Thus, the lowest hardness values were measured at SC regions. The lowest decrease in VFM of SC was calculated as 19,37% at lowest heat input weld (0.10kj/mm). The highest decrease in VFM of SC was calculated as 25,74% at highest heat input weld (0.22 kj/mm).
8. The tempered martensite phases in the SC regions dispersed more homogeneously at low heat input welds. But they were clustered at high heat input welds. As a result, the increase in heat input increased the accumulation of the tempered martensites due to high amount of martensite decomposition obtained at the higher temperatures.
9. Increase in heat input decreased the hardness distribution measurements and increased the distance to maximum softening from FZ. The welding condition of 23^{th} Run which had the lowest welding heat input (0.10kj/mm), thus had also the highest hardness distribution. The hardness of SC on this sample was measured as 220HV. The lowest Vickers hardness distribution was observed on the welding cross-section of 12^{th} Run condition which had the highest heat input (0.22kj/mm). The lowest hardness value (197 HV) of this cross-section were measured on the SC region.

10. Because of the renucleation of martensite phase in IC regions, the VFM of IC regions were higher than the SC regions for all samples. Also, IC region had a significant spike in hardness compared to the adjacent SC region. While heat input was increasing, the martensite tempering increased and hardness decreased in IC region, too. The IC region of 23th Run condition which had the lowest heat input and also the highest VFM (46,84%) and finest microstructure among the inspected four IC regions. Also, while heat input was increasing, the tempered martensite percentage and grain size of IC region increased. Also, accumulation of the tempered martensite increased.
11. The hardness increased further upon entering the GR region. The finest grain structure was observed in GR regions. Upon cooling after welding austenite in this region transformed to massive martensite. On the other hand, while heat input was increasing in GR region, the quenching effect decreased due to lower cooling rate. Therefore the martensite tempering and grain growing effects increased; hardness decreased.
12. The highest percentage of VFM and hardness values were measured on the GG region where the largest grain sizes were also observed. The interior of these large grains transformed to massive martensite and acicular ferrite upon cooling after welding. But, increase in heat input decreased the percentage of VFM in GG region. This caused decrease in local hardness.
13. The compositions of the fusion zones were mostly ER70S-6 electrode material with a small amount of melted BM from the DP1000 steel. The measured VFM in FZ’s were 43,73%, 44,18%, 42,63% and 41,14%. Although, there was no big difference among 4 samples, rise in the heat input had an reducing effect on the percentage of VFM and hardness in fusion zones. The average hardness of the FZ was lower than the hardness of DP1000 BM and higher than the hardness of SC region.

14. The 100% of welded DP1000 samples fractured in the HAZ during uniaxial transverse weld tensile tests. Because, increased material flow in the SC regions likely caused localized necking to occur in the SC region.
15. A certain relation between the VFM of SC region and tensile strength was proved. When the heat input was increased, martensite tempering increased and thus UTS decreased.
16. The minimum decrease in UTS was calculated as 21.85% and the highest decrease in UTS was calculated as 26.55%.
17. In ANOVA analysis, the R-Sq value was defined as 87,06 %. The noise factors with 12.94% could be resulted from electricity fluctuation, cooling rated differences, difference in ambient temperature and other undefined factors.
18. Welding speed, wire feed rate and voltage had 30.41%, 26.58% and 18,30% effects respectively on the UTS of DP1000 steel welding. Therefore, welding speed had greatest effect on UTS because it affected almost directly proportional to heat input.
19. While welding speed was increasing, heat input and martensite tempering effect decreased and UTS of welded plates increased. But, extremely fast welding speeds caused lack of penetration which also decreased the UTS and made weld quality worse. Therefore, highest welding speed was limited as 380mm/min, whose some applications had already lack of fusion in the available design.
20. When the wire feed rate and welding current were increased; the UTS increased due to provided full penetration and enlargement of FZ cross-section area. But as the welding current continued to increase, heat input increased. Therefore martensite tempering effect and grain growth decreased the UTS of DP1000 welding. As a result, the optimum WFR was defined as 2.2m/min for full welding penetration.

21. The 17.5V was generally sufficient for the full welding penetration to provide higher UTS. But, higher voltage levels decreased the UTS of the welding and caused welding defects.
22. Voltage-wire feed rate interaction had a decreasing effect and welding speed-wire feed rate interactions had an increasing effect on UTS of DP1000 welding. There was no effect of voltage-welding speed interaction because p-value of the interaction found as 0.148, which was higher than 0.05.
23. As a result of physical tests and statistical analysis of Minitab-17 software, the optimum butt welding parameter combination was defined as 17.5V arc voltage, 380mm/min welding speed and 2.2m/min wire feed rate to provide the maximum UTS in GMAW of 1.20mm DP1000 plates.

REFERENCES

Aghakhani, M., Mehrdad, E., Hayati, E., August 2011. Parametric Optimization of Gas Metal Arc Welding Process by Taguchi Method on Weld Dilution. International Journal of Modeling and Optimization, Mechanical Engineering Department of University of Razi, 1(3):216-220.

Ashrafi, H., Shamanian, M., Emadi, R., Saeidi, N., February 2017. Microstructure, Tensile Properties and Work Hardening Behavior of GTA-Welded Dual-Phase Steels. Isfahan University of Technology, Journal of Materials Engineering and Performance, 26(3):1414–1423.

Belinga, E., M., 2012. Application and Benefits Of Adaptive Pulse GMAW. Research Gate, Lappeenranta University of Technology, 124.

Biro, E., Lee, A., May 2004. Welded Properties of Various DP600 Chemistries. Sheet Metal Welding Conference XI, American Welding Society, Miami, 23(7):2-5.

Biro, E., 2013. HAZ Softening Kinetics In Dual Phase and Martensitic Steels. Ph.D. Thesis, Materials Science and Engineering Department, McMaster University, Hamilton, Ontario, 167.

Biro, E., Jiang, C., Lyttle, K., 2008. Correlation Between Failure Location and Tensile Strength of AHSS GMAW Lap Joint. Sheet Metal Welding Conference XIII, Livonia, American Welding Society, Miami, 27(12):1-13.

Brooks, C., R., 1996. Principles of the Heat Treatment of Plain Carbon and Low Alloy Steels. ASM International, Material Science and Engineering Department, The University of Tennessee, Knoxville,498.

Burns T., J., 04.2009.Weldability of a Dual-Phase Sheet Steel by the Gas Metal Arc Welding Process. MSc. Thesis at University of Waterloo, Ontario, Canada,260.

Chu, K., P., February 2007. Welding Of Sheet Metal Using Modified Short Arc MIG/MAG Welding Process. MSc. Thesis at Department of Mechanical Engineering Department, Lappeenranta University of Technology,72.

Conrardy, C., Kapustka, N., Albright C., May 2006. Effect of Material and GMAW Process Conditions on AHSS Welds. Sheet Metal Welding Conference XII, Livonia American Welding Society, Miami, 2-5.

Davies, R., 1978. Influence of Martensite Composition and Content on the Properties of Dual Phase Steels. Metallurgical Transactions A, 9(5):671-679.

Elliott, A., N., A., 2010. Gas Metal Arc Welding Of Advanced High Strength Steel; Developments For Optimized Weld Control And Improved Weld Quality, Great Designs in Steel Seminar, 24.

Ghosh, P., 1990. Thermal Cycle and Microstructure of Heat Affected Zone of Flash Butt Welded Mn-Cr-Mo Dual-phase Steel. ISIJ International, 3(4):317-324.

Hernandez, V., H., B., Nayak, S., S. And Zhou, Y., 18 May 2011. Tempering of Martensite in Dual Phase Steels and Its Effects on Softening Behavior. The Minerals, Metals & Materials Society and ASM International,15.

Hsu, C., Soltis, P., Carroscia, M., Barton, D., Occhialini, C., 2004. Weldability of Dual-Phase Steel with Arc Welding Processes. Sheet Metal Welding Conference XI, Sterling Heights, MI. American Welding Society, Miami, 23(7):1-5.

Kang, M.J., So, W.J., Kim, D.C., 01.01.2010.Weldability Of Pulse GMAW Joints Of 780 MPa Dual-Phase Steel. Department of Mechanical Engineering, Hanyang University, 17 Haengdang-Dong, Seoul, Korea, 41(1):53-60.

Kapustka, N., Conrardy, C., Babu, S., and ALBRIGHT, C., 8 June 2008. Effect of GMAW Process and Material Conditions on DP 780 and TRIP 780 Welds. American Welding Society, 87(3):135-148.

Koganti, R., Elliott A., Jiang, C., November 2010. Gas Metal Arc Welding (GMAW) Process Optimization of a 1.4 mm Uncoated Dual Phase 980 (DP980) Joint for Automotive Body Structural Applications. ASME 2010 International Mechanical Engineering Congress and Exposition, British Columbia, Canada, 42(9): 647-655.

Lawson, R., Matlock, D., Krauss, G., 1981. The Effect of Microstructure on the Deformation Behavior and Mechanical Properties of a Dual-Phase Steel. The fundamentals of dual-phase steels: Proceedings of a symposium. Warrendale, PA: Metallurgical Society of AIME, 38(16): 347-381.

Mukherjee, K., Ramazani, A., Yang, L., Prahl, U., Bleck, W., Reisgen, U., Schleser, M., Abdurakhmanov, A., December 2011. Characterization of Gas Metal Arc Welded Hot Rolled DP600 Steel. RWTH Aachen University Institute for Ferrous Metallurgy, Steel Research International, 82(12):1708-1416.

Tansal M., 2008. Lection Notes of Welding Technology. Middle East Technical University, Ankara, 117-156.

Na, H., H., Kim, I.S., Kang, B.Y., April 2011. A Experiment Study For Welding Optimization Of Fillet Welded Structure. Department of Mechanical Engineering, Mokpo National University, South Korea, 45(2):178-187.

Okamoto, A., Takahashi, M., 1981. Control of Strength and R-Value in Box-Annealed Dual-Phase Steel Sheet. Fundamentals of Dual Phase Steels: Proceedings of a symposium, Warrendale, PA: Metallurgical Society of AIME, 32(11): 427-445.

Park, Y., Coldren, A., Morrow, J., 1981. Effect of Martensite Bands and Elongated Manganese Sulfide Inclusions on the Formability of Dual-Phase Steels. Fundamentals of Dual Phase Steels: Proceedings of a symposium, Warrendale, PA: Metallurgical Society of AIME, 32(14): 485-497.

Pouranvari, M., 2010. Tensile Strength And Ductility Of Ferrite-Martensite Dual Phase Steels. Association of Metallurgical Engineers of Serbia, Islamic Azad University, Dezful Branch, Dezful, Iran, 16:187-194.

Ramazani, A., Li, Y., Mukherjee, K., Prahl, U., Bleck, W., Abdurakhmanov, A., Schleser, M., Reisgen U., 13 September 2012. Microstructure Evolution Simulation In Hot Rolled DP600 Steel During Gas Metal Arc Welding. Computational Materials Science, Department of Ferrous Metallurgy, RWTH Aachen University, Germany, 68:107-116.

Rocha, I., C., L., Machado, I., G., Mazzaferro, C., C., P., 2015. Mechanical and Metallurgical Properties of DP1000 Steel Square Butt Welded Joints With GMAW. . International Journal of Engineering & Technology, Federal University of Rio Grande do Sul, PPGE3M, Welding & Related Techniques Laboratory, 4(1): 26-34.

Rodrigues, D., M., Menezes, L., F., Loureiro, A., 2004. The Influence of The HAZ Softening on The Mechanical Behaviour of Welded Joints Containing Cracks in The Weld Metal. Engineering Fracture Mechanics, 14(13): 2053-2064.

Salamci, E., Kabakci, F., 8.03.2011. Influence of Microstructure on Tensile Properties of Dual Phase Steel. J. Fac. Eng. Arch. Gazi University, 26(2):263-272.

Sodjit, S., Uthaisangsuk, V., 2012. A Micromechanical Flow Curve Model for Dual Phase Steels. Department of Mechanical Engineering, Faculty of Engineering, King Mongkut’s University Technology Thonburi, Bangkok, Thailand, 22(1):87-97.

Sudersanan, P., D., Kempaiah, U., N., 2012. The Effect Of Heat Input and Travel Speed On The Welding Residual Stress By Finite Element Method. Department of Mechanical Engineering, Dr.T. Thimmaiah Institute of Technology, K.G.F, India, 4(2):50-43.

Tiziani, A., Ferro, P., Cervo, R., Durante, M., 2011. Effects of Different Welding Technologies on Metallurgical and Mechanical Properties of DP600 Steel Welded Joints. University of Padova,27-34.

Tsipouridis, P., 2016. Mechanical Properties of Dual Phase Steels. MSc. Thesis at Technical University Munich,122.

Van, M., 4 June 2007. Micromechanical Modeling Of a Dual Phase Steel. Technische Universiteit Eindhoven, 18(7): 27.

Wang, J., Yang, L., Sun M., Liu, T., Li, H., January 2016. Effect of Energy Input on The Microstructure and Properties of Butt Joints in DP1000 Steel Laser Welding. School of Materials Science and Engineering, Tianjin University, Tianjin 300072, PR China, 90:642-649.

http://www.gedikwelding.com/product/sg-2-gas-shielded-arc-welding-wire-rod, 2017. Gas Metal Arc Welding Consumables. Pendik, Istanbul, Turkey.

http://www.lincolnelectric.com, 2014. Gas Metal Arc Welding. The Lincoln Electric Company, 22801 Saint Clair Avenue, Cleveland, OH, 44117, U.S.A.

http://www.ssab.com.tr/products/brands/docol/products/docol-1000dp, 2009. Welding Of Domex And Docol Advanced High Strength Steels. SSAB Tunnplåt AB SE-781 84 Borlänge, Sweden.

CURRICULUM VITAE

Murat KARATAŞ was born on 02.04.1985 in Konya. He graduated from The Chamber of Commerce of Adana Anatolian High School in 2003. Same year, he enrolled in Mechanical Engineering Department of Çukurova University. He graduated from the department of Mechanical Engineering in 2008. He began his engineering career at Baris Technological Mechanical Installation Company and he had worked as a site chief at Zeugma Museum Project in Gaziantep for a year. Then, he deserved to get the international welding engineering (IWE) diploma and welding inspector (IWI-C) at the end of the six mounts. He continued his career as the construction production chief at Setkon Machinery Company between 2010 and 2011. Then, he worked in TEMSA GLOBAL (The Bus Producer in Adana) from 2011 to 2015 as a R&D Engineer. He managed the scientific project which was defined with 1120147 project number in TUBITAK (The Scientific and Research Council of TURKEY) during TEMSA years. This project was directly related to weight reduction of bus structure by using DP steels and HSLA steels. He has been working at Gedik Welding Company as a Regional Sales Manager for 3 years.